A BEAM TRANSPORT SYSTEM FOR THE MEDICAL FACILITY AT TRIUMF

by

ROBERT WILLIAM HARRISON

B.Sc., University of Victoria, 1968

A THESIS SUBMITTED IN PARTIAL FULFILLMENT

OF THE REQUIREMENTS FOR THE DEGREE OF

MASTER OF SCIENCE

in the Department

of

Physics

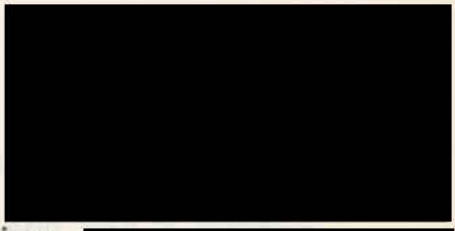

We accept this thesis as conforming
to the required standard

Accepted by the Faculty of Graduate Studies

on _____ by _____ Dean of Faculty

ABSTRACT

Supervisor: Dr. D. E. Lobb

Preliminary experiments indicate that a beam of negatively charged pions should have a depth-dose pattern that is much more favorable for irradiation of deep-seated malignant tumors than any other type of radiation beam. Consequently, it is proposed that a beam transport system to transmit a pion beam for radiobiological testing of this possibility be built in conjunction with the TRIUMF cyclotron to take advantage of the pions that will be available when the high energy, high intensity proton beam strikes a target in Beam Line I. The beam transport system that is the subject of this thesis should be able to transmit a beam that forms a solid angle of 10 msr at the target and has a momentum spread of ±10% of the central momentum to deliver a 100 rad dose to a volume of 10 cm x 10 cm x 8 cm thick.

An achromatic system consisting of two 45 degree bending magnets and five quadrupole focussing magnets has been designed to first order. In addition, the second order aberrations and methods for their correction are discussed; two sextupole magnets should be included in the system to correct some of these geometric and chromatic aberrations. The second order design meets all of the

requirements for radiobiology experiments and pre-clinical testing of the potentialities of pions for radiotherapy.

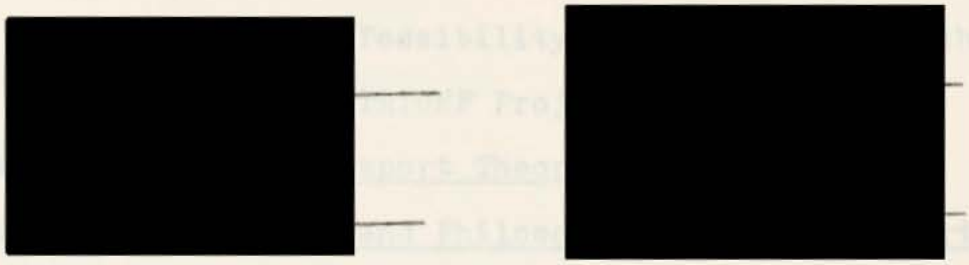

TABLE OF CONTENTS

TABLE OF CONTENTS (continued)

ACKNOWLEDGEMENTS

The author wishes to express his appreciation for the patient supervision of Dr. D. E. Lobb, under whose guidance this work was performed.

For reading the manuscript and offering many valuable comments, the author is indebted to Dr. G. Friedmann, Dr. H. Dosso, and Mrs. J. Hunt.

Financial support from TRIUMF made this research possible and is therefore gratefully acknowledged.

LIST OF TABLES

LIST OF FIGURES

1. INTRODUCTION

1.1 The Possibility of Pions for Radiotherapy.

With the advent of a new generation of accelerators that produce very intense beams of elementary particles, negatively charged pions may be produced in beams of sufficient intensity to allow consideration of these particles for cancer therapy. Interest in this possibility is such that facilities for the necessary radiobiology and radiotherapy studies are now being constructed in conjunction with three large accelerators: The Los Alamos Meson Physics Facility (LAMPF) at Los Alamos, New Mexico; the Swiss Institute for Nuclear Research (SIN) near Zurich, Switzerland; and TRIUMF in Vancouver, British Columbia. The purpose of this thesis is to present the design of a beam transport system that will transmit the desired beam of pi mesons to the Radiobiology-Radiotherapy Laboratory that is planned as part of the TRIUMF Project. It must be emphasized that much experimental radiobiology and many studies of radiation dosimetry must be carried out before the use of these beams for cancer treatment can be considered more than an exciting possibility.

The principal aim of cancer research is to find some method of treatment that will destroy malignant tissue

and not do irreparable damage to healthy tissue surrounding a tumor. In certain cases, radiation therapy is such a method. If the cancerous tissue is more susceptible to damage from ionizing radiation than is normal tissue, then the tumor is said to be radio-sensitive. A radio-sensitive tumor may be completely eradicated by a dose of radiation that healthy tissue will survive. In some other instances, healthy cells will repair tissue damage more quickly than malignant cells. In these cases, by dividing the radiation treatment into several successive exposures a tumor may be progressively destroyed while the normal tissues recover sufficiently between radiation doses that they are not destroyed, even though they may suffer as much damage at each dose of radiation as does the cancer tissue. Such a treatment procedure is called dose fractionation, and is widely used in radiotherapy. In other cases, such as in skin cancer, the radiation dose can be localized so that only the cancer and the immediately adjacent tissue receive the radiation dose, but for a deep-seated tumor, such as cancer of the large intestine, there is no possibility for dose localization using conventional methods.

Another common procedure in radiotherapy is to irradiate a tumor from several different directions. This technique, called multiple field treatment, distributes the radiation dose over a large volume of healthy

tissue so that any point in the surrounding tissue receives less dose than the tumor.

It can also happen that cancer tissue is less susceptible to radiation damage than healthy tissue. Dose fractionation and multiple field irradiation are of little avail in such cases because the total dose is limited to a non-curative level by the sensitivity of the healthy tissue surrounding and even inside the tumor.

To put into perspective the possibility of using pions for radiotherapy of deep-seated tumors, we shall briefly summarize the methods of production and the physical properties of the various types of radiation that are available. For a more complete treatment of these topics and others in the field of radiology, Johns (1969) and Meredith and Massey (1968) are suggested. Among the choices of particles are x-ray and γ-ray photons, protons, neutrons, electrons, some light nuclei, and more recently, pions. Each different choice has its own relative advantages and disadvantages.

To begin with production, some particle beams are easy to produce while others are extremely difficult. The easiest of all to produce are γ-rays, which result from the radioactive decay of some unstable nuclei. The most

common decay scheme used is that of Co^{60}. The stable isotope Co^{59} is irradiated with low-energy neutrons in a nuclear reactor and converted into Co^{60}. In the subsequent decay into Ni^{60}, two γ-rays with energies of 1.17 and 1.33 MeV are emitted. Cobalt is preferred for this application because of its long half-life (5.26 years) and its ease of production with very high activity. Sources with activities of 5 kilo-curies (1 curie = 3.7×10^{10} disintegrations per second) are readily available.

Also very easy to produce are x-rays, which differ from γ-rays only in the means of production and the type of energy spectrum. X-rays may be produced by several different processes, but the usual method is to allow energetic electrons from a high voltage electron gun to strike a target. There a small fraction of the electron kinetic energy is converted into x-rays by the slowing down of the incident electrons by the atomic electrons in the target material. The x-ray production process is called bremsstrahlung (see, for example, Leighton (1959)), and results in a continuous spectrum of energies, as opposed to the discrete line spectrum characteristic of γ-rays. If the electron energy in the incident beam is high enough, the x-ray spectrum will have superimposed intensity peaks characteristic of the target material that result from high energy radiative transitions of the atomic electrons.

Since most of the energy of the electron beam is converted into heat in the target, the intensity of the x-ray beam is usually limited by the rate at which the target can dissipate this heat. The desired properties of an x-ray beam to be used for radiotherapy do not require a small electron beam spot at the target, so large electron beam spots may be used to generate very intense x-ray beams. Consequently, dose rate is rarely a limiting factor in x-ray cancer therapy.

For some deep-therapy applications, electrons with energies of millions of electron volts are used to produce more penetrating rays. Below about 10 MeV, a linear accelerator is commonly used to produce the electron beam, while for even higher energies, a betatron can be used. The maximum energy for the x-rays, which is equal to the kinetic energy of the incident electrons, can thus be made larger than the energies available from γ-rays.

In general, charged particles have a much shorter range than do photons with the same kinetic energy because the charged particles interact more strongly with the electrons in the absorber. Consequently, in order that charged particle beams be useful for radiotherapy, they must have much higher energies than the commonly used x-rays and γ-rays. The usual device for producing energetic charged

particles is an accelerator of some type. Protons are usually accelerated with a cyclotron and light nuclei with a Van de Graaff accelerator. Linear accelerators may also be used to accelerate any type of charged particle.

The production of an intense beam of neutrons is even more difficult because neutrons do not occur naturally outside nuclei. Their instability means that some nuclear reaction must be used to create free neutrons. Also, since neutrons are uncharged, they cannot be controlled or accelerated by electric and magnetic fields as charged particles are. Neutrons are produced in great numbers in a nuclear reactor, but the problems involved in extraction and collimation of a useful beam are probably insurmountable. High energy neutrons are produced when protons from an accelerator strike a target, but these neutrons are usually too high in energy to be useful for radiobiology. A promising nuclear reaction that is discussed by Bacon (1969) is the so-called D-T reaction; accelerated deuterons bombard a tritium target and release 14 MeV neutrons. These neutrons are approximately equivalent in range to the x-rays produced by 4 MeV electrons, and intensities of 10^{11} neutrons per second are readily attainable. If neutrons are ever extensively used for radiotherapy, a reaction such as this one will probably be used.

Pions are highly unstable elementary particles that may be produced in very energetic nuclear collisions. Some properties of pions are summarized in Appendix I. Pions are produced as secondary particles when a proton beam with energy greater than 150 MeV strikes a metallic target, or when a proton beam with energy greater than 293 MeV strikes a hydrogen target. Other particles are produced as well: there are scattered protons, neutrons, energetic electrons, γ-rays, nuclear fragments such as deuterons and alpha particles, and muons, the decay product of pions. In order to use a pion beam for radiotherapy, it is necessary to separate the pions from all these other particles with electromagnetic fields and shielding. That is, one must design a beam transport system to select particles of the desired type with the proper charge and momentum from the spray of particles produced by the proton beams. It is this selection system that is the subject of this thesis.

In order to justify the research and design effort that must go into the development of a radiotherapeutic beam of pions, one must examine the mechanisms of the absorption of radiation from a beam and the effects of different types of radiation on tissue. The analysis of the loss of energy from a radiation beam is complicated by the number of possible interactions that can occur. Each type of particle has several basic modes of interaction with matter, the

dominant process being determined by the particle energy and the atomic number of the absorbing material. In fact, the radiation type may change many times and many secondary particles may be produced before the energy of a single incident particle is finally dissipated. Photons interact by the processes of photoelectric electron emission, the Compton effect, and electron-positron pair production. Charged particles, especially electrons, produce bremsstrahlung, while the heavier particles lose most of their energy through electron scattering. Neutrons, having no charge, can only interact through nuclear scattering and absorption. Quantitative description of these processes are given in Meyerhof (1967) or Weinstein (1964).

In Compton scattering of photons, some of a photon's energy and momentum are transferred to an electron with the resulting emission of a scattered photon and an electron. In the photoelectric effect, all of the photon's energy is transferred to an electron; some of this energy is used to overcome the binding energy of the electron to the atom and the rest appears as kinetic energy of the ejected electron. The atom is left in an excited state due to the removal of the electron, but it quickly decays to the ground state with the emission of one or several photons with lower energy than the incident photon.

If the original photon carries sufficient energy, an electron-positron pair may be created when the photon scatters off a nucleus or off an electron. The positron will eventually recombine with an electron and two 0.51 MeV γ-rays will be produced by the resulting annihilation of the pair. For photons with energies greater than 50 MeV, pair production is the dominant mode of interaction. The Compton effect predominates between 200 keV and 2 MeV, and the photoelectric effect is most important below 50 keV. Between 50 keV and 200 keV, the photoelectric effect and the Compton effect are of nearly equal importance, and between 2 MeV and 50 MeV, interactions by pair production are nearly as numerous as those by the Compton effect. The results quoted here are those if water or soft tissue is the absorbing medium.

The relative importance of these different effects is dependent on the atomic number of the absorbing material as well as on the photon energy. For example, the absorption by pair production varies as the atomic number, Z and the absorption by the photoelectric effect varies approximately as Z^3. This means that tissues with a high atomic weight, such as bone, will suffer more effect per gram than will adjacent soft tissue, and the effect will be from different atomic processes in the two different tissue types.

The photoelectric effect and pair production are 'one-shot' interactions. That is, a photon may travel a long distance in an absorber before it interacts, but once it does, all of the photon energy (now carried by secondary particles) is absorbed within a short distance from the point of interaction. This means that a given thickness of absorber will attenuate the photon beam by a definite fraction, and the energy in the beam will be absorbed according to a negative exponential law as shown in Figure 1.1. Also shown on this graph is the dose build-up that occurs for high energy photon beams. This effect is due to the predominant forward scattering of the electrons that come from photons interacting near the surface of the absorber. This 'skin-sparing' effect is one of the major reasons for using γ-rays and megavoltage x-rays for radiotherapy instead of lower energy x-rays. It should be pointed out that the curves in Figure 1.1 are plotted as a fraction of the maximum dose as a function of depth in the absorber. Because of the negative exponential absorption law, however, it is not possible to deliver more than about 20% of the energy in a photon beam to a deep-seated tumor located between 12 - 20 cm depth in soft tissue. The result is, of course, that more than 80% of the energy from x-rays and γ-rays either is absorbed by healthy tissue or escapes from the body.

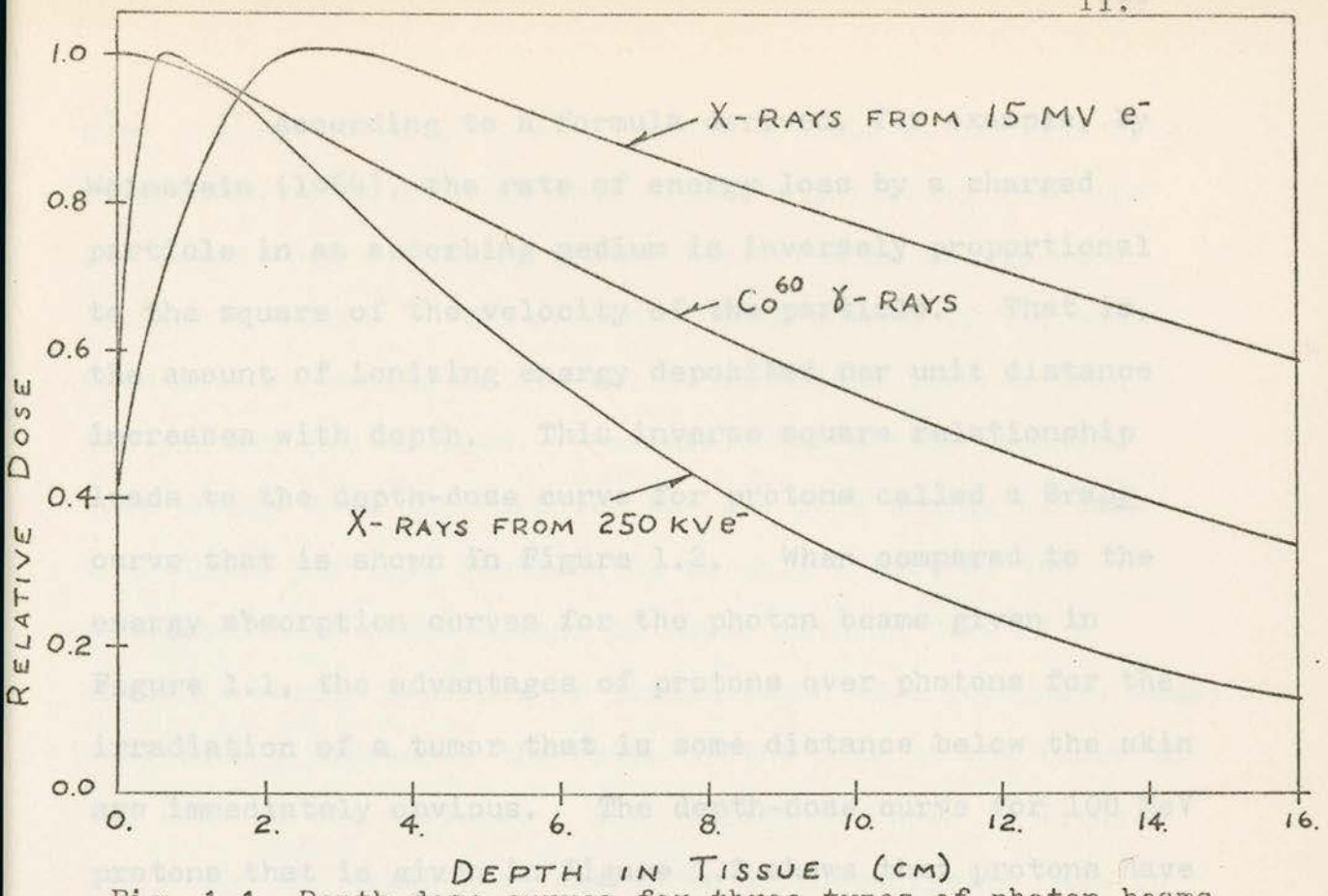

Fig. 1.1 Depth dose curves for three types of photon beams.

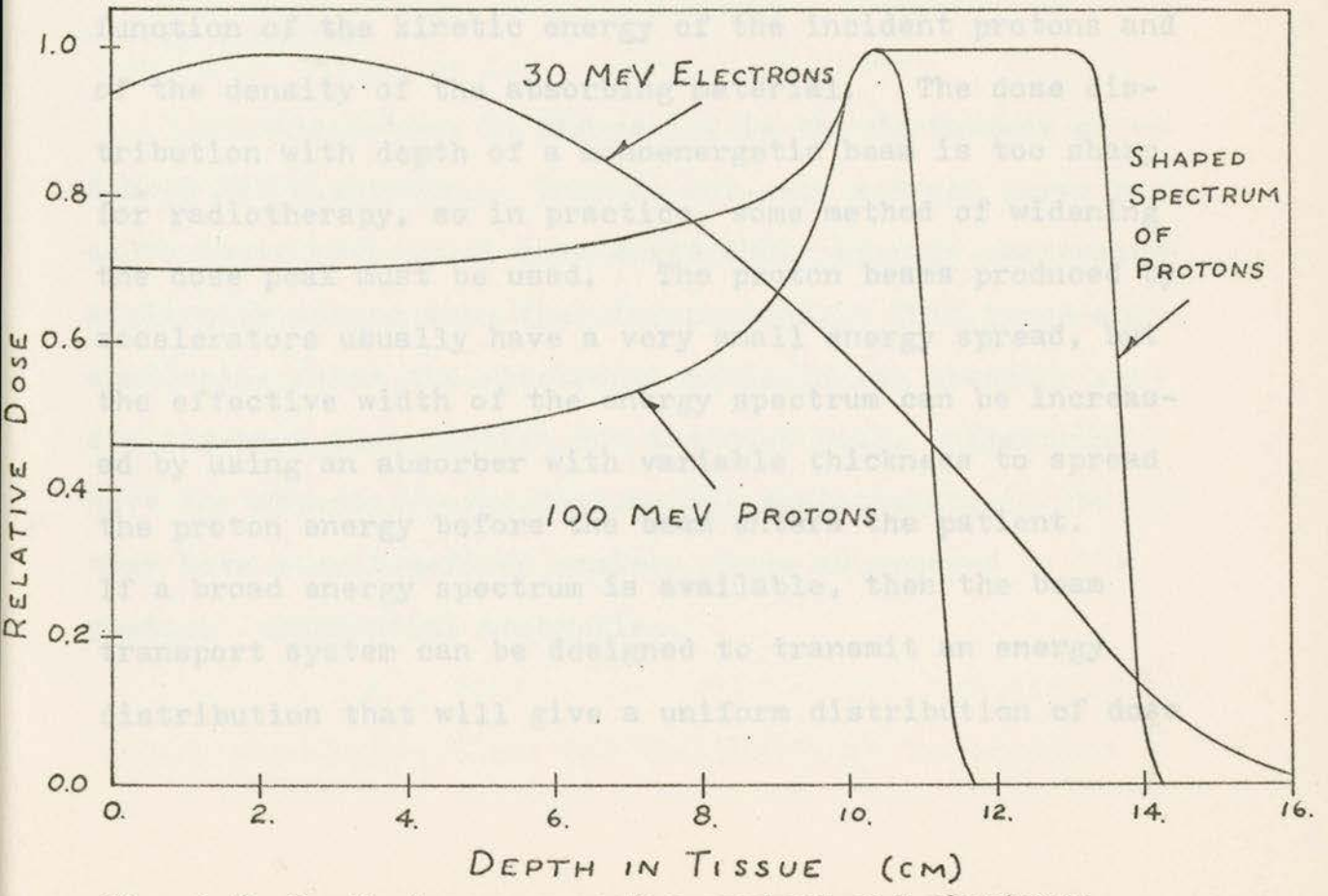

Fig. 1.2 Depth dose curves for protons and electrons.

According to a formula derived, for example, by Weinstein (1964), the rate of energy loss by a charged particle in an absorbing medium is inversely proportional to the square of the velocity of the particle. That is, the amount of ionizing energy deposited per unit distance increases with depth. This inverse square relationship leads to the depth-dose curve for protons called a Bragg curve that is shown in Figure 1.2. When compared to the energy absorption curves for the photon beams given in Figure 1.1, the advantages of protons over photons for the irradiation of a tumor that is some distance below the skin are immediately obvious. The depth-dose curve for 100 MeV protons that is given in Figure 1.2 shows that protons have a very well-defined range in an absorber. This range is a function of the kinetic energy of the incident protons and of the density of the absorbing material. The dose distribution with depth of a monoenergetic beam is too sharp for radiotherapy, so in practice, some method of widening the dose peak must be used. The proton beams produced by accelerators usually have a very small energy spread, but the effective width of the energy spectrum can be increased by using an absorber with variable thickness to spread the proton energy before the beam enters the patient. If a broad energy spectrum is available, then the beam transport system can be designed to transmit an energy distribution that will give a uniform distribution of dose

over a given range of depth. Such a broad energy spectrum of protons would be available from the particles that are scattered when a primary proton beam from an accelerator strikes a target. The secondary beam formed by the scattered protons would, of course, be much less intense than the primary proton beam. Because every proton deposits some energy near the surface, but the peak energy of each individual particle contributes to only a part of the broadened dose peak, either of these methods (use of a variable energy degrader or transmission of a secondary beam) unavoidably decreases the ratio of the dose at the tumor to the dose at the surface. This effect is shown in Figure 1.2 where the depth-dose curve for a monoenergetic beam is compared with that of a beam that has a specially shaped energy spectrum.

Also shown in Figure 1.2 is the depth-dose curve for 30 MeV electrons. They do not show a Bragg curve because their very small mass makes their average scattering angle much larger than that for protons. This large-angle scattering makes the electrons' paths in the absorber random zig-zags that flatten out the dose peak. Electrons have the advantage over photons for radiotherapy in that they have a well-defined maximum range as opposed to the photons' exponential absorption.

When pions are slowing down in an absorbing material, they exhibit the Bragg curve characteristic of heavier charged particles, but when negative pions come to rest they have the singular property of causing the fission of any nucleus they enter. A negatively charged pion can replace an electron in an atomic orbit, but since the pion is much more massive than an electron, the orbit is much closer to the nucleus. The pion quickly makes transitions to orbits even closer to the nucleus, emitting low energy x-rays as it does so. Eventually the pion enters the nucleus, which immediately breaks up into fragments and releases about 100 MeV of energy. Much of this energy is carried off by neutrons and γ-rays, but at least 30 MeV is carried by protons and light nuclear fragments that have a range in tissue of less than one centimeter. Guthrie et al. (1968) summarize results of measurements by Fowler and Mayes (1967) and Anderson (1964) to determine the energies of the products of pion stars, and discuss calculations of energy distributions using a nuclear model. The results quoted by Guthrie are given here as Table 1.1. When a pion stops in tissue, it will most likely be absorbed by C^{12}, or O^{16}, so the figures in this table are those of most concern in radiobiology.

In 1961, Fowler and Perkins (1961) realized that a beam of negative pions had the potential for giving a

	Particle type	Calculation		Experiment	
		Number per π^- capture	Energy per π^- capture (MeV)	Number per π^- capture	Energy per π^- capture (MeV)
^{16}O	Neutron	2.94	60.65	2.7	69
	Proton	1.25	20.03	0.95	15.2
	Deuteron	0.21	2.45		
	Triton	0.06	0.68		
	^3He	0.03	0.48		
	Alpha	1.08	10.62	0.99	7.8
	Other	0.63	2.42	0.78	4.4
^{12}C	Neutron	2.79	64.16	2.68	68
	Proton	1.03	20.14	1.00	17.5
	Deuteron	0.26	2.82		
	Triton	0.08	1.03		
	^3He	0.03	0.38		
	Alpha	1.10	16.84	0.92	7.0
	Other	0.33	1.52	0.60	4.0

Table 1.1 Multiplicities and energy partition from pion capture in ^{16}O and ^{12}C. (Guthrie et al. (1968))

radiotherapist precise control over the depth in the body at which a radiation dose is delivered. They estimated that 30 MeV of ionizing energy is released in a pion star and is absorbed within 0.5 cm of the pion stopping point. In addition, the range-energy curve for mesons (Appendix I) which shows that the range of a 15 MeV pion to be approximately 1 cm, so that a stopping pion deposits 15 MeV of energy in the last centimeter of travel. Therefore, nearly 45 MeV is deposited in the last centimeter, while less than 5 MeV per centimeter is deposited some distance before the pion comes to rest. The resulting depth-dose curve for a pure pion beam is shown in Figure 1.3.

A beam of negative pions should have other advantages as well over the more conventional photon beams. Photons are relatively sparsely ionizing radiation as measured by their Linear Energy Transfer (LET). The LET, which is only meaningful for charged particles, is defined as the amount of kinetic energy lost by the particle and absorbed locally in the medium per unit distance travelled. Since the LET depends on the composition of the absorbing medium, the values given here will be those for soft tissue. The electrons set in motion by Co^{60} γ-rays have an LET value of approximately 0.3 keV per micron, and this is the value assigned to the photon beam.

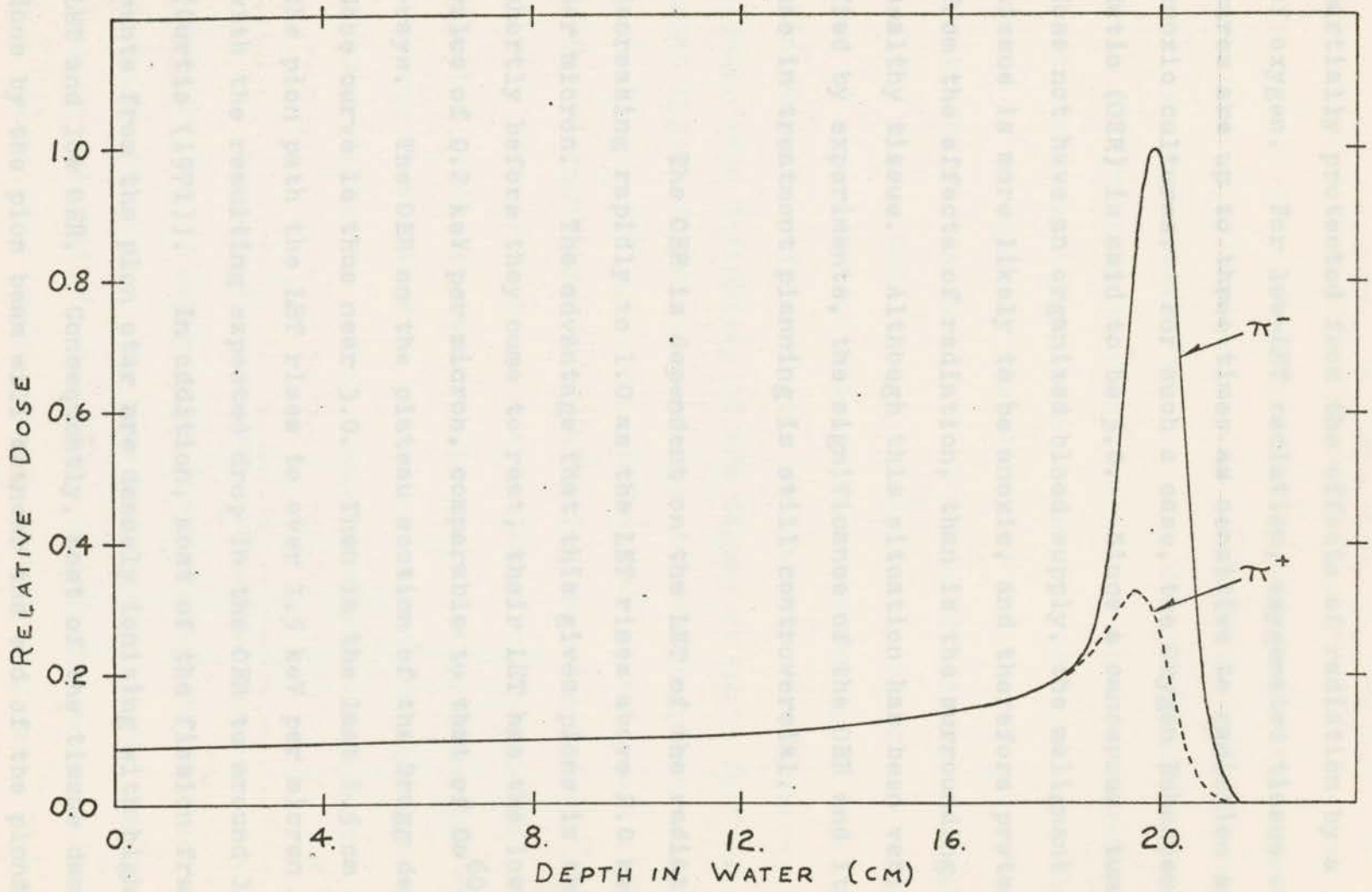

Fig. 1.3 Theoretical depth dose curves for uncontaminated pion beams.

In the lower region of LET values, cells may be partially protected from the effects of radiation by a lack of oxygen. For low-LET radiation, oxygenated tissue cultures are up to three times as sensitive to radiation as anoxic cultures. For such a case, the Oxygen Enhancement Ratio (OER) is said to be 3.0. Since a cancerous tumor does not have an organized blood supply, the malignant tissue is more likely to be anoxic, and therefore protected from the effects of radiation, than is the surrounding healthy tissue. Although this situation has been verified by experiments, the significance of the OER and its use in treatment planning is still controversial.

The OER is dependent on the LET of the radiation, decreasing rapidly to 1.0 as the LET rises above 2.0 keV per micron. The advantage that this gives pions is that, shortly before they come to rest, their LET has the low value of 0.2 keV per micron, comparable to that of Co^{60} γ-rays. The OER on the plateau section of the Bragg depth-dose curve is thus near 3.0. Then in the last 1.5 cm of the pion path the LET rises to over 1.5 keV per micron with the resulting expected drop in the OER to around 1.8 (Curtis (1971)). In addition, most of the fission fragments from the pion star are densely ionizing with high LET and low OER. Consequently, most of the tissue damage done by the pion beam will be near the end of the pions' range.

Table 1.2 summarizes these properties of pions and compares them with the properties of Co^{60} γ-rays. Figure 1.4, taken from Fowler (1965) compares the expected effectiveness of several types of radiation beam for treatment of a deep-seated tumor. The figures of merit for these different types of ionizing radiation are based on theoretical depth-dose curves and a treatment volume between 10 and 15 cm depth. Also included in the figures of merit are the values assumed for the OER of 3.0 for photon beams, 1.5 for pions, and 1.0 for heavy ions. Since the effectiveness of the radiation depends on the tumor type, depth and thickness, as well as on the sensitivity of the surrounding tissue, this definition of the figure of merit for the different types of radiation is open to some argument. In any case, Figure 1.4 gives some indication of the possibilities of the various beams for minimizing the side effects of radiation therapy that are due to damage to the normal tissue. Negative pions are shown to be ten times as effective as photons and three times as effective as protons when the ratios of tumor damage to normal tissue damage are compared.

Many people have done extensive surveys of the possibilities of using pions for radiological studies and radiation therapy. For more information on the use of pions in this field, the reader is referred to Rosen (1968), Raju and Richman (1969), Kaplan (1970), and Boone (1971).

	Co^{60} γ-rays	Fast pions	Stopping pions
Linear energy transfer (keV/μ)	0.3	0.2	1.5
Oxygen enhancement ratio	3.0	3.0	1.8
Relative biological effectiveness	1.0	1.0	2 to 5

Table 1.2 A comparison of the properties of γ-rays, fast pions, and stopping pions.

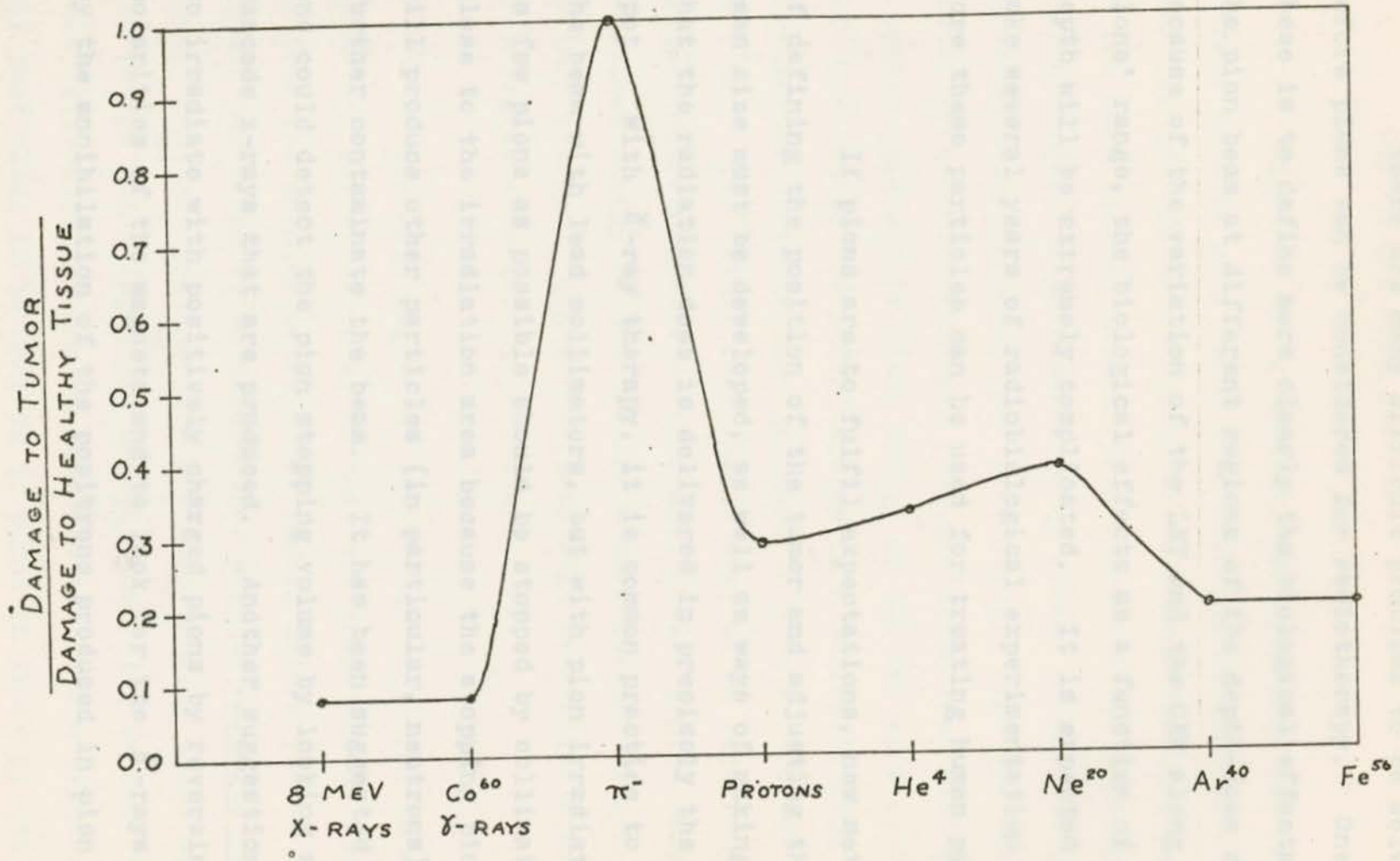

Fig. 1.4 A comparison of the effectiveness of several types of radiation beam for treatment of a tumor at a depth of 10 to 15 cm. (Fowler, 1965)

There are many difficult problems to be solved before pions can be considered for radiotherapy. One of these is to define more clearly the biological effects of the pion beam at different regions of the depth-dose curve. Because of the variation of the LET and the OER along the pions' range, the biological effects as a function of depth will be extremely complicated. It is expected to take several years of radiobiological experimentation before these particles can be used for treating human patients.

If pions are to fulfil expectations, new methods of defining the position of the tumor and adjusting the pion beam size must be developed, as well as ways of making certain that the radiation dose is delivered in precisely the right spot. With γ-ray therapy, it is common practice to define the beam with lead collimators, but with pion irradiation, as few pions as possible should be stopped by collimators close to the irradiation area because the stopping pions will produce other particles (in particular, neutrons) to further contaminate the beam. It has been suggested that one could detect the pion stopping volume by looking at the cascade x-rays that are produced. Another suggestion was to irradiate with positively charged pions by reversing the polarities of the magnets and to look for the γ-rays produced by the annihilation of the positrons produced in pion decay.

1.2 The TRIUMF Project

Negative pions have not yet been used for radiotherapy because pion beams from existing accelerators have been far too low in intensity to be useful for this purpose. In the near future, intense pion beams will be created for radiobiological experimentation by proton beams from the three accelerators mentioned previously. The SIN accelerator is a sector-focussed ring cyclotron that will produce a proton beam with a fixed energy of 590 MeV at a current of 100 μA, while the LAMPF machine is a half-mile long linear accelerator that has been designed to give an 800 MeV beam at 1 mA. The TRIUMF accelerator will be an isochronous sector-focussed cyclotron that will give a proton beam with a maximum energy of 500 MeV and a beam current of 100 μA at this energy. Higher currents will be available at lower energies from this accelerator.

The main magnet of the TRIUMF cyclotron is made up of six spiral sectors, so that six beams may be extracted from the machine between the magnet return yokes. The actual particles to be accelerated will be negative hydrogen ions; that is, protons each with two loosely bound electrsons. The reason for using these unusual particles is that this makes extraction of proton beams versatile and efficient. All that needs to be done is to place in front of the circulating beam a thin stripping foil that removes the two

electrons from each ion. Since the protons have the opposite charge to the H^- ions, and thus have the opposite direction of curvature in the magnetic field of the cyclotron, they curve out of the accelerator with essentially 100% extraction efficiency. By moving the stripping foil closer to the center of the machine, beams of lower energy may be extracted. This extraction system has been described by Vogt and Burgerjon (1966).

For the early stages of operation, only Beam Lines I and IV will be used as shown in Figure 1.5. Beam Line IV will be used for nuclear experimentation with the proton beam, while the proton beam in Beam Line I will be passed through two targets for the production of secondary beams of mesons. The first target will be quite thin, probably 4 gm/cm^2, and the second will be thick, equivalent to 20 gm/cm^2 of carbon.

Low energy pions will be accepted off the second target for the muon experimental area, the low energy pion area, and the medical facility. It is proposed that the medical channel take the pions from this target at an angle of 30^o above the forward direction of the proton beam, bend the pion beam through two 45^o bends, and deliver a horizontal beam into the irradiation cave of the medical facility through seven feet of dense shielding. The proposed medical laboratory for the TRIUMF Project is described

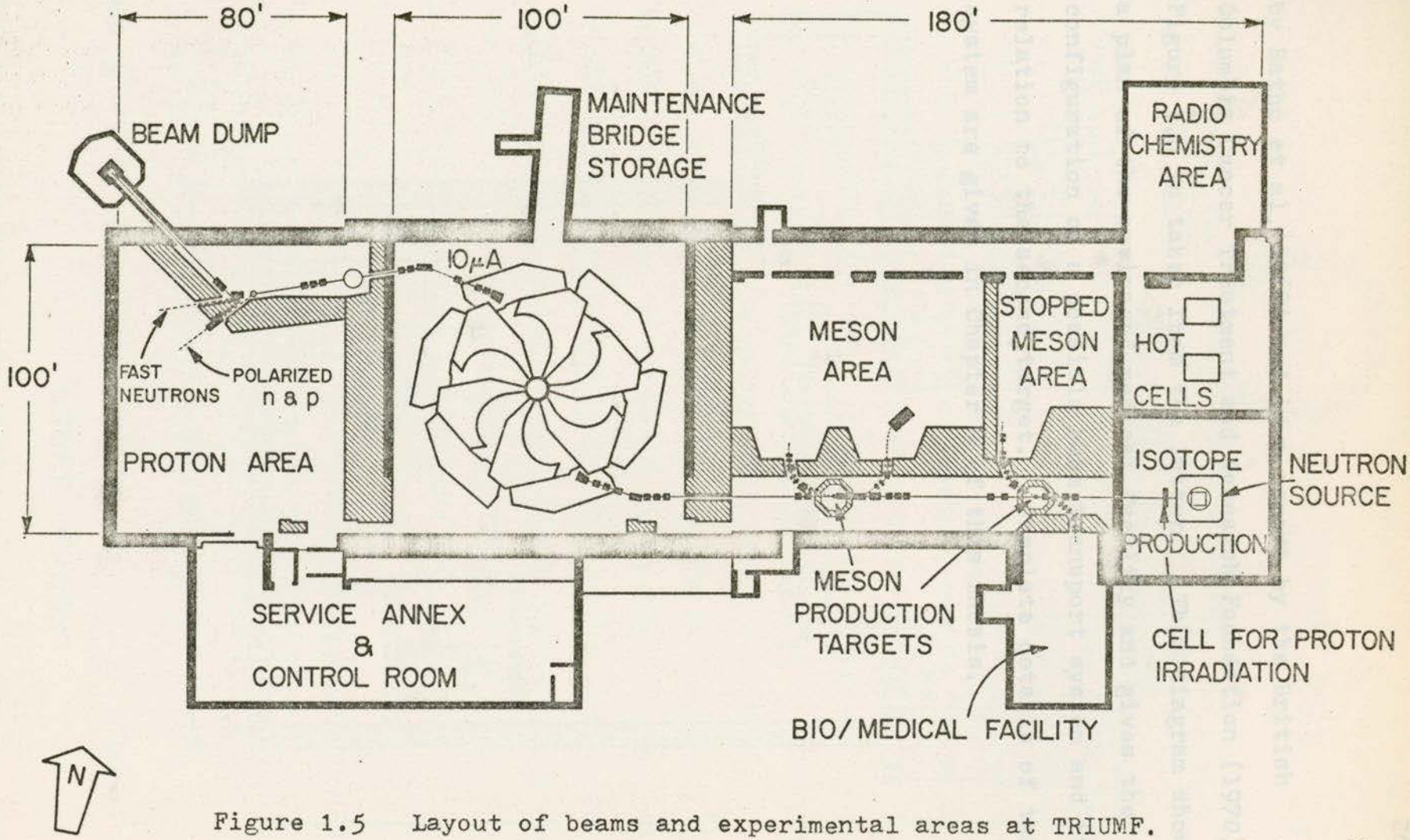

Figure 1.5 Layout of beams and experimental areas at TRIUMF.

(April, 1971)

by Batho et al.(1968) and in a report by the British Columbia Cancer Treatment and Research Foundation (1970). Figure 1.6 is taken from the latter. This diagram shows a plan of the envisaged medical facility and gives the configuration of a possible beam transport system and its relation to the second target. Complete details of this system are given in Chapter 4 of this thesis.

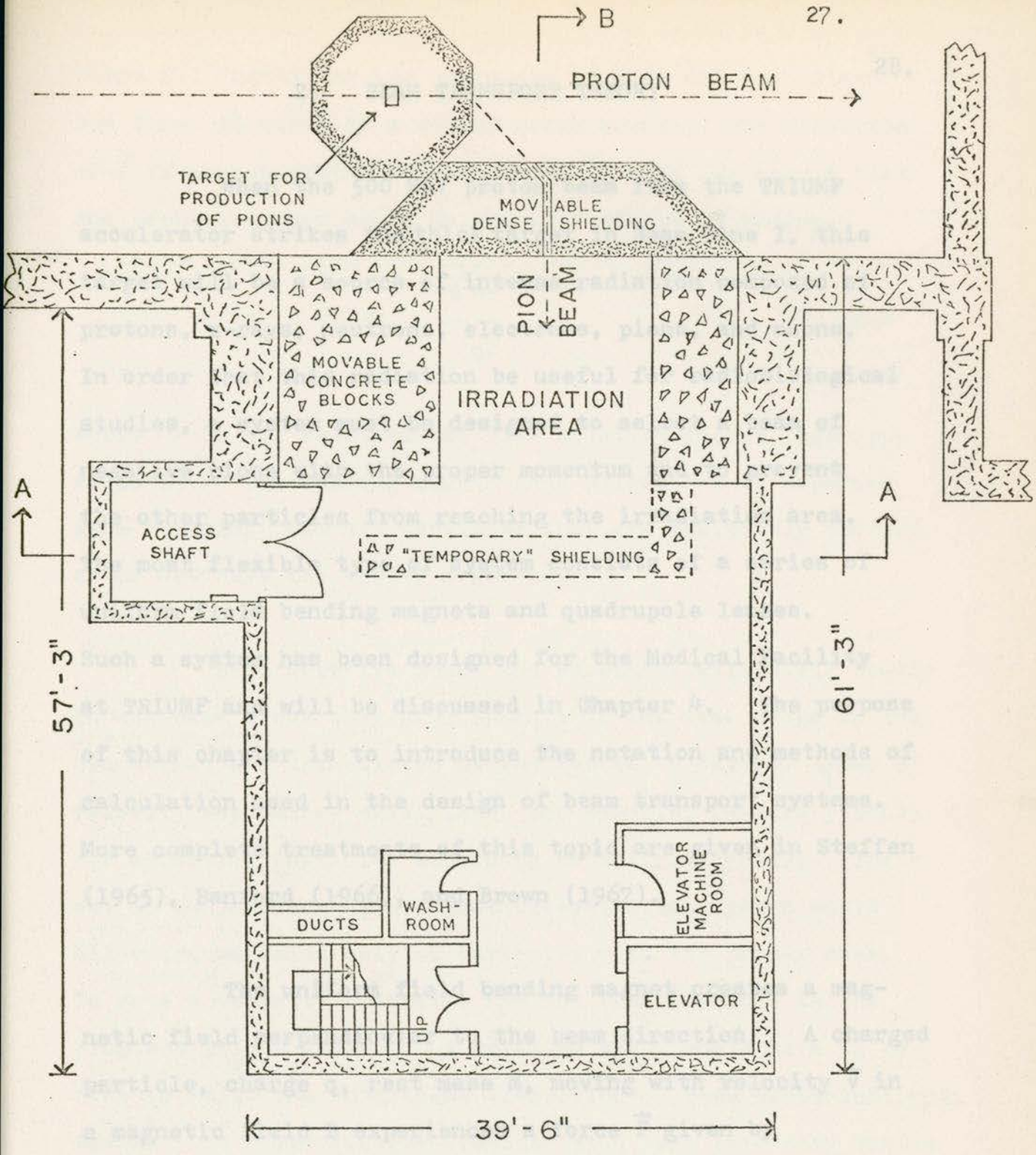

SCALE: $\frac{3}{32}$" = 1'-0"

ELEV. = 270'-6"

LOWER FLOOR

Fig. 1.6 Plan view of the Radiobiology-Radiotherapy Laboratory.

2. BEAM TRANSPORT THEORY

When the 500 MeV proton beam from the TRIUMF accelerator strikes the thick target in Beam Line I, this target will be a source of intense radiation composed of protons, x-rays, neutrons, electrons, pions, and muons. In order that this radiation be useful for radiobiological studies, a system must be designed to select a beam of negative pions with the proper momentum and to prevent the other particles from reaching the irradiation area. The most flexible type of system consists of a series of uniform field bending magnets and quadrupole lenses. Such a system has been designed for the Medical Facility at TRIUMF and will be discussed in Chapter 4. The purpose of this chapter is to introduce the notation and methods of calculation used in the design of beam transport systems. More complete treatments of this topic are given in Steffen (1965), Banford (1966), and Brown (1967).

The uniform field bending magnet creates a magnetic field perpendicular to the beam direction. A charged particle, charge q, rest mass m, moving with velocity $\vec{v}$ in a magnetic field B experiences a force $\vec{F}$ given by

$$\vec{F} = q \vec{v} \times \vec{B} \qquad 2.1$$

where all quantities are expressed in MKSA units. Since the force is given as a vector cross product, the direction of $\vec{F}$ is perpendicular to both $\vec{v}$ and $\vec{B}$, with the result that the particle moves along an arc of a circle of radius

$$r = \frac{\gamma mv}{qB} \qquad 2.2$$

where γ is the relativistic time dilation factor (see Appendix I). The bending magnet thus allows one to separate from the pion beam all particles that are positively charged or do not have the proper momentum.

Some negative muons and electrons will still remain in the beam since they have momenta in the same range as the pions that are transmitted by the system. Several types of velocity separators exist (see, for example, Banford (1966)) for selecting particles according to their velocity. Their use in conjunction with a momentum-selection system would allow transmission only of particles with the proper mass. To date a velocity separator has not been included in the proposed TRIUMF design. A detailed study would have to be done to weigh the advantages (reduction of beam contamination) against the disadvantages (reduced pion beam intensity due to probable beam quality deterioration). In particular, the raw beam contamination and the biologically tolerable contamination would have to be known; such data are best obtained in the initial phase of an operating facility.

In order to design a beam transport system, there must be a mathematical description of the beam and of the effects of the different types of magnetic field. The basic mathematical methods for describing the action of a beam transport system were developed by Penner (1961) who introduced the matrix notation for charged particle optics, and by Brown (1967) who developed the 6 x 6 formalism and incorporated second order effects into the matrix formalism.

A moving particle in free space has six degrees of freedom - - three co-ordinates to specify the position and three to give the direction of motion. The notation that will be used here is as follows: the horizontal displacement from the optic axis for the system will be denoted by x, the horizontal component of the slope by x', the vertical displacement by y, the vertical component of the slope by y', the longitudinal displacement from the center of the beam pulse by L, and the fractional deviation of momentum from the design momentum of the system by δ. The units that will be used throughout this work are centimeters for x and y, milliradians for x' and y', and percent for δ. The L co-ordinate is superfluous for this work but will be retained for consistency of notation with other authors.

If a particle with initial displacement and slope x_o and x'_o travels a distance d (in meters) in field-free

space, the equations of motion are

$$x = x_o + \frac{d}{10} x'_o \qquad 2.3$$

and $$x' = x'_o \qquad 2.4$$

(x is in cm, x' is in mrad, and d is in meters)

It may be seen that these equations correspond to the multiplication of a vector by a matrix as follows:

$$\begin{pmatrix} x \\ x' \end{pmatrix} = \begin{pmatrix} 1 & \frac{d}{10} \\ 0 & 1 \end{pmatrix} \times \begin{pmatrix} x_o \\ x'_o \end{pmatrix} \qquad 2.5$$

Analogous equations will apply for the vertical components of the charged particle's trajectory. The action of a bending magnet or a quadrupole lens on a beam may also be expressed in the form of equation 2.5. For a development of the exact form of the transformation matrices for these magnets, see, for example, Penner (1961).

This 2 x 2 matrix formalism is limited in use to monoenergetic beams and to transport systems that have no coupling terms between the horizontal and vertical planes. The first generalization to a formalism capable of describing beams that contain a range of momenta requires the increase of the dimension of the transfer matrix to 3 x 3. The

third component of the vector representing the co-ordinates of a particle will be the fractional change in momentum from the design momentum of the system, δ . The 3 x 3 formalism is thus able to describe the dispersion of the beam that occurs in a bending magnet.

The most general description of the action of a beam transport system is given by a full 6 x 6 matrix notation. The transfer matrices operate on vectors whose components are the six components required to specify any trajectory that were defined previously. For example, the transformation of a trajectory by a drift length is given by

$$\begin{pmatrix} x \\ x' \\ y \\ y' \\ L \\ \delta \end{pmatrix} = \begin{pmatrix} 1 & \frac{d}{10} & 0 & 0 & 0 & 0 \\ 0 & 1 & 0 & 0 & 0 & 0 \\ 0 & 0 & 1 & \frac{d}{10} & 0 & 0 \\ 0 & 0 & 0 & 1 & 0 & 0 \\ 0 & 0 & 0 & 0 & 1 & 0 \\ 0 & 0 & 0 & 0 & 0 & 1 \end{pmatrix} \times \begin{pmatrix} x_o \\ x_o' \\ y_o \\ y_o' \\ L_o \\ \delta_o \end{pmatrix} \qquad 2.6$$

in the 6 x 6 formalism.

In general, the equation of motion of a charged particle travelling in a static magnetic field may be given in the form of a Taylor series such as equation 2.7.

$$x_i = \sum_{j=1}^{6} R_{ij}(x_j)_o + \sum_{j=1}^{6}\sum_{k=j}^{6} T_{ijk}(x_j)_o(x_k)_o + \ldots \qquad 2.7$$

The first order approximation that is often used in the study of beam optics involves using only the first term of the series given above. If the power series coefficients R_{ij} are considered as the components of a 6 x 6 matrix, the first order approximation can be seen to be identical with equation 2.6. This approximation greatly simplifies the calculations and is often sufficiently accurate that no higher terms need to be considered. For a tabulation of the first and second order matrix coefficients, see Brown (1967). Brown also shows that, for static magnetic fields with mid-plane symmetry, the transformation matrices take the form

$$\underset{\sim}{R} = \begin{pmatrix} R_{11} & R_{12} & 0 & 0 & 0 & R_{16} \\ R_{21} & R_{22} & 0 & 0 & 0 & R_{26} \\ 0 & 0 & R_{33} & R_{34} & 0 & R_{36} \\ 0 & 0 & R_{43} & R_{44} & 0 & R_{46} \\ R_{51} & R_{52} & 0 & 0 & 1 & R_{56} \\ 0 & 0 & 0 & 0 & 0 & 1 \end{pmatrix} \qquad 2.8$$

The common elements of a beam transport system create magnetic fields symmetric about the mid-plane of the magnet, so this reduction of the number of matrix components can often be used. Usually, there is only a single dispersion plane,

by convention defined to be the x plane. In this case, $R_{36} = R_{46} = 0$ as well.

Each of these components has a special meaning. If the term R_{11} (or R_{33}) is equal to zero, then the beam transport system will take a ray that is initially parallel to the optic axis in the x (or y) plane and bring it to a focus on the optic axis at the end of the system. This is called, for obvious reasons, a parallel-to-focus system. If the coefficient R_{12} (or R_{34}) is zero, the system is focus-to-focus in the x plane (or y plane). If R_{21} (R_{43}) is zero, the system is parallel-to-parallel in the x plane (y plane) and if the coefficient R_{22} (R_{44}) is zero, the system is focus-to-parallel in the x plane (y plane). If the beam is not monoenergetic, then the terms R_{16} and R_{26} must be included in the calculations. If R_{16} is zero, then the displacement of a particle is independent of its momentum, and if R_{26} is equal to zero, the divergence is independent of momentum. If both of these terms are zero, the system is said to be doubly achromatic in the x-plane and the beam behaves as if it were achromatic in the first order approximation.

With this matrix formalism, one may trace any particle through a beam transport system if the initial coordinates are known. However, it would be very tedious to trace enough rays through the system to be able to examine the beam characteristics in all parts of the system. In

some cases, characteristic rays may be traced that will give certain desired properties; e.g. the outline, or envelope of the beam (Lobb (1970), Larson (1971)). Usually, due to the mid-plane symmetry of the magnetic fields, there is no first-order coupling between the horizontal and vertical planes. That is, if the transformation matrix has the form of Eq. 2.8, the horizontal displacement and divergence are completely independent of the vertical displacement and divergence. Consequently, if the beam is monoenergetic or if the system is achromatic, the beam may be described by an area in each of two orthogonal two-dimensional planes called phase spaces. For example, a point in the horizontal phase space gives the horizontal components x and x' of a trajectory; the set of all points in phase space corresponding to trajectories of particles in the ion beam forms a connected set whose area is called the phase space area, or emittance of the beam.

Banford (1966) shows that in some cases, the representation of a charged particle beam in phase space may be approximated by an ellipse. An example of such a beam is a primary beam from an accelerator. An ellipse requires only three parameters to be completely specified. In the notation of Steffen (1965), the equation of an ellipse is

$$\gamma x^2 + 2\alpha x x' + \beta (x')^2 = \epsilon \qquad 2.9$$

and the parameters are related by

$$\gamma\beta - \alpha^2 = 1 \qquad 2.10$$

The ellipse described by this equation is shown in Figure 2.1. If the ellipse parameters are put into the form of a matrix as

$$\underset{\sim}{E} = \begin{pmatrix} \gamma & \alpha \\ \alpha & \beta \end{pmatrix} \qquad 2.11$$

the ellipse may be shown to undergo the transformation

$$\underset{\sim}{E} = (\underset{\sim}{R}^{-1})^T \underset{\sim}{E}_0 \underset{\sim}{R}^{-1} \qquad 2.12$$

as the beam travels down the transport system. In equation 2.12, $\underset{\sim}{R}$ denotes the 2 x 2 submatrix composed of the horizontal (or vertical) components of the 6 x 6 transfer matrix, and $\underset{\sim}{R}^{-1}$ is the inverse and $(\underset{\sim}{R}^{-1})^T$ is the transpose of the inverse of $\underset{\sim}{R}$. These equations are discussed in more detail by Steffen (1965) and by Tautz (1968).

Liouville's theorem of statistical mechanics (see, for example, Goldstein (1950)) states that, under certain conditions, the volume of phase space occupied by the points representative of a system of particles remains a constant. Assuming that the number of particles is also a constant, then

the density of the points in phase space is also a constant. One consequence of this theorem is that the determinant of a first order transfer matrix must have the value 1.0. A more direct consequence of Liouville's theorem is that, since the transformation of an ion beam by static magnetic fields satisfies the conditions under which the theorem holds, the phase space area occupied by a charged particle beam is a constant, called the beam emittance. The area of the ellipse shown in Figure 2.1 is given by the coefficient ϵ, the emittance of the beam that the ellipse represents.

Since the general equation for a trajectory in field-free space is given by equation 2.3 and 2.4 the transformation of the beam by a drift length corresponds to a skewing of the phase space ellipse. The fact that x' is a constant for each trajectory implies that all points within the ellipse travel parallel to the displacement axis. Those points corresponding to a positive slope travel to the right and those for a negative slope to the left. Thus the ellipse in Figure 2.1 describes a beam that is increasing in size, or defocussing as it travels along the drift distance. An ellipse that represents a focussing beam would be tilted the opposite way in phase space. If the ellipse is upright, the ellipse coefficient α is equal to zero and the beam size is at a minimum for its travel in the drift space. Where the phase space ellipse is upright, the beam is said to be at a waist. Steffen

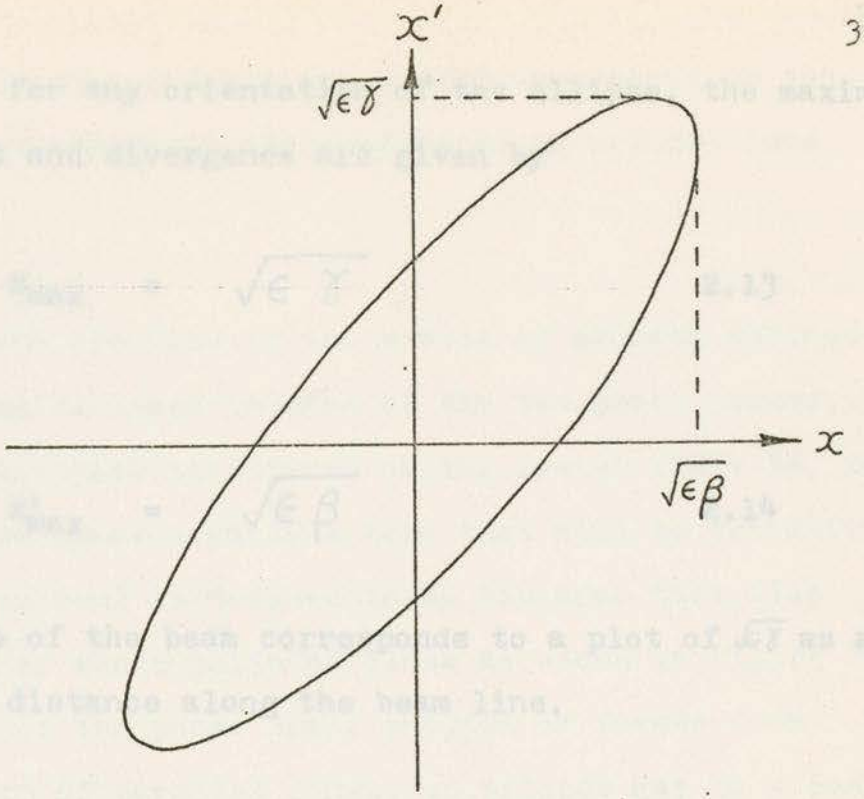

Fig. 2.1 An ellipse in x-x' phase space ($\alpha < 0$ as shown).

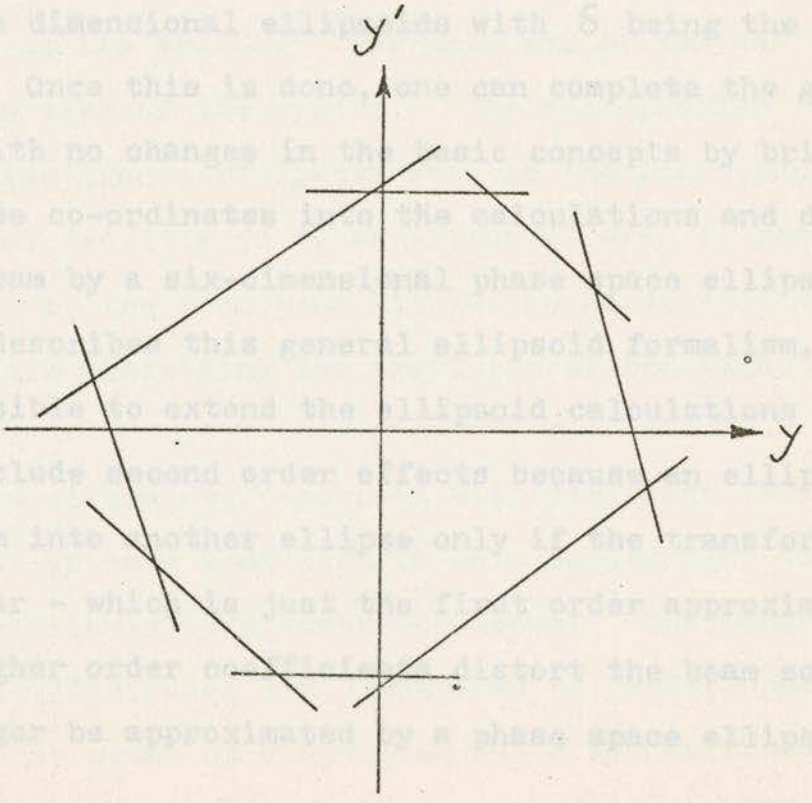

Fig. 2.2 A phase space polygon in the y-y' phase space.

shows that, for any orientation of the ellipse, the maximum displacement and divergence are given by

$$x_{max} = \sqrt{\epsilon \gamma} \qquad 2.13$$

and

$$x'_{max} = \sqrt{\epsilon \beta} \qquad 2.14$$

The envelope of the beam corresponds to a plot of $\sqrt{\epsilon\gamma}$ as a function of distance along the beam line.

These simple ellipse calculations that use the 2 x 2 transfer matrices cannot be used for a dispersed beam. To perform such calculations, one must generalize the formalism to treat three dimensional ellipsoids with δ being the third co-ordinate. Once this is done, one can complete the generalization with no changes in the basic concepts by bringing the other three co-ordinates into the calculations and describing the beam by a six-dimensional phase space ellipsoid. Brown (1967) describes this general ellipsoid formalism. It is not possible to extend the ellipsoid calculations any further to include second order effects because an ellipse will transform into another ellipse only if the transformation is linear - which is just the first order approximation. Second and higher order coefficients distort the beam so that it can no longer be approximated by a phase space ellipsoid.

These second-order effects are roughly analogous to the spherical and chromatic aberrations of an optical lens system.

Each aperture in the system of magnets defines a pair of parallel lines in each of the two phase planes, and the phase space acceptance of the system (that is, the maximum phase space area of a beam that will be transmitted by the system) is defined to be the area that lies between all of these pairs of lines as shown in Figure 2.2. Notice that if the phase space polygon is formed from several pairs of parallel lines, an ellipse may be a reasonable approximation to the polygon. It is usual to give the phase space acceptance polygon at the beginning of the system for easy comparison with the configuration of the particle beam at its origin. The beam may or may not fill the acceptance area of the system. The main problem in designing a beam transport system such as the pion channel for the medical facility is to maximize the area in phase space occupied by the pion beam within the acceptance of the system while minimizing the apertures of the magnets.

Several computer programs with different levels of sophistication have been used in this design work to carry out the calculations described above. The program TRIUMF (Tautz (1968)) uses 3 x 3 matrices to perform calculations in the plane of dispersion and 2 x 2 matrices

for the calculations in the orthogonal plane. The program TRANSPORT (Brown and Howry (1970)) is a more powerful program that uses the 6 x 6 formalism and can calculate the second order coefficients. Other programs that were used are ACCEPTANCE (Harrison and Lobb (1968)) for calculating the maxumum phase space polygons that will pass through a beam transport system, TRANS (Chan and Lobb (1970)), a first order version of TRANSPORT, and NPFLUX (Hutson (1970)), written to calculate the actual distribution of particles at any point in a system. These computer programs are described in more detail in Appendix II.

3. CRITERIA AND PHILOSOPHY OF BEAM TRANSPORT SYSTEM DESIGN

The beam transport system for the Medical Facility at TRIUMF must satisfy many specifications on pion beam intensity, magnet sizes, momentum resolution, achromaticity, and so on. One of the most important requirements is that of beam intensity. The pion intensity at the irradiation location is set by the factors of proton beam intensity and energy, the thickness and composition of the pion production target, the length of the beam transport system, and the acceptance of the system. For this work, the proton beam will be considered to be 100 μA at 500 MeV, and the pion production target is assumed to be 10 cm of carbon.

The take-off angle for the beam transport system was chosen to be 30 degrees above the forward direction. The forward direction was chosen for the higher energy (pion kinetic energies up to 110 MeV are required) and greater intensity of the pion beam. There is also higher beam contamination with electrons and neutrons in the forward direction, but the sacrifice of beam purity for intensity must be made in order to achieve an adequate dose rate. The angle of 30 degrees was chosen because this is the smallest angle that will allow the first magnet of the pion beam transport system to clear one of the magnets belonging to the proton beam transport system downstream of the target.

It is desired to irradiate tumor volumes of up to 800 cc (10 x 10 cm, thickness 8 cm) with a radiation dose of 100 rads, A rad requires the deposition of 100 ergs per gram of tissue, so that if body tissue is assumed to have the density of water, then a total of 8×10^6 ergs is the required energy dose. If the conservative estimate of the energy dose of 40 MeV per stopping pion is used, the number of pions stopping in the tumor volume is 1.25×10^{11} for a 100 rad dose. To irradiate a depth of 20 cm requires a pion energy of 80 MeV, and at this energy, 52% of the pions will decay before they reach the end of a seven meter beam transport system. Because of this decay, at least 2.5×10^{11} pions of the appropriate energy must be created at the target during the irradiation period.

The pion production cross section has not been measured very accurately at 500 MeV, but the best figures available for a proton energy near that of TRIUMF (Hirt et al. (1969)) give the cross section for production of 100 MeV pions by 600 MeV protons incident on a carbon target to be approximately 5.0 microbarns per MeV-steradian at 21.5 degrees from the forward direction of the proton beam. The proton beam from TRIUMF is expected to have an intensity of 6.3×10^{14} protons per second, so that the production of negative pions from a 10 cm carbon target in Beam Line I should be approximately 3.0×10^9 particles per MeV-steradian per second. If the maximum irradiation time is specified as 500 seconds, then the required acceptance of the beam transport system

is 0.17 MeV-steradians. To irradiate a range in tissue between 10 and 18 cm requires pions in the energy range of 50 to 70 MeV. This depth requirement implies that the transport system must be able to transmit a solid angle of 10 millisteradians at the pion production target and a beam momentum band of ±10% of the design momentum. This solid angle and momentum width are within the capabilities of a bending magnet-quadrupole lens system. In order that the pion beam have sufficient penetration for deep-therapy applications, the system should be capable of transmitting pions with energies up to 110 MeV (30 cm range in water).

Another requirement is that the pion beam be achromatic in the irradiation area. If there is dispersion of the beam (that is, if the matrix element R_{16} is not equal to zero), the pion energy and therefore the depth of penetration will depend on position in the radiation field. To construct a beam transport system that is doubly achromatic ($R_{16} = R_{26} = 0.$) requires at least two bending magnets and one quadrupole lens between the bending magnets. The first bend will disperse the pion beam just as a prism disperses white light. The quadrupole focussing lens is necessary to direct the diverging trajectories into the aperture of the second bending magnet where they are recombined into an achromatic beam. A slit may be placed in the beam where it is dispersed to define the energy range of the pions that reach the irradiation area. The momentum resolution that is provided by the slit depends on the size of the beam

at that point and on the magnitude of the dispersion. If the beam is large, and the dispersion is small, then a wide range of momenta will overlap and the resolution will be poor. However, if the beam size is very small for pions with a single energy and the dispersion is large, then the different momenta will be well separated in space and the momentum-defining aperture will give very good resolution.

Because of the statistical nature of the pion's interactions as it slows down, there is an uncertainty in the range of a pion in an absorber even if its momentum is known exactly (range straggling; see, for example, Evans (1955)). In fact, the range straggling for a 75 MeV pion is equivalent to a 1% spread in the momentum of the incident particles. Thus, the momentum resolution required by a radiobiology experiment is not stringent - - only about 1%.

The effective source of the pions is a cylinder 10 cm long with a diameter the same as that of the proton beam - - approximately 0.4 cm. Therefore, since the transport system views this cylinder at a 30° angle, the pion beam has an initial x size of 0.4 cm and an initial y size of 5.0 cm. With this pion source configuration and assum-

ing an angular acceptance of ± 50 mrad in both planes, the vertical emittance is 500 cm-mrad and the horizontal emittance is only 40 cm-mrad. The initial phase space polygons for this beam are shown in Figures 3.1 and 3.2. The smaller emittance in the horizontal planemeans that the pion beam can be made very small in the plane of the dispersion. Consequently, the resolution can be made as small as 0.2% if this take-off angle is used while even 1% momentum resolution would be difficult to achieve with a horizontal take-off.

It was mentioned that a uniform distribution of radiation dose over a range of depth requires a special distribution of the momenta of the particles in the beam. The reason for this is the fact that a uniform momentum distribution will give a non-uniform depth-dose distribution. The uniform momentum distribution of Figure 3.3 gives a much higher dose to the shallow portion of the tumor than it does to the deeper areas because every particle contributes some energy to the dose at the shallow end, but the pions that stop before the end of the treatment volume do not contribute to the dose at the end of the range. The resulting depth-dose distribution is shown in Figure 3.4, which was taken from Rosen (1968). In order to correct this situation, many more of the high energy pions must be transmitted than low energy ones as shown by Figure 3.5.

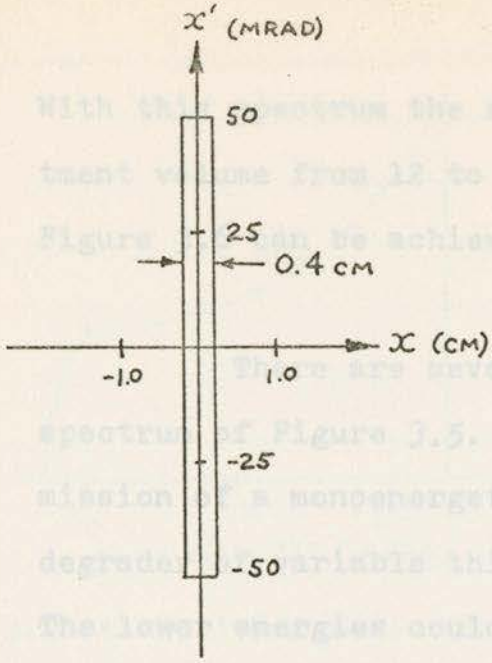

Fig. 3.1 The initial polygon of the pion beam in x-x' phase space.

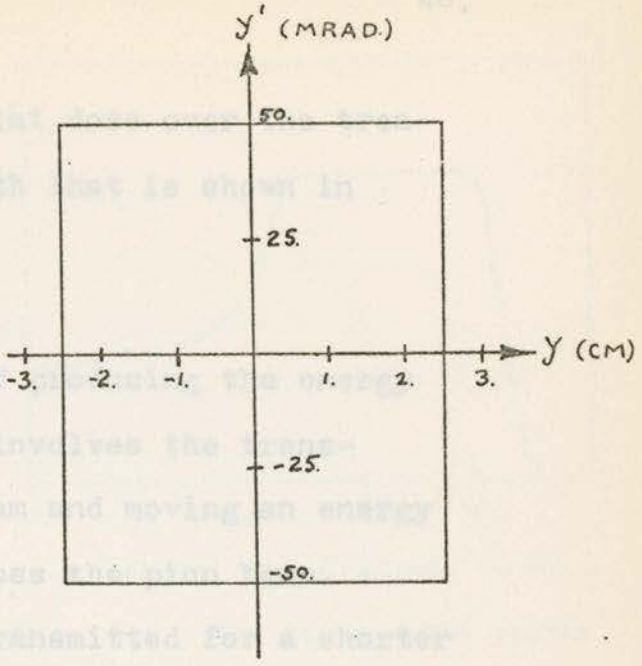

Fig. 3.2 The initial polygon of the pion beam in y-y' phase space.

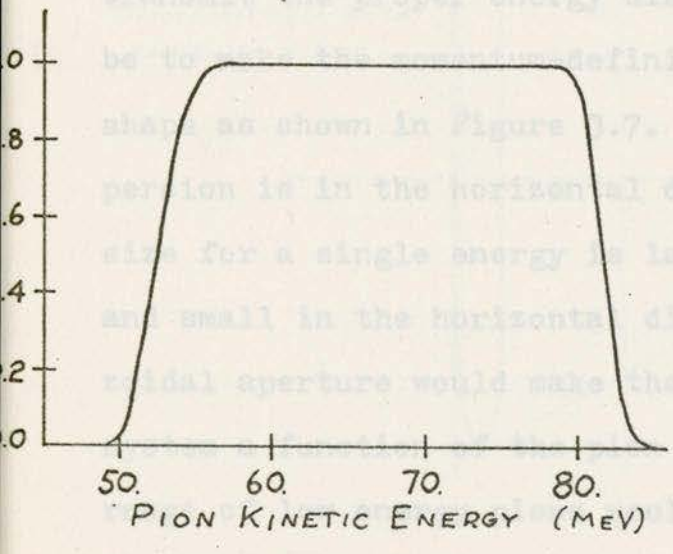

Fig. 3.3 A uniform momentum distribution.

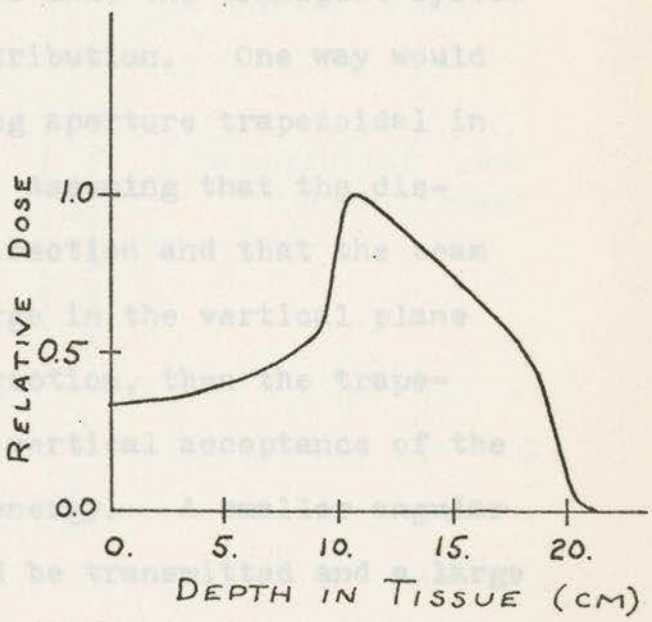

Fig. 3.4 The depth dose curve due to the momentum distribution of Figure 3.3.

With this spectrum the resulting flat dose over the treatment volume from 12 to 20 cm. depth that is shown in Figure 3.6 can be achieved.

There are several ways of producing the energy spectrum of Figure 3.5. One way involves the transmission of a monoenergetic pion beam and moving an energy degrader of variable thickness across the pion beam. The lower energies could thus be transmitted for a shorter length of time than the higher energies. This method would make treatment times much longer because to make the beam monoenergetic many of the pions would be stopped at a momentum-defining aperture.

It is also possible to make the transport system transmit the proper energy distribution. One way would be to make the momentum-defining aperture trapezoidal in shape as shown in Figure 3.7. Assuming that the dispersion is in the horizontal direction and that the beam size for a single energy is large in the vertical plane and small in the horizontal direction, then the trapezoidal aperture would make the vertical acceptance of the system a function of the pion energy. A smaller angular range of low energy pions would be transmitted and a large angular range of high energy particles would pass through the aperture. It should be possible to adjust the edges of the trapezoid so that a distribution such as that of

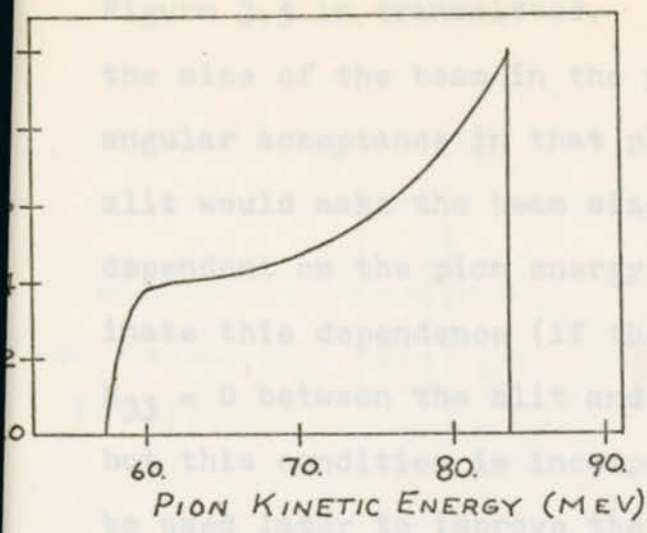

g. 3.5 A specially shaped momentum stribution.

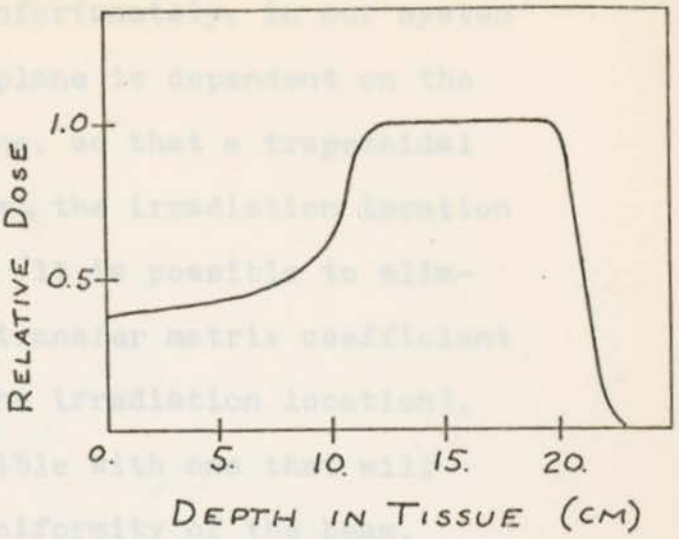

Fig. 3.6 The depth dose curve due to the distribution shown in Figure 3.5.

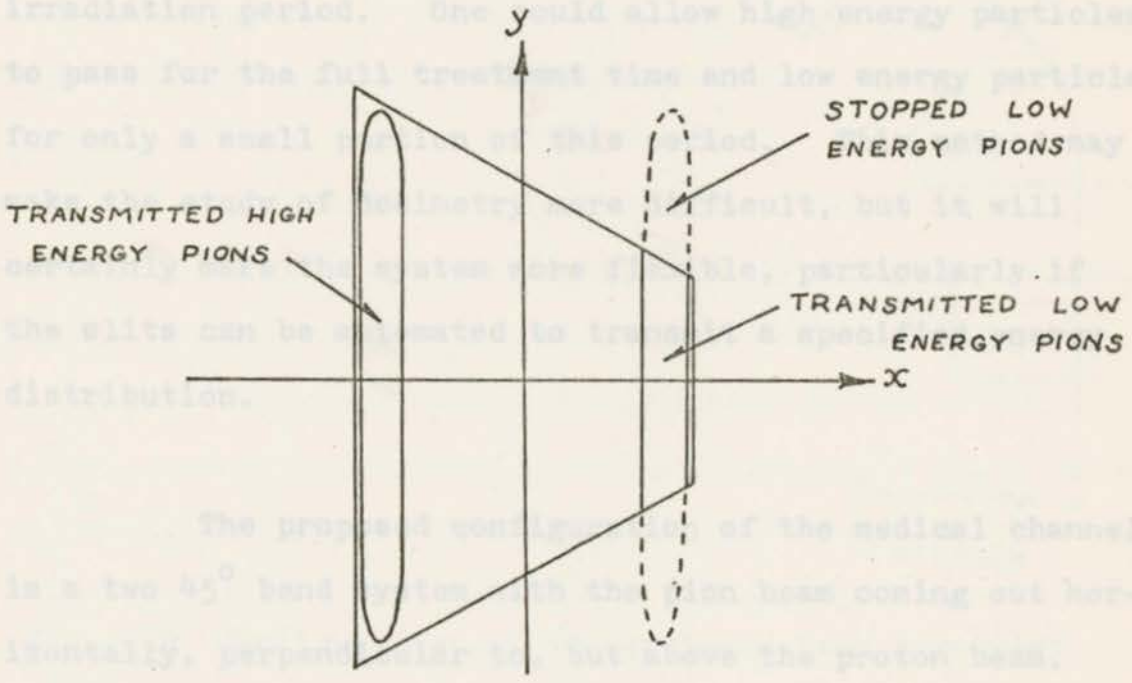

Fig. 3.7 A trapezoidal momentum-defining aperture.

Figure 3.5 is transmitted. Unfortunately, in our system the size of the beam in the y plane is dependent on the angular acceptance in that plane, so that a trapezoidal slit would make the beam size at the irradiation location dependent on the pion energy. It is possible to eliminate this dependence (if the transfer matrix coefficient $R_{33} = 0$ between the slit and the irradiation location), but this condition is incompatible with one that will be used later to improve the uniformity of the beam.

Another way to tailor the energy spectrum, and the way that we propose be used for the medical channel at TRIUMF, is to have the momentum slit move during the irradiation period. One could allow high energy particles to pass for the full treatment time and low energy particles for only a small portion of this period. This method may make the study of dosimetry more difficult, but it will certainly make the system more flexible, particularly if the slits can be automated to transmit a specified energy distribution.

The proposed configuration of the medical channel is a two 45° bend system with the pion beam coming out horizontally, perpendicular to, but above the proton beam. The design requires the use of five quadrupole focussing magnets in the arrangement given in Figure 3.8. The bending magnets serve the purpose of permitting the passage only

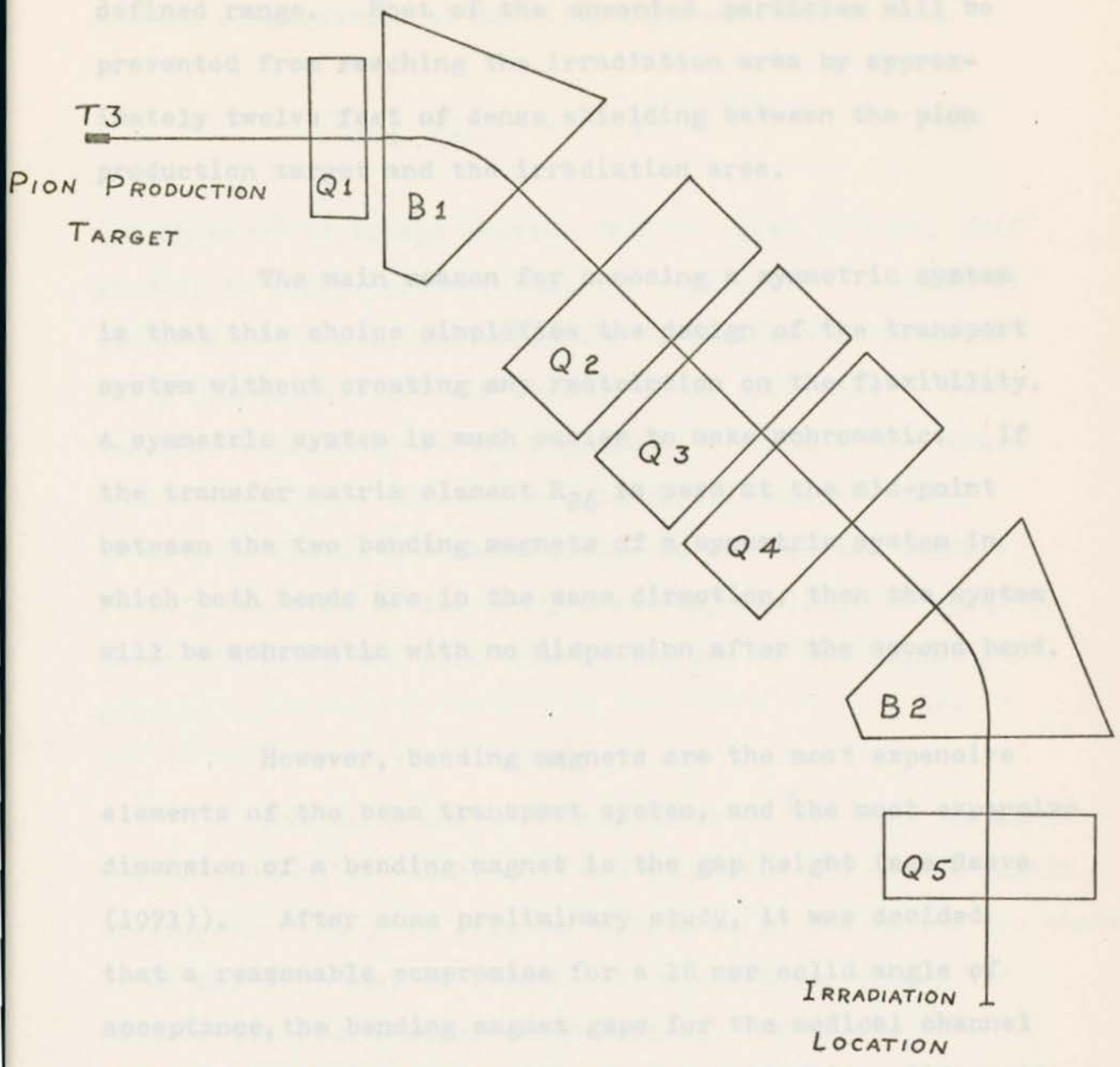

Fig. 3.8 Configuration of the proposed beam transport system in the plane of the two bends.

of particles with negative charge and momentum in a well-defined range. Most of the unwanted particles will be prevented from reaching the irradiation area by approximately twelve feet of dense shielding between the pion production target and the irradiation area.

The main reason for choosing a symmetric system is that this choice simplifies the design of the transport system without creating any restriction on the flexibility. A symmetric system is much easier to make achromatic. If the transfer matrix element R_{26} is zero at the mid-point between the two bending magnets of a symmetric system in which both bends are in the same direction, then the system will be achromatic with no dispersion after the second bend.

However, bending magnets are the most expensive elements of the beam transport system, and the most expensive dimension of a bending magnet is the gap height (see Reeve (1971)). After some preliminary study, it was decided that a reasonable compromise for a 10 msr solid angle of acceptance, the bending magnet gaps for the medical channel was 6 in. It is not possible to transmit this solid angle with fewer than four quadrupole magnets before the second bend. Arrangements other than that given in Figure 3.8 are possible, but have been rejected on grounds of lack of space or their requirements for larger magnet apertures.

From Chapter 2 (Equations 2.13 and 2.14), it may be seen that the product of the maximum divergence and the maximum displacement of an elliptical beam is given by

$$y_{max}\ y'_{max} = \epsilon\sqrt{1 + \alpha^2} \qquad 3.1$$

and since α^2 is always greater than or equal to zero, this product is always greater than the emittance. Because of the take-off angle, the emittance of the beam is large in the y plane, and for this reason, it is difficult to make the beam size small in the y plane. A small y size would mean a very large divergence which would require strong quadrupole fields and short distances between the magnets. It is preferable to let the y size stay as large as possible without letting the pion beam strike any of the magnet apertures.

The solid angle of acceptance of the beam transport system depends on the size of the pion beam and on the magnet apertures. The most critical apertures in the system are those of Q1 and B1 (refer to Figure 3.8) since after these, the size of the pion beam is under control. When the beam leaves the target, it is diverging in both the x and the y

planes. The first magnet determines the angular acceptance of the system in that magnet's focussing plane. If this magnet is a quadrupole, as it is for the medical channel, the beam diverges strongly in one plane between the first and second magnets. For the medical channel, the first quadrupole focusses in the y plane and defocusses in the x plane, with the result that the beam size in the x plane grows very rapidly between the first quadrupole and the first bending magnet. The minimum aperture needed for the quadrupole magnet is 6 in., and the aperture of the bending magnet should be at least 6 in. in the y direction and 10 in. in the x direction. The drift distance between Q1 and B1 has been kept as short as possible to minimize the increase in beam size between these magnets. After B1, the magnet spacing is not nearly so critical to the acceptance of the system.

For several reasons, the first drift length has been set at one meter. The first quadrupole Q1 must be mounted above the collimators and quadrupoles for the proton beam. At a distance of one meter and with a take-off angle of 30°, Q1 barely clears these elements. The magnet Q1 should be mounted as close as possible to the target so that the aperture of this magnet subtends the largest solid angle possible at the target without suffering unacceptable radiation damage. It is believed that if the

magnet coils are made radiation resistant with special insulation, Q1 will have a reasonably long lifetime in the radiation field if the first drift length is one meter in length. The expected lifetime of the magnet coils and methods for handling such radioactive magnets have not yet been studied extensively.

The remaining requirements of the beam transport system pertain to the variability of beam size and the beam uniformity at the irradiation location. Beam sizes between 3 x 3 cm and 10 x 10 cm are required, and the pion intensity should be uniform to $\pm$ 5% across the radiation field. It has been found possible to meet these requirements with a single moveable quadrupole lens after the second bending magnet. The horizontal size of the pion beam at the irradiation location can easily be made as small as 1 cm, but the vertical size is limited by the maximum strength of the last quadrupole. Vertical sizes below 3 cm should be available, however.

Whether or not the beam is uniform in intensity over the irradiation field depends on several different factors. Where the phase space area is large, as in the y plane for this system, the intensity distribution can be found from the outline of the phase space area at the end of the system. It is assumed that the angular distribution of the pions at the source is uniform, an accurate

enough assumption for the small angular range accepted by the beam transport system. If the beam occupies the phase space polygon shown in Figure 3.9, then by calculating the beam angular range that arrives at each position in the field, one can plot the intensity distribution shown in Figure 3.10. This is a very undesirable distribution because it is peaked in the center and falls off rapidly at the sides of the field. However, if the phase space distribution looks like Figure 3.11, a parallelogram with two of the sides vertical, then every point in the field receives the same angular range of pions in the beam. The resulting intensity distribution is shown in Figure 3.12. As was mentioned previously, the effect of a drift length is to skew the phase space distribution of a beam, so that the beam representation in phase space looks like Figure 3.12 at only one or two points along the drift distance after Q5. Therefore the beam can only be made uniform at a specified point, and it will not be as uniformly distributed either before or after that point. There is, however, a certain distance either side of the position of uniformity where the distribution will still be acceptable.

Where the phase space area of the beam is very small, as in the x plane of this system, the beam is nearly always uniform to first order because the phase

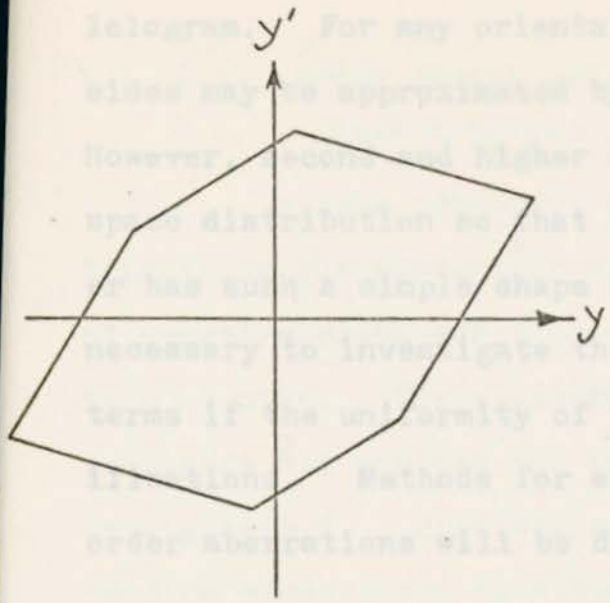

Fig. 3.9 A phase space polygon.

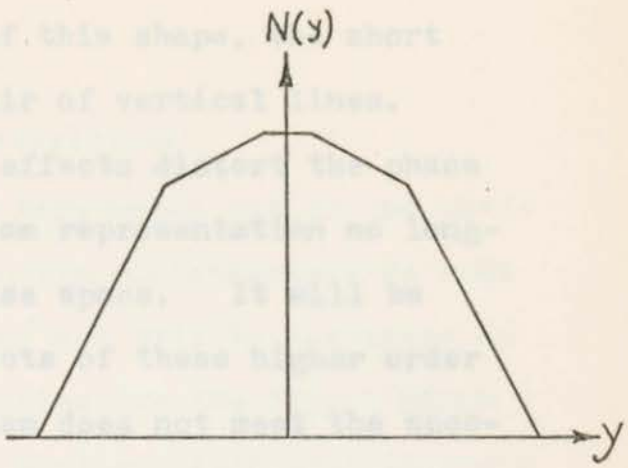

Fig. 3.10 Distribution of pions in the beam at the same position as the polygon of Fig. 3.9.

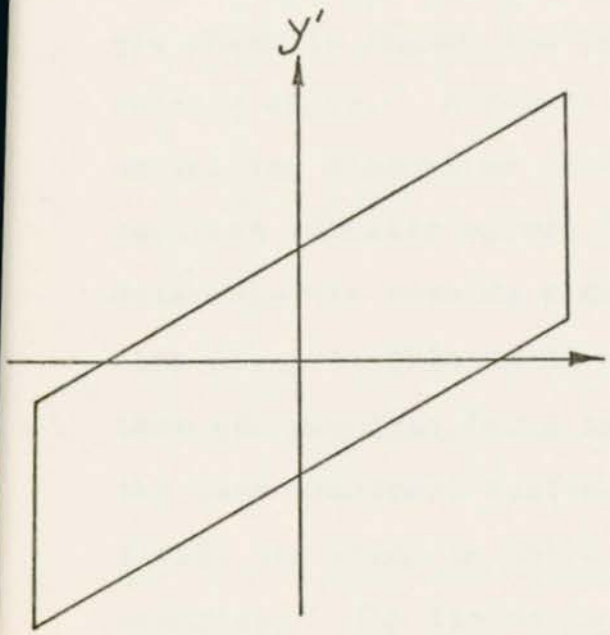

Fig. 3.11 A phase space parallelogram.

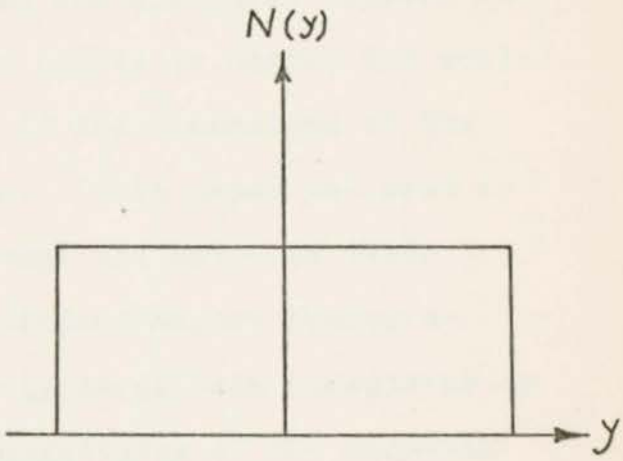

Fig. 3.12 Pion distribution at the position of the phase space parallelogram of Fig. 3.11.

space representation of the beam is a long, thin parallelogram. For any orientation of this shape, the short sides may be approximated by a pair of vertical lines. However, second and higher order effects distort the phase space distribution so that the beam representation no longer has such a simple shape in phase space. It will be necessary to investigate the effects of these higher order terms if the uniformity of the beam does not meet the specifications. Methods for eliminating some of the second order aberrations will be discussed in Chapter 4.

CHAPTER 4. DESIGN PARAMETERS AND SYSTEM PROPERTIES.

4.1 First order Properties.

4.1.1 Beam transport characteristics.

A beam transport system that meets all of the specifications for production of a useable radiotherapeutic beam of negative pions has been designed and will be discussed in this chapter. The recommended design has the layout shown in Figure 4.1 and has the optical configuration that is shown in Figure 4.2. This design requires two 45 degree sector bending magnets and five quadrupole focussing magnets to bring the pions into the irradiation location in a well- defined, uniform, achromatic beam. Since the dimensions of the magnets will not be known until final designs for these magnets are chosen, the distances between the magnet centers are shown in Figure 4.1 rather than the distances between the outside edges. A report by Reeve (1971) is useful for estimating the dimensions of a magnet if the dimensions of the required magnetic volume are known. This paper was used to determine the outside dimensions that are given in Table 4.1. Also given in this table are the minimum magnet apertures that are required for a sufficiently large beam acceptance by the beam transport system. The magnitudes of the magnetic fields are given in Table 4.2 for several different pion energies. The fields in the bending magnets and the field gradients of the quadrupoles scale directly with the momentum of the particles to be transmitted. Table 4.3 gives the

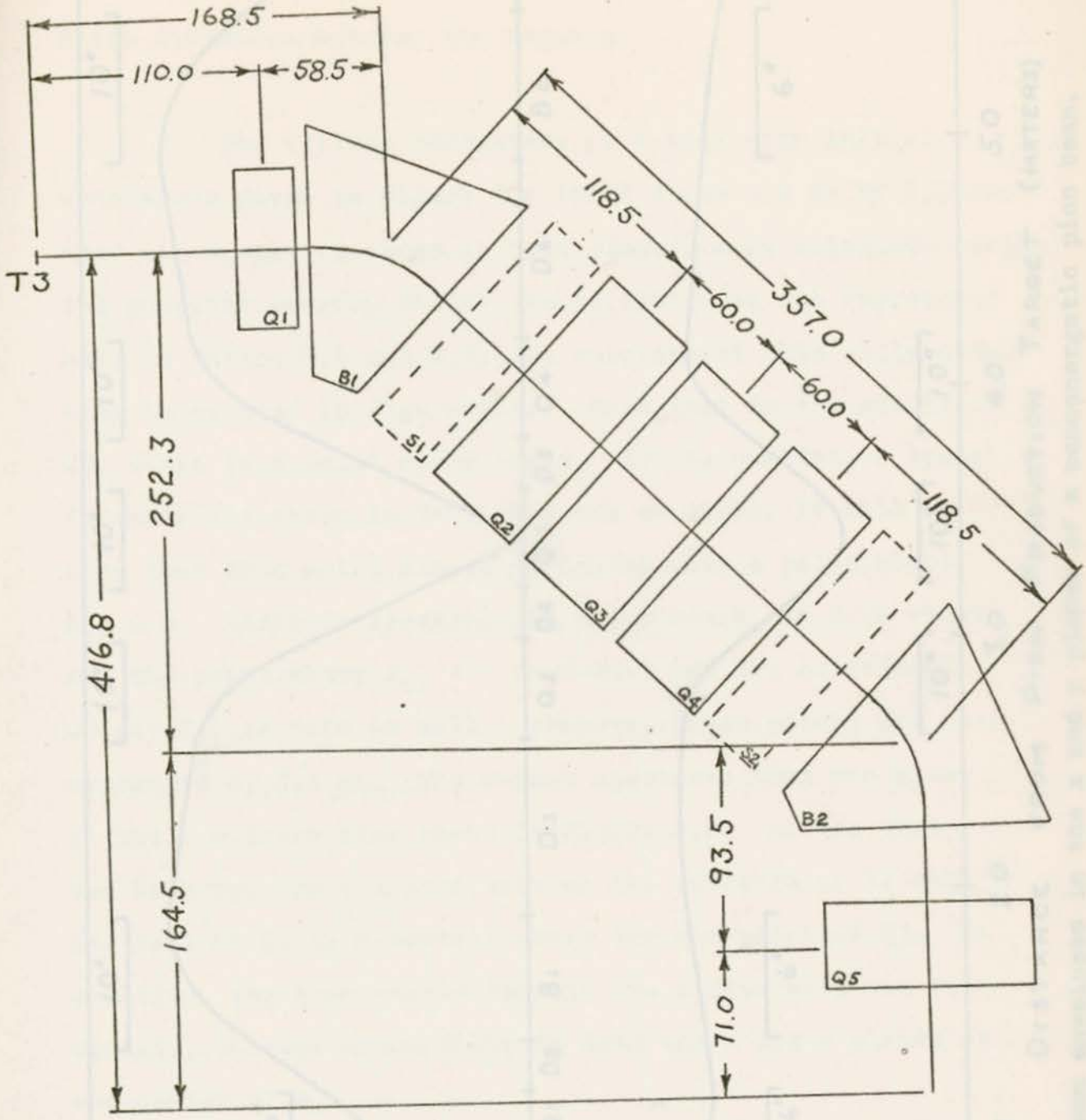

Fig. 4.1 Layout and dimensions of the beam transport system in the bending plane (dimensions in cm). Distances between the centers of the magnets are given rather than the distances between the outside edges. For a discussion of the purpose of sextupole magnets S1 and S2, see Section 4.2.

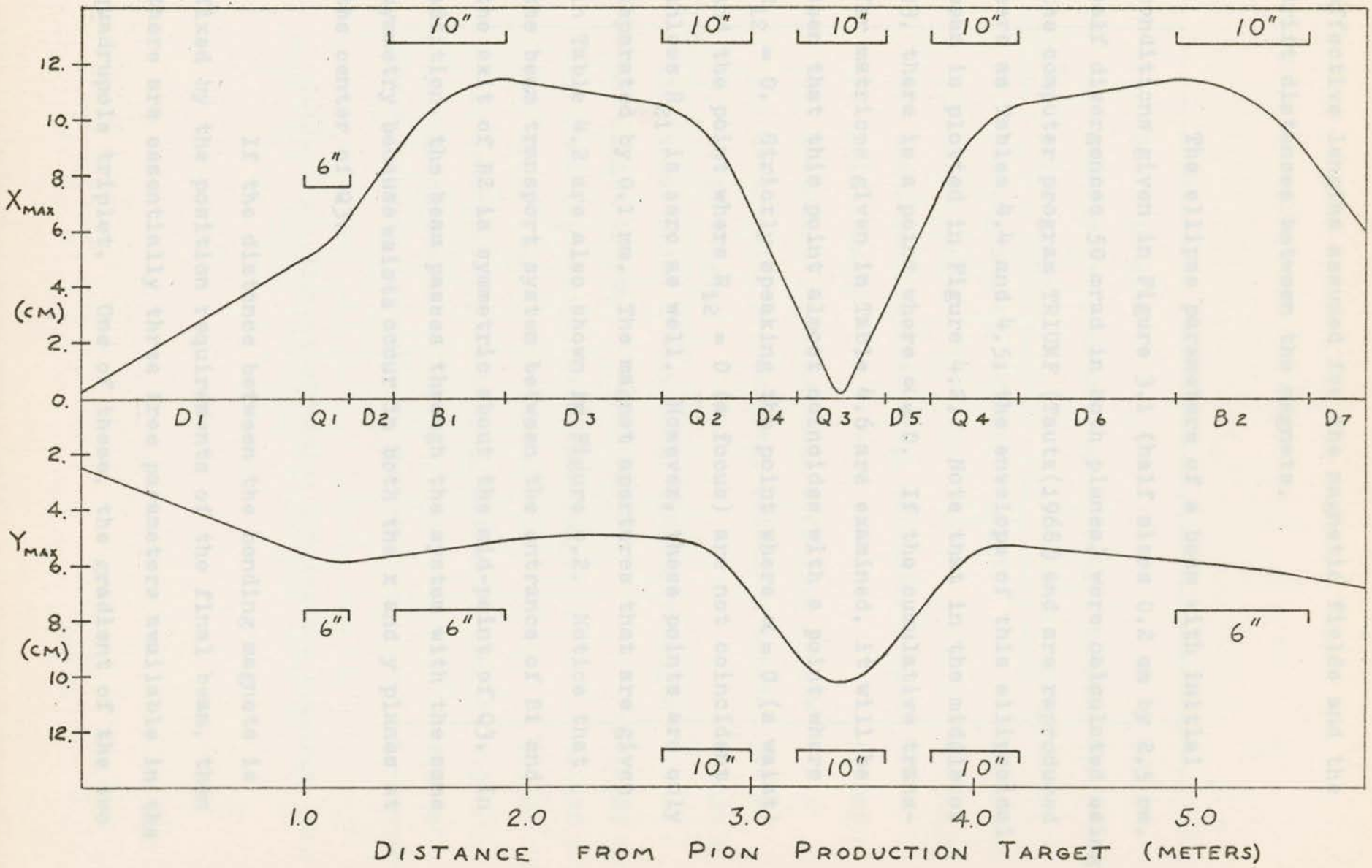

Fig. 4.2 Beam envelopes in the x and y planes of a monoenergetic pion beam.

effective lengths assumed for the magnetic fields and the drift distances between the magnets.

The ellipse parameters of a beam with initial conditions given in Figure 3.1 (half sizes 0.2 cm by 2.5 cm, half divergences 50 mrad in both planes) were calculated using the computer program TRIUMF (Tautz(1968)) and are reproduced here as Tables 4.4 and 4.5; the envelope of this ellipsoidal beam is plotted in Figure 4.2. Note that in the middle of Q3, there is a point where $\alpha = 0$. If the cumulative transfer matrices given in Table 4.6 are examined, it will be seen that this point almost coincides with a point where $R_{12} = 0$. Strictly speaking the point where $\alpha = 0$ (a waist) and the point where $R_{12} = 0$ (a focus) are not coincident unless R_{21} is zero as well. However, these points are only separated by 0.1 mm. The magnet apertures that are given in Table 4.2 are also shown in Figure 4.2. Notice that the beam transport system between the entrance of B1 and the exit of B2 is symmetric about the mid-point of Q3. In addition, the beam passes through the system with the same symmetry because waists occur in both the x and y planes at the center of Q3.

If the distance between the bending magnets is fixed by the position requirements of the final beam, then there are essentially three free parameters available in the quadrupole triplet. One of these, the gradient of the two

1.	Drift length	1.0 m
2.	Quadrupole, y-focussing, effective length	0.2 m
3.	Drift length	0.2 m
4.	Bending magnet, effective length	0.5420 m
5.	Drift length	0.6975 m
6.	Quadrupole, x-focussing, effective length	0.4 m
7.	Drift length	0.2025 m
8.	Quadrupole, y-focussing, effective length	0.2 m
9.	Quadrupole, y-focussing, effective length	0.2 m
10.	Drift length	0.2025 m
11.	Quadrupole, x-focussing, effective length	0.4 m
12.	Drift length	0.6975 m
13.	Bending magnet, effective length	0.5420 m
14.	Drift length	0.5 m
15.	Quadrupole, y-focussing, effective length	0.3 m
16.	Drift length	0.56 m

Table 4.3 Element effective lengths and spacings (m).

Magnet	Aperture (in)	Effective length (cm)	Pole iron length (cm)	Overall length x width x height (cm)
Q1	8	20	13.4	29 x 102 x 55
B1 B2	10 x 6	54.2	41.3	71 x 102 x 107
Q2 Q3 Q4	10	40	27.3	52 x 127 x 127
Q5	8	30	19.8	39 x 102 x 102

Table 4.1 Magnet dimensions for the medical pion channel.

π energy (MeV)	110	100	90	80	70	60
π momentum (MeV/c)	206.9	194.7	182.3	169.5	156.3	142.7
Q1 gradient (G/cm)	350.	329.4	308.4	286.7	264.4	241.4
B1, B2 field (kG)	10.	9.410	8.881	8.192	7.554	6.897
Q2, Q4 gradient (G/cm)	279.5	280.0	262.1	243.7	224.7	205.2
Q3 gradient (G/cm)	361.3	340.0	318.3	296.0	272.9	249.2
Q5 max gradient (G/cm)	500.	470.	440.	410.	378.	345.

Table 4.2 Magnet fields for the medical pion channel.

	γ $(\frac{rad}{100}/cm)$	α —	β $(cm/\frac{rad}{100})$	X_{max} (cm)	X'_{max} (rad/100)
	25.00000	0.0	0.04000	0.20000	5.00000
1	25.0000	-25.0000	25.0400	5.0040	5.0000
2	115.8297	-70.5259	42.9501	6.5536	10.7624
3	115.8297	-93.6918	75.7936	8.7060	10.7624
4	1.7226	14.9394	130.1426	11.4080	1.3125
5	1.7226	13.7373	110.1402	10.4948	1.3125
6	287.9746	112.2238	43.7370	6.6134	16.9698
7	287.9746	53.9089	10.0952	3.1773	16.9698
8	235.1468	0.0195	0.0043	0.0652	15.3345
9	287.8799	-53.8521	10.0773	3.1745	16.9670
10	287.8799	-112.1477	43.6922	6.6100	16.9670
11	1.7313	-13.7684	110.0711	10.4915	1.3158
12	1.7313	-14.9760	130.1203	11.4070	1.3158
13	115.7573	93.6724	75.8096	8.7069	10.7591
14	115.7573	35.7938	11.0766	3.3281	10.7591
15	87.2522	3.4437	0.1474	0.3839	9.3409
16	87.2522	-45.4174	23.6526	4.8634	9.3409

Table 4.4 Beam ellipse and envelope parameters in the x plane. (α, β, γ defined in Eq. 2.9)

	γ $(\frac{rad}{100}/cm)$	α —	β $(cm/\frac{rad}{100})$	y_{max} (cm)	y_{max} (rad/100)
	2.00000	0.0	0.50000	2.50000	5.00000
1	2.0000	-2.0000	2.5000	5.5902	5.0000
2	0.4933	0.6164	2.7971	5.9130	2.4833
3	0.4933	0.5177	2.5703	5.6682	2.4833
4	0.4933	0.2503	2.1540	5.1889	2.4833
5	0.4933	-0.0938	2.0448	5.0557	2.4833
6	9.0263	-5.9434	4.0242	7.0924	10.6221
7	9.0263	-7.7712	6.8014	9.2205	10.6221
8	0.1197	-0.1331	8.5027	10.3094	1.2232
9	8.5433	7.6089	6.8937	9.2828	10.3340
10	8.5433	5.8788	4.1624	7.2132	10.3340
11	0.4477	-0.1511	2.2844	5.3437	2.3657
12	0.4477	-0.4634	2.7130	5.8235	2.3657
13	0.4477	-0.7061	3.3469	6.4681	2.3657
14	0.4477	-0.9299	4.1649	7.2154	2.3657
15	1.4691	2.1315	3.7733	6.8678	4.2853
16	1.4691	1.3088	1.8467	4.8046	4.2853

Table 4.5 Beam ellipse and envelope parameters in the y plane.

Horizontal plane

	R_{11}	R_{12} mm/mrad	R_{21} mrad/mm	R_{22}	R_{16} cm	R_{26} rad/100
1	1.0000	1.0000	0.0	1.0000	0.0	0.0
2	1.1032	1.3100	1.0489	2.1521	0.0	0.0
3	1.3129	1.7404	1.0489	2.1521	0.0	0.0
4	1.4403	2.2809	-0.6035	-0.2614	20.2132	70.7097
5	1.0193	2.0986	-0.6035	-0.2614	69.5332	70.7097
6	0.4730	1.3225	-1.9695	-3.3931	72.0433	-58.8889
7	0.0741	0.6355	-1.9695	-3.3931	60.1183	-58.8889
8	-0.3258	0.0006	-2.0990	-3.0658	54.3302	0.0024
9	-0.7951	-0.6341	-2.6758	-3.3917	60.1191	58.8940
10	-1.3369	-1.3209	-2.6758	-3.3917	72.0452	58.8940
11	-1.8532	-2.0970	0.2445	-0.2630	69.5362	-70.7091
12	-1.6827	-2.2804	0.2445	-0.2630	20.2167	-70.7091
13	-1.0706	-1.7408	1.8969	2.1505	0.0028	-0.0031
14	-0.1221	-0.6656	1.8969	2.1505	0.0012	-0.0031
15	0.4549	-0.0746	2.0246	1.8664	0.0004	-0.0024
16	1.5886	0.9706	2.0246	1.8664	-0.0009	-0.0024

Vertical plane

	R_{33}	R_{34} mm/mrad	R_{43} mrad/mm	R_{44}	R_{36}	R_{46}
1	1.0000	1.0000	0.0	1.0000	0.0	0.0
2	0.9003	1.0936	-0.9803	-0.0801	0.0	0.0
3	0.7042	1.0776	-0.9803	-0.0801	0.0	0.0
4	0.1728	1.0342	-0.9803	-0.0801	0.0	0.0
5	-0.5109	0.9783	-0.9803	-0.0801	0.0	0.0
6	-1.1363	1.2997	-2.3242	1.7784	0.0	0.0
7	-1.6070	1.6599	-2.3242	1.7784	0.0	0.0
8	-1.8904	1.8325	-0.4606	-0.0825	0.0	0.0
9	-1.7848	1.6280	1.4977	-1.9264	0.0	0.0
10	-1.4816	1.2379	1.4977	-1.9264	0.0	0.0
11	-1.3522	0.8277	-0.8141	-0.2412	0.0	0.0
12	-1.9200	0.6595	-0.8141	-0.2412	0.0	0.0
13	-2.3613	0.5287	-0.8141	-0.2412	0.0	0.0
14	-2.7683	0.4081	-0.8141	-0.2412	0.0	0.0
15	-2.6845	0.2916	1.3619	-0.5204	0.0	0.0
16	-1.9218	0.0002	1.3619	-0.5204	0.0	0.0

Table 4.6 Cumulative transfer matrices from the target to the ends of the beam transport elements.

outer quadrupoles Q2 and Q4, is taken up by the requirement of achromaticity. The remaining two, which are the distance between the quadrupoles and the gradient of Q3, are chosen to satisfy the double waist condition at the symmetry point. Actually, this condition is important only in that it assures that all of the pions that reach the center of the system will be transmitted to the irradiation location and not be stopped in the second half of the system. If the size of the beam passing through the second half of the system could be made smaller without adversely affecting the acceptance of the first half, then it should be done in order to minimize the required magnet apertures. However, to make the beam sizes smaller in the second half of the system requires the magnets of the quadrupole triplet to be placed closer together. Although there is 20 cm between the edges of the magnetic fields, the overall magnet dimensions are such that the magnet coils will be nearly touching. If the outside dimensions of the quadrupoles are so large that the magnets cannot be put this close together, then some of the pion beam must be intercepted in the second half of the beam transport system.

A similar problem arises with the space between Q1 and B1. To minimize the x size of the pion beam in the bending magnet and in Q2, the first quadrupole should be as close to the bending magnet as possible. The strength of Q1 is then set by the maximum size of the pion beam in the

next three magnets. If the field is two weak in Q1, then the y size of the beam is too large in Q3. If it is too strong, the x size is too large in Q2. Since the range of possible values for the magnetic field in Q1 is so restricted, variation within this range has little effect on the condition of having a double waist in Q3.

It has been assumed thus far that the apertures of the quadrupole magnets are circular. If fact other shapes are possible. The vacuum tube inside which the beam travels may be elliptical, as shown in Figure 4.3, or cruciform, as shown in Figure 4.4. These apertures make more efficient use of the magnetic fields in a quadrupole because they allow the passage of particles that would be intercepted by a circular beam tube. Usually, however, the beam is large in only one dimension at a time. The reason for this is that a quadrupole magnet that focusses in one plane defocusses in the other. Consequently a beam transport system is usually designed so that the beam is being alternately focussed and defocussed. For example, in Q2 of the medical channel, the beam is large in the focussing (horizontal) plane and small in the defocussing (vertical) plane. In the next magnet, Q3, the beam is again large in the focussing (vertical) plane and small in the defocussing (horizontal) plane. Because the beam is large in only one direction at a time, elliptical apertures would probably be

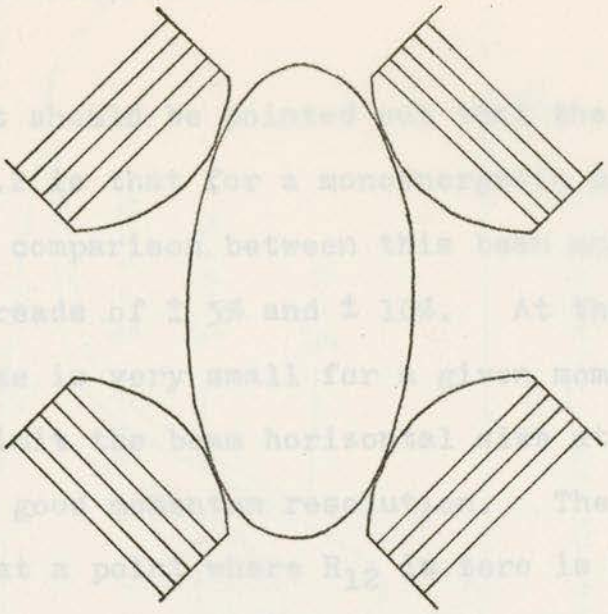

Fig. 4.3 A quadrupole magnet with an elliptical beam tube.

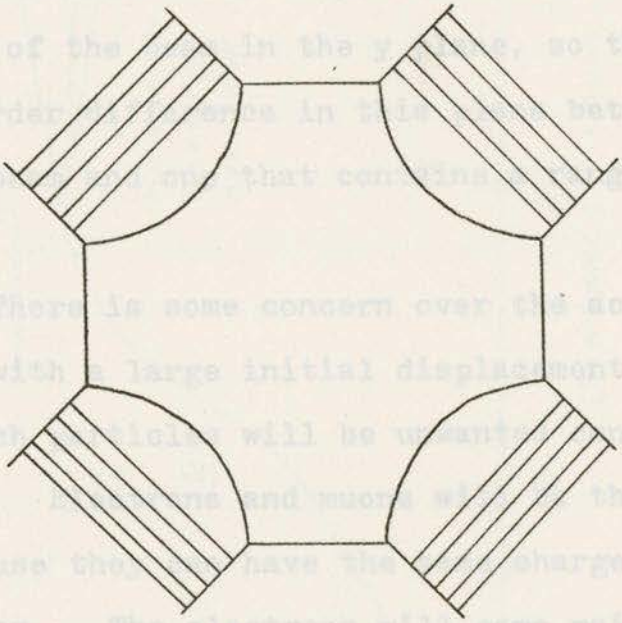

Fig. 4.4. A quadrupole magnet with a cruciform aperture.

as useful as cruciform ones.

It should be pointed out that the beam envelope in Figure 4.2 is that for a monoenergetic beam. Figure 4.5 gives a comparison between this beam and those with momentum spreads of ± 5% and ± 10%. At the center of Q3, the beam size is very small for a given momentum, so that a slit to limit the beam horizontal size at this point should give good momentum resolution. The definition of resolution at a point where R_{12} is zero is the product of the initial beam size (0.4 cm) and the magnification (R_{11}, which is equal to 0.33 at the center of Q3) divided by the dispersion (R_{16}, 0.54 cm/%). With this definition, the first order momentum resolution is 0.24%. There is no dispersion of the beam in the y plane, so that there is no first order difference in this plane between a monoenergetic beam and one that contains a range of momenta.

There is some concern over the acceptance of particles with a large initial displacement from the target because such particles will be unwanted contaminants of the pion beam. Electrons and muons will be the main contaminants because they can have the same charge and momentum as the pions. The electrons will come mainly from interactions of protons in the target and surrounding shielding, while the muons will be created by pions that decay along the beam transport system. If the phase space acceptance

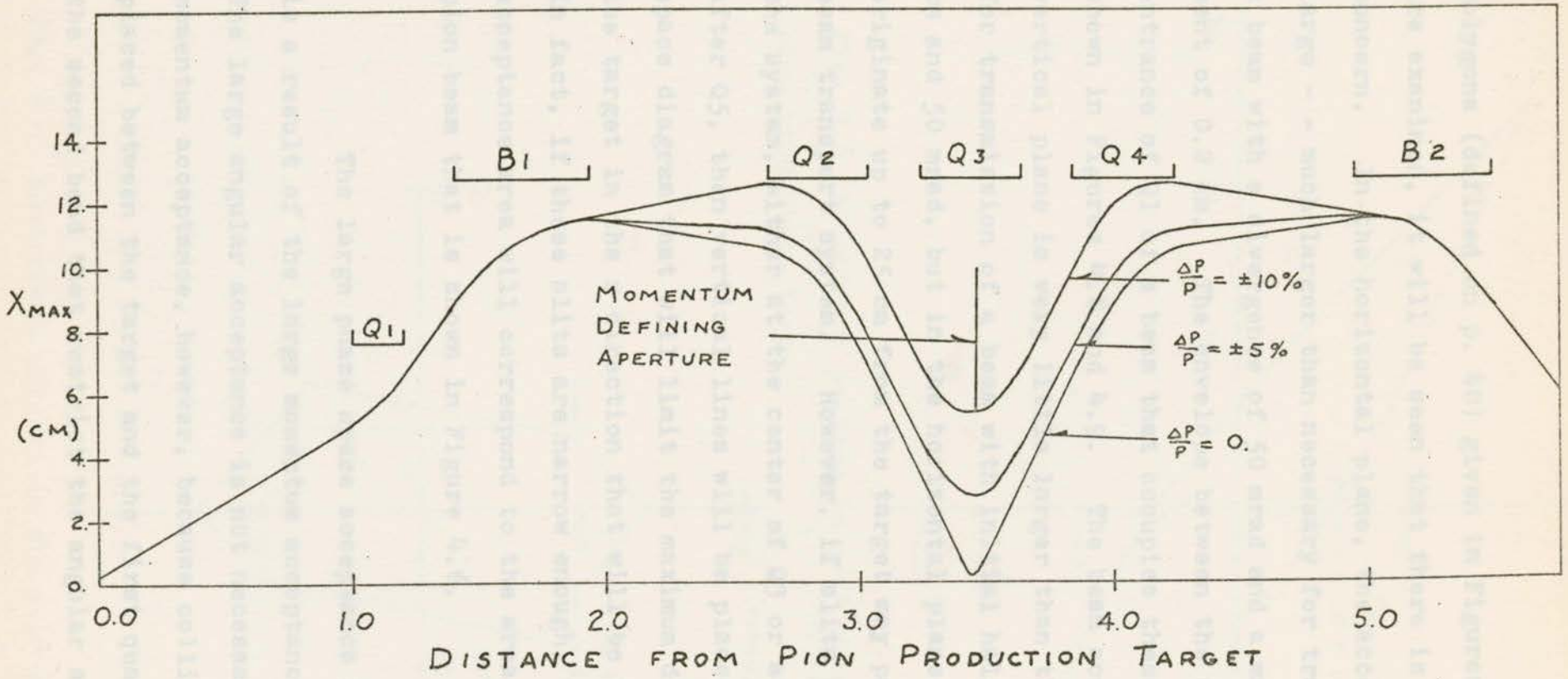

Fig. 4.5 Beam envelopes in the x plane of beams with momentum spreads of 0.0%, ±5%, and ± 10% of the central momentum.

polygons (defined on p. 40) given in Figures 4.6 and 4.7 are examined, it will be seen that there is cause for some concern. In the horizontal plane, the acceptance is very large - - much larger than necessary for transmission of a beam with a divergence of 50 mrad and a maximum displacement of 0.2 cm. The envelope between the target and the entrance of Q1 of a beam that occupies these polygons is shown in Figures 4.8 and 4.9. The beam accepted in the vertical plane is very little larger than that required for transmission of a beam with initial half sizes of 2.5 cm and 50 mrad, but in the horizontal plane, particles that originate up to 25 cm from the target may pass through the beam transport system. However, if slits are placed in the system, either at the center of Q3 or at the x waist after Q5, then vertical lines will be placed on the x phase space diagram that will limit the maximum displacement from the target in the x direction that will be transmitted. In fact, if these slits are narrow enough, the x phase space acceptance area will correspond to the area occupied by the pion beam that is shown in Figure 4.6.

The large phase space acceptance in the x plane is a result of the large momentum acceptance of the system. The large angular acceptance is not necessary for a large momentum acceptance, however, because collimators may be placed between the target and the first quadrupole or after the second bend that restrict the angular acceptance with-

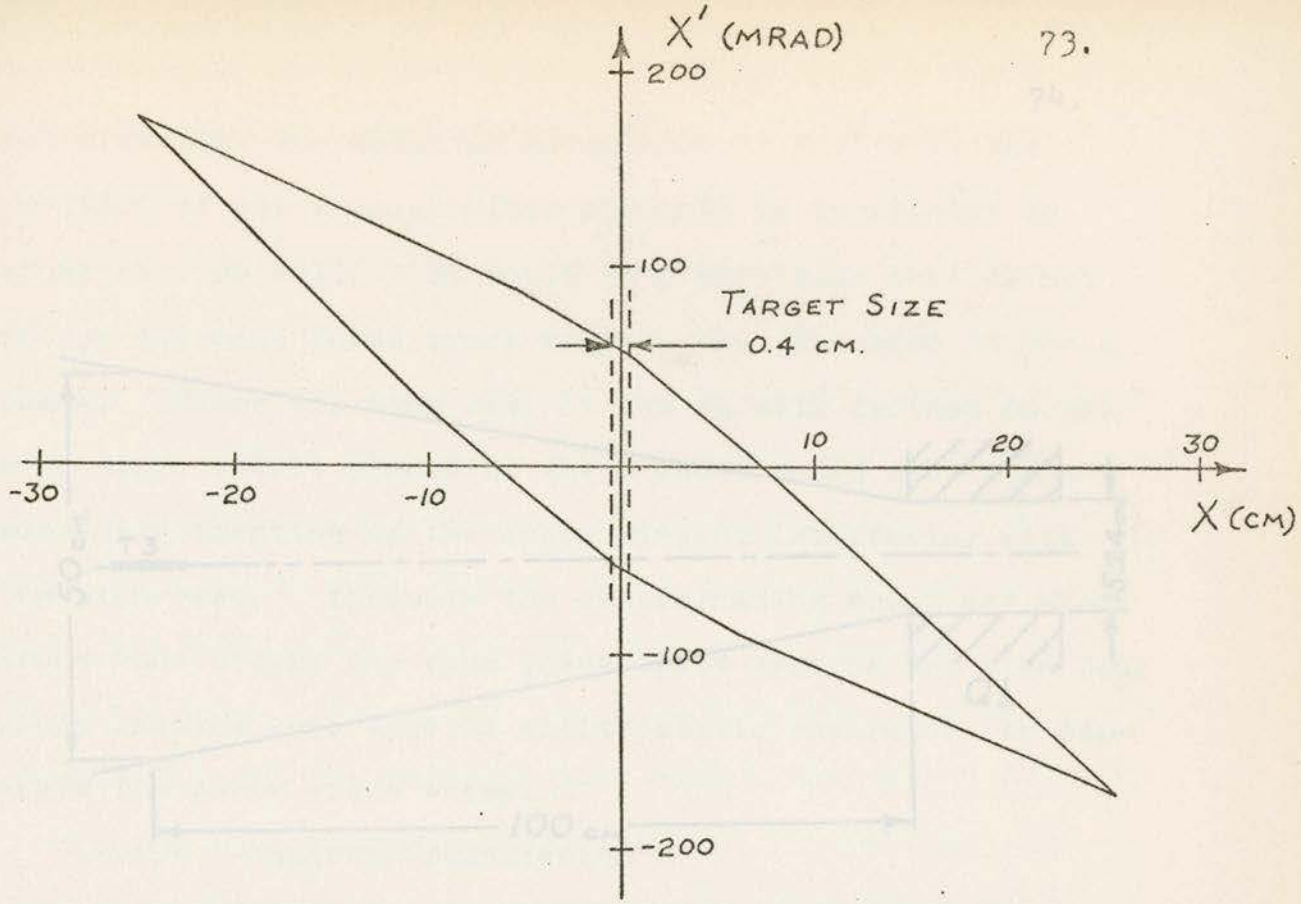

Fig. 4.6 Acceptance polygon in x-x' phase space at the pion production target.

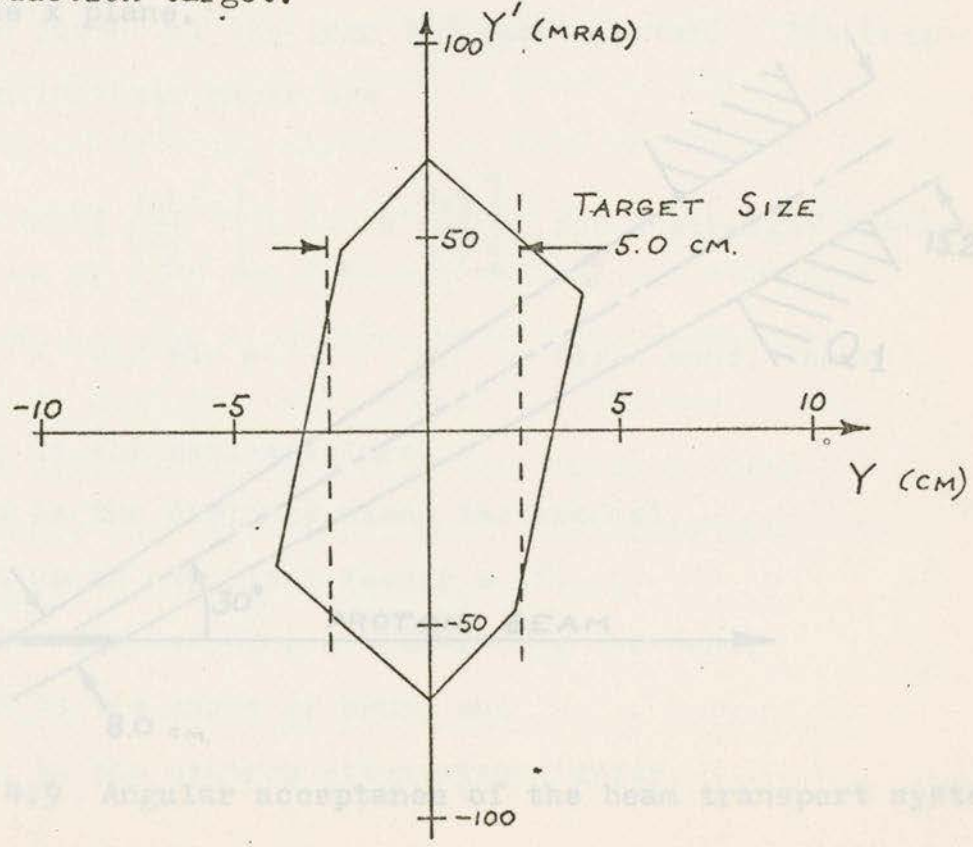

Fig. 4.7 Acceptance polygon in the y-y' phase space at the pion production target.

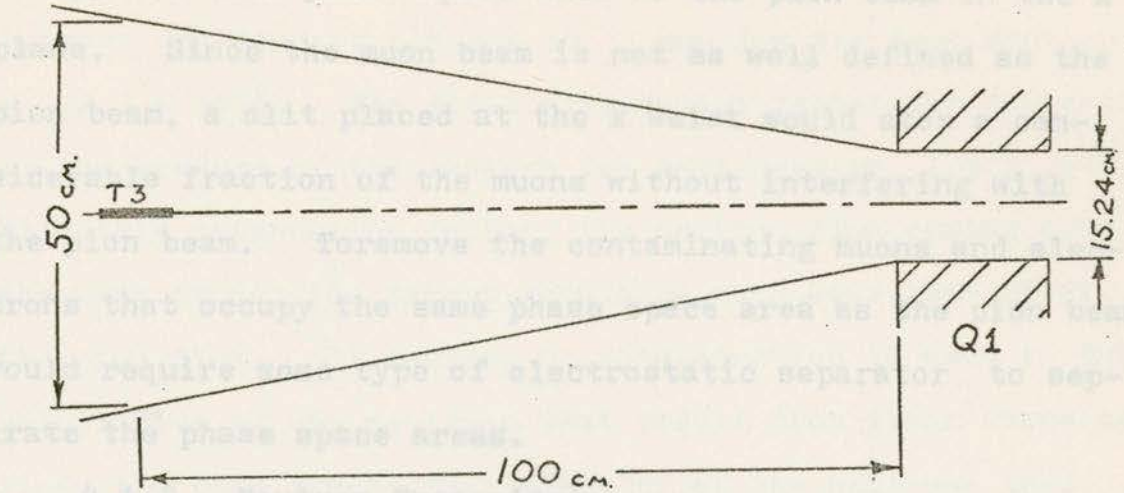

Fig. 4.8 Angular acceptance of the beam transport system in the x plane.

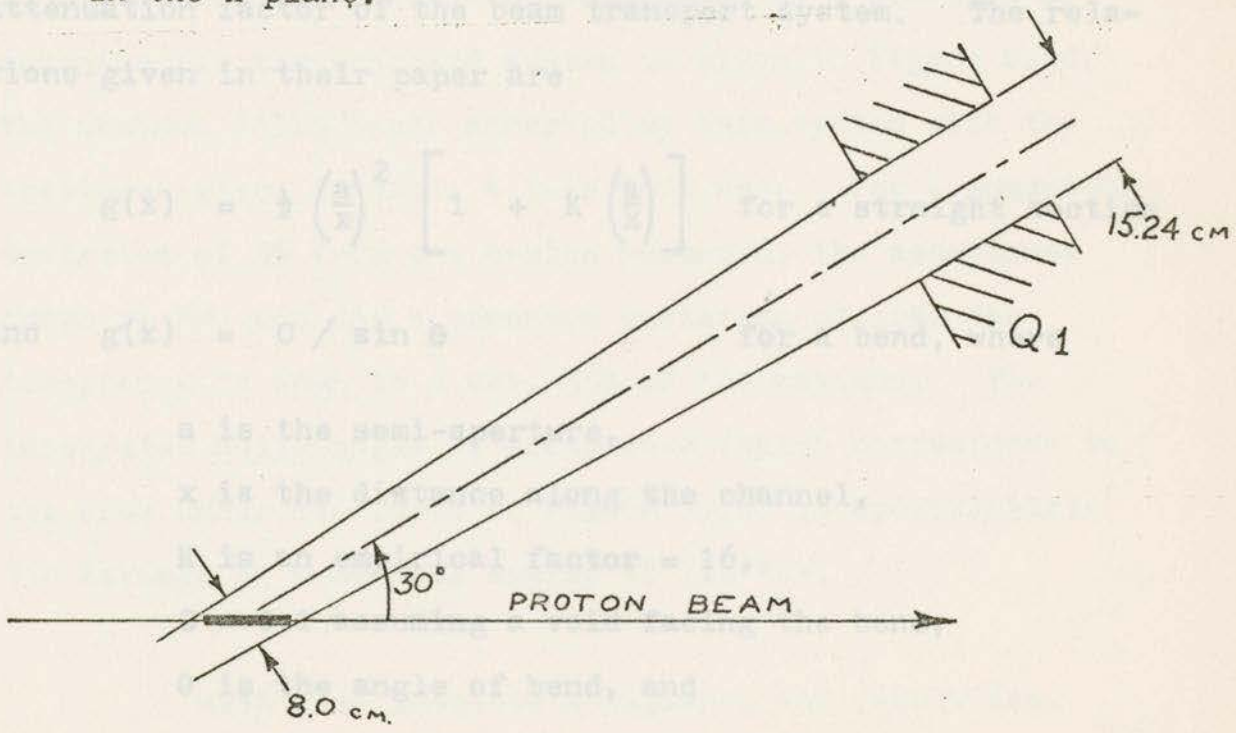

Fig. 4.9 Angular acceptance of the beam transport system in the y plane.

out affecting the momentum acceptance. A slit at the position of the x waist after Q5 would be beneficial in other ways as well. It would stop particles that do not occupy the same phase space area as the pion beam in the x plane. Since the muon beam is not as well defined as the pion beam, a slit placed at the x waist would stop a considerable fraction of the muons without interfering with the pion beam. Toremove the contaminating muons and electrons that occupy the same phase space area as the pion beam would require some type of electrostatic separator to separate the phase space areas.

4.1.2 Neutron Transmission

Following empirical formulas given by Cochran and Jacobson (1966), it is possible to estimate the neutron attenuation factor of the beam transport system. The relations given in their paper are

$$g(x) = \tfrac{1}{2}\left(\frac{a}{x}\right)^2\left[1 + K\left(\frac{a}{x}\right)\right] \quad \text{for a straight section}$$

and $g(x) = C / \sin\theta$ for a bend, where

a is the semi-aperture,

x is the distance along the channel,

K is an empirical factor = 16,

C = 0.1 assuming a void facing the bend,

θ is the angle of bend, and

g is the neutron attenuation factor.

Using these relations, assuming an 8 inch beam tube before B1 and after B2 and a 12 inch beam tube between the bends, the attenuation factor for the section up to B1 is 5.7×10^{-3}, for each of the bends, $g = 0.14$; for the section between the bends $g = 5.6 \times 10^{-4}$, and for the last section $g = 2.3 \times 10^{-2}$. The total attenuation factor for the system is the product of the factors for each section, 1.4×10^{-9}. With this attenuation factor, the neutron flux coming from the pion production target should be much less than 1% of the pion flux. Of course, no consideration is made in this calculation of the neutrons that result from pions stopping along the beam transport system, or of the neutrons that are created when the pions stop in the irradiated volume.

4.1.3 Momentum Acceptance and Beam Uniformity

The solid angle of acceptance as a function of momentum for the proposed system is given in Figure 4.10. The maximum solid angle accepted by this system with the apertures given in Table 4.1 is 10.9 msr. For a momentum deviation of 5% from the design momentum, the acceptance drops by 8%, and for a momentum deviation of 10%, the acceptance is down to 6 msr, 55% of the maximum. The integrated solid angle of acceptance (which corresponds to the area under the curve of Figure 4.10) is approximately 350 MeV-msr at a central energy of 110 MeV.

With this adequate acceptance and resolution, the parameters of the system up to and including B2 can

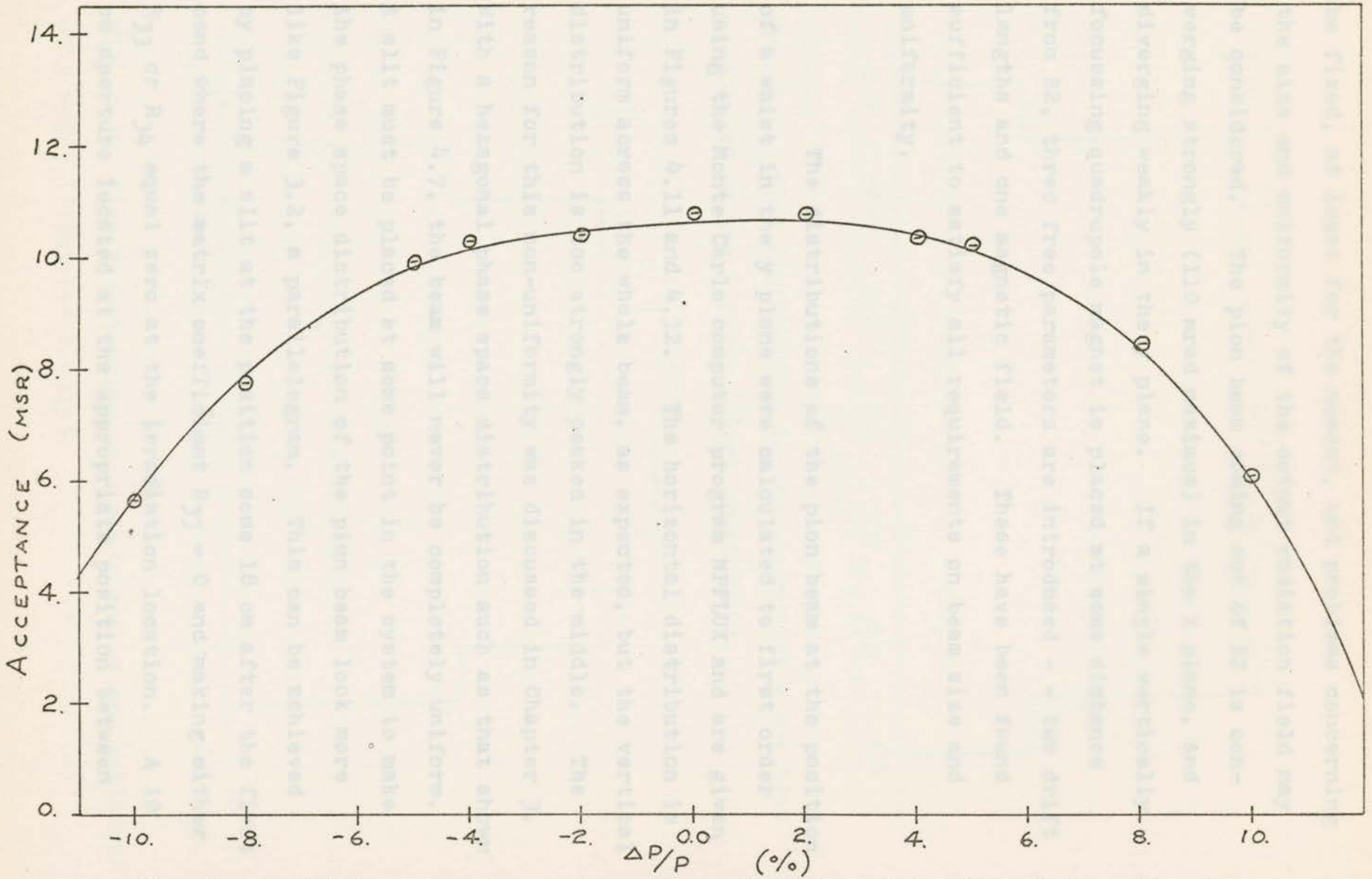

Fig. 4.10 Solid angle of acceptance as a function of fractional deviation from the design momentum.

be fixed, at least for the moment, and problems concerning the size and uniformity of the output radiation field may be considered. The pion beam coming out of B2 is converging strongly (110 mrad maximum) in the x plane, and diverging weakly in the y plane. If a single vertically focussing quadrupole magnet is placed at some distance from B2, three free parameters are introduced - - two drift lengths and one magnetic field. These have been found sufficient to satisfy all requirements on beam size and uniformity.

The distributions of the pion beam at the position of a waist in the y plane were calculated to first order using the Monte Carlo computer program NPFLUX and are given in Figures 4.11 and 4.12. The horizontal distribution is uniform across the whole beam, as expected, but the vertical distribution is too strongly peaked in the middle. The reason for this non-uniformity was discussed in Chapter 3. With a hexagonal phase space distribution such as that shown in Figure 4.7, the beam will never be completely uniform. A slit must be placed at some point in the system to make the phase space distribution of the pion beam look more like Figure 3.2, a parallelogram. This can be achieved by placing a slit at the position some 18 cm after the first bend where the matrix coefficient $R_{33} = 0$ and making either R_{33} or R_{34} equal zero at the irradiation location. A 10 cm aperture located at the appropriate position between

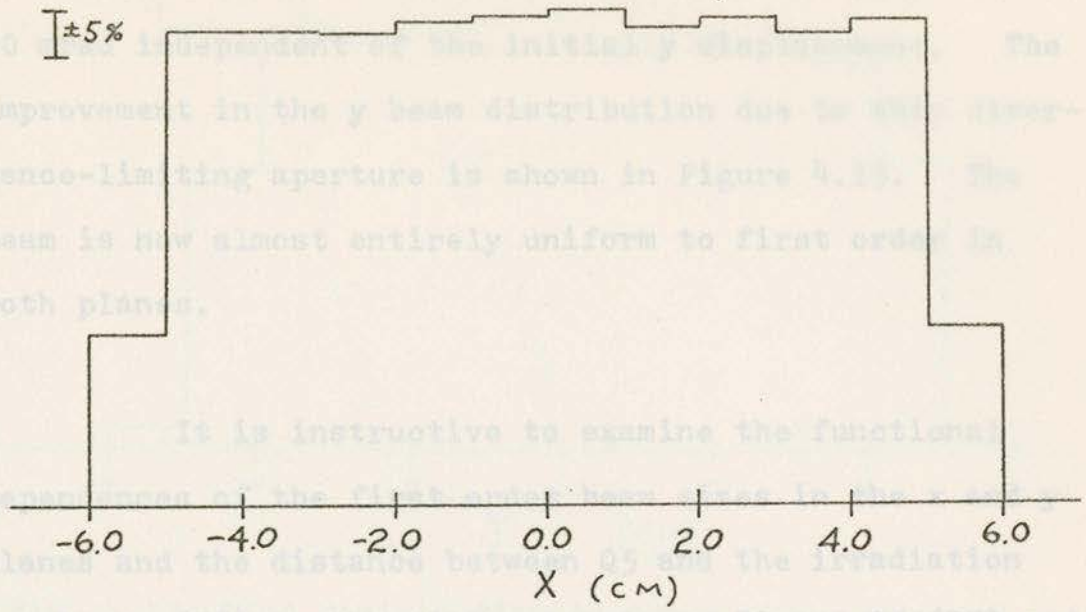

Fig. 4.11 Pion distribution in the x plane at a position of a waist in the y plane (first order only).

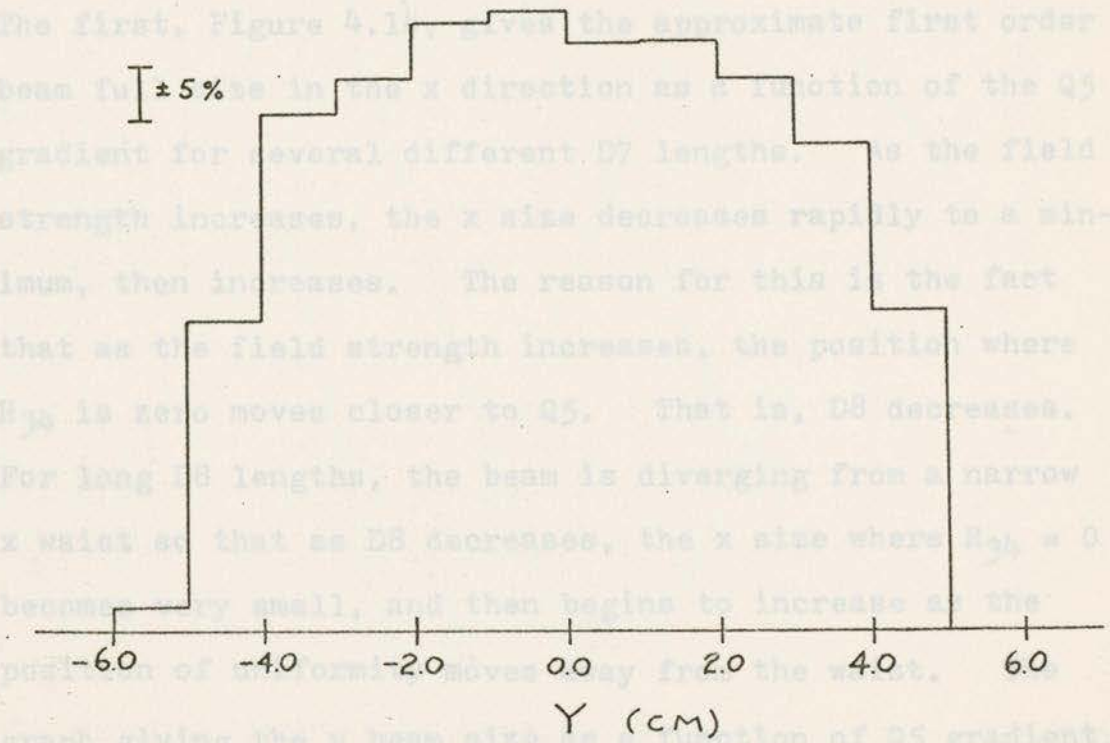

Fig. 4.12 Pion distribution in the y plane at the position of a waist (first order only).

B1 and Q2 will intercept approximately 1 msr of the pion beam and limit the initial divergence of the pion beam to 50 mrad independent of the initial y displacement. The improvement in the y beam distribution due to this divergence-limiting aperture is shown in Figure 4.13. The beam is now almost entirely uniform to first order in both planes.

It is instructive to examine the functional dependences of the first order beam sizes in the x and y planes and the distance between Q5 and the irradiation location (D8) on the distance between B2 and Q5 (D7) and on the magnetic field gradient in Q5. These dependences are given in the next six graphs, Figures 4.14 to 4.19. The first, Figure 4.14, gives the approximate first order beam full size in the x direction as a function of the Q5 gradient for several different D7 lengths. As the field strength increases, the x size decreases rapidly to a minimum, then increases. The reason for this is the fact that as the field strength increases, the position where R_{34} is zero moves closer to Q5. That is, D8 decreases. For long D8 lengths, the beam is diverging from a narrow x waist so that as D8 decreases, the x size where $R_{34} = 0$ becomes very small, and then begins to increase as the position of uniformity moves away from the waist. The graph giving the y beam size as a function of Q5 gradient, Figure 4.15, shows that the y size is much less dependent

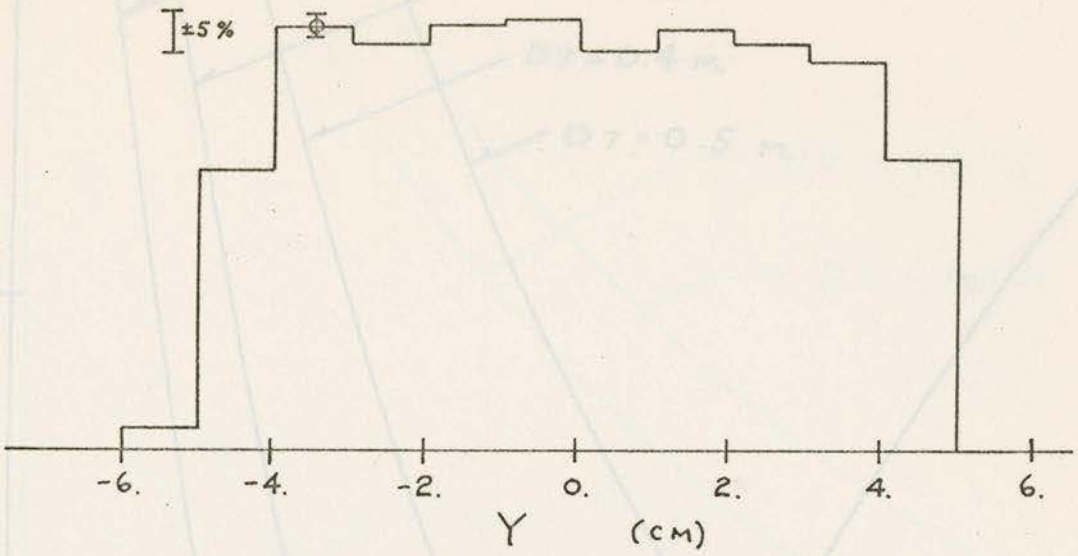

Fig. 4.13 Pion distribution in the y plane using a 10 cm divergence-limiting aperture to improve the beam uniformity (first order).

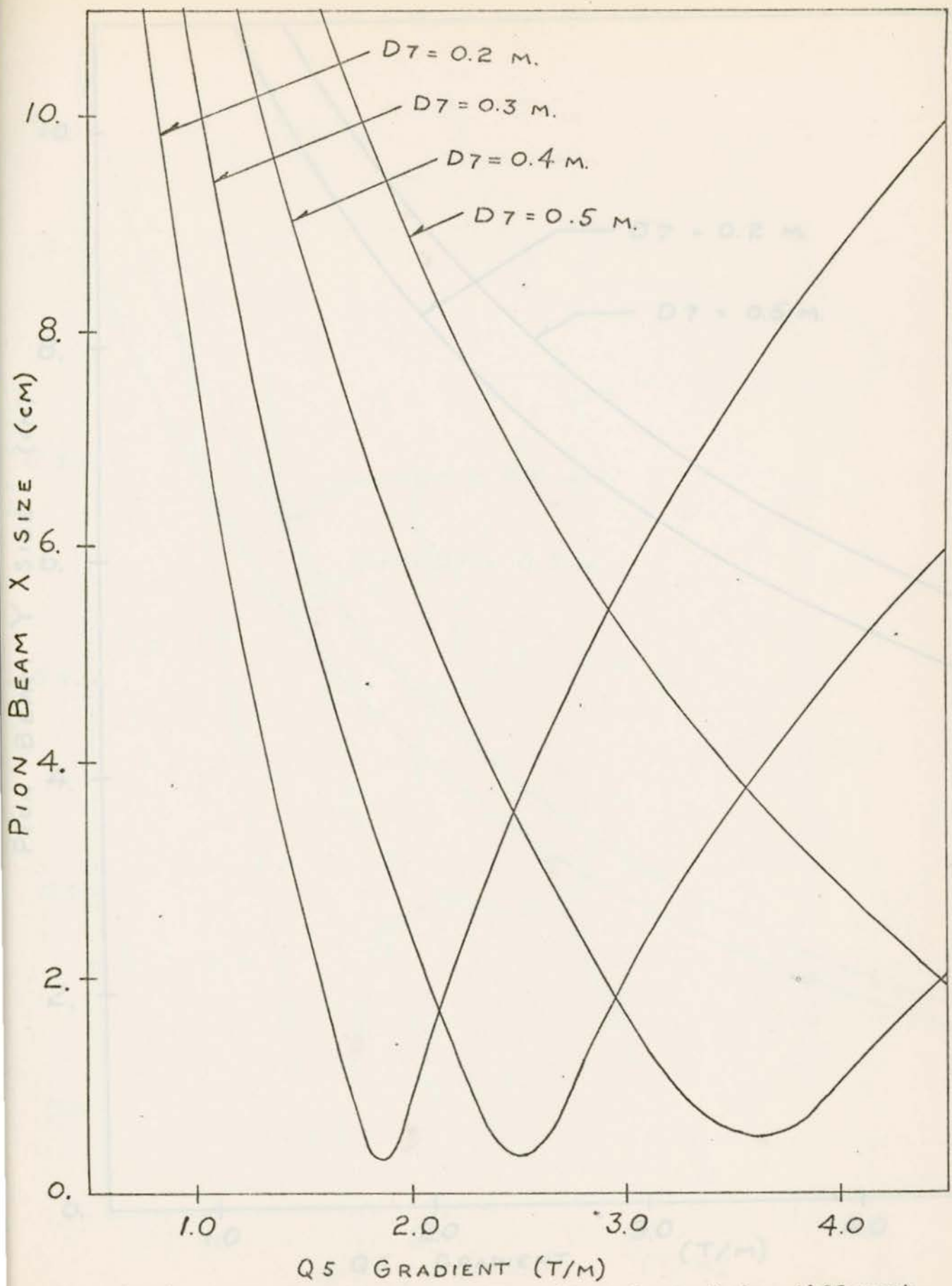

Fig. 4.14 Beam size in the x plane where $R_{34} = 0$ for different Q5 gradients and D7 lengths.

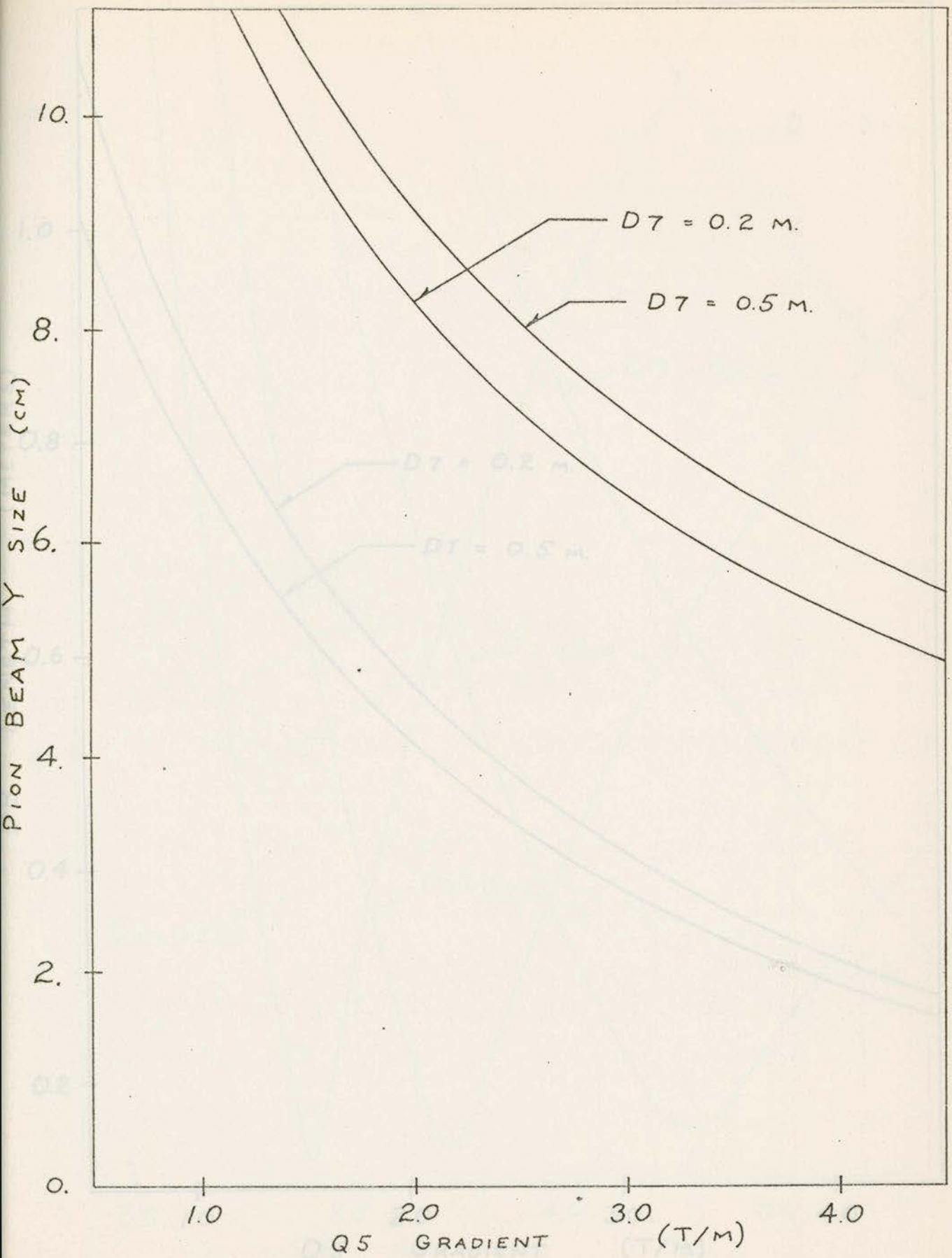

Fig. 4.15 Beam size in the y plane where R34 = 0 as a function of Q5 gradient and D7 length.

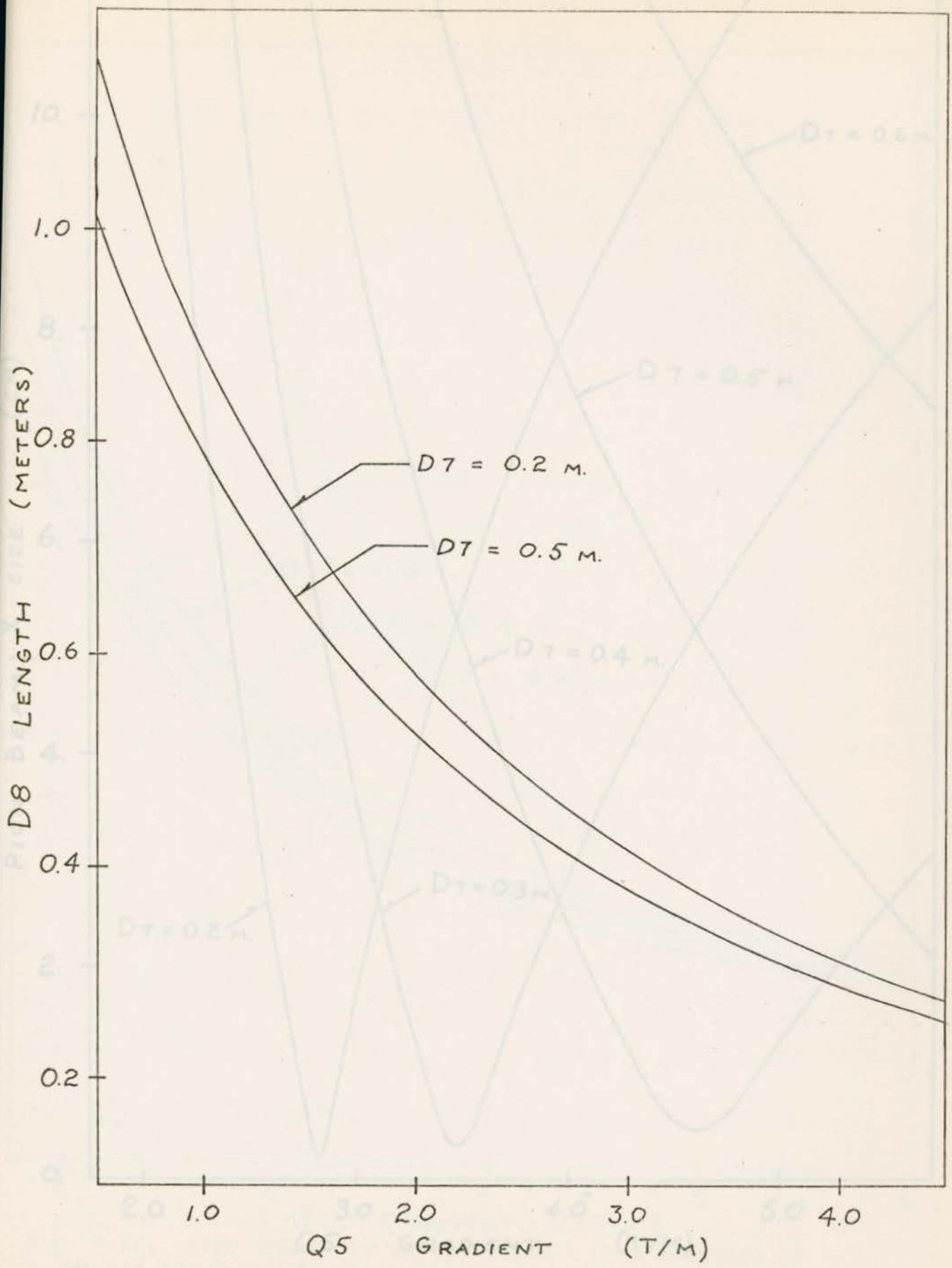

Fig. 4.16 Drift distance from Q5 to a position where $R_{34} = 0$.

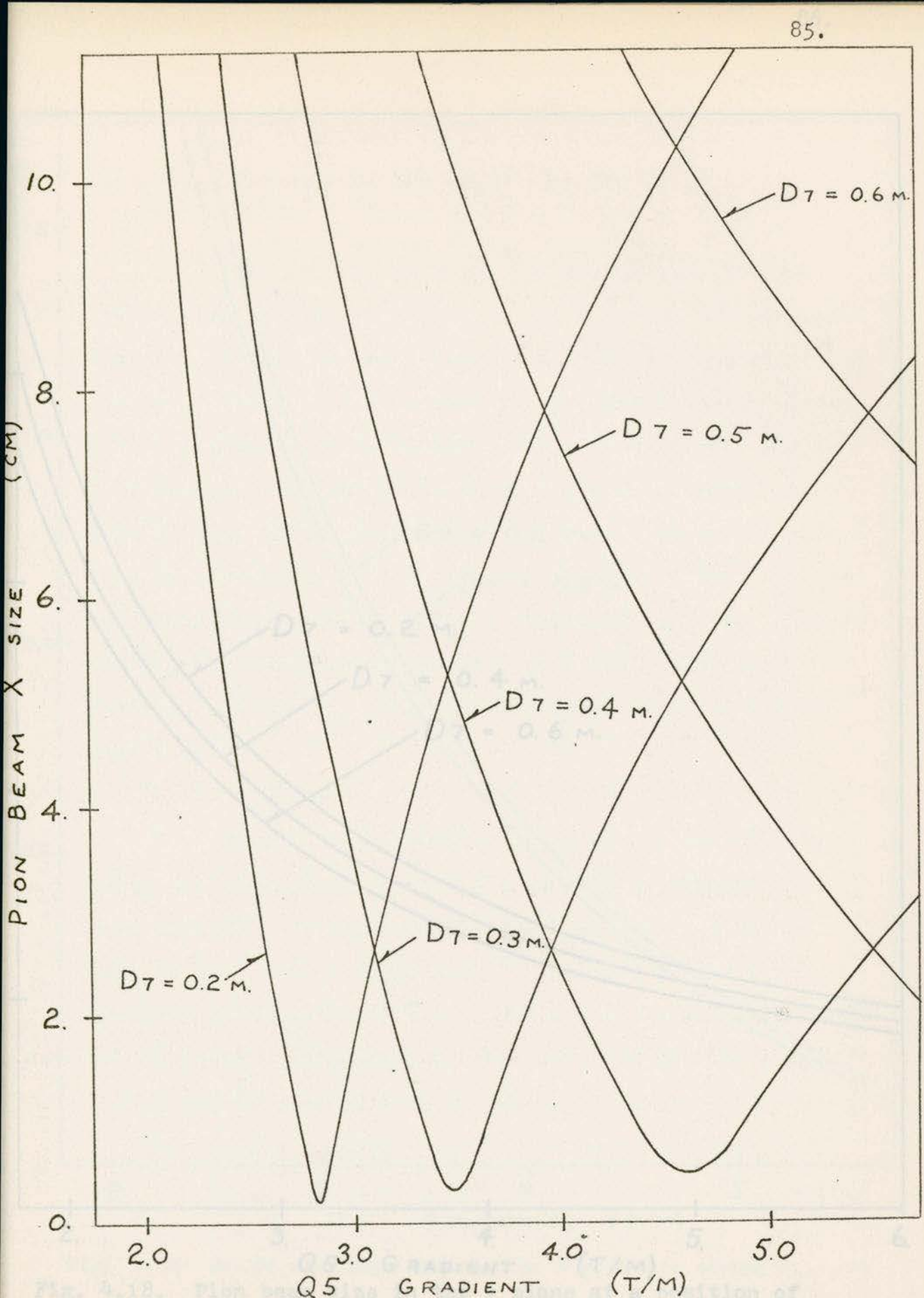

Fig. 4.17 Beam size in the x plane at a position where $R_{33} = 0$ for values of Q5 field gradient and D7 length.

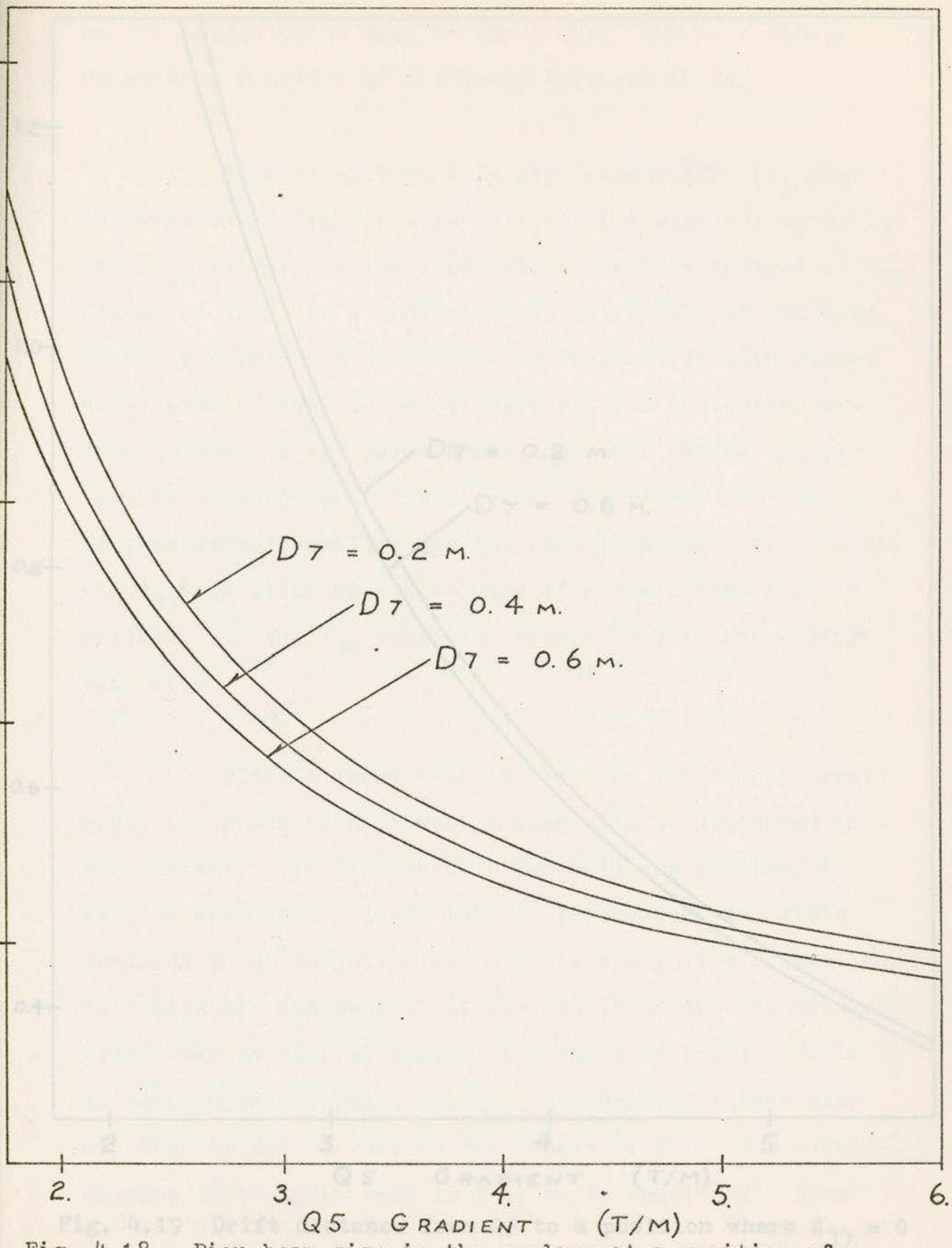

Fig. 4.18. Pion beam size in the y plane at a position of uniformity ($R_{33} = 0$).

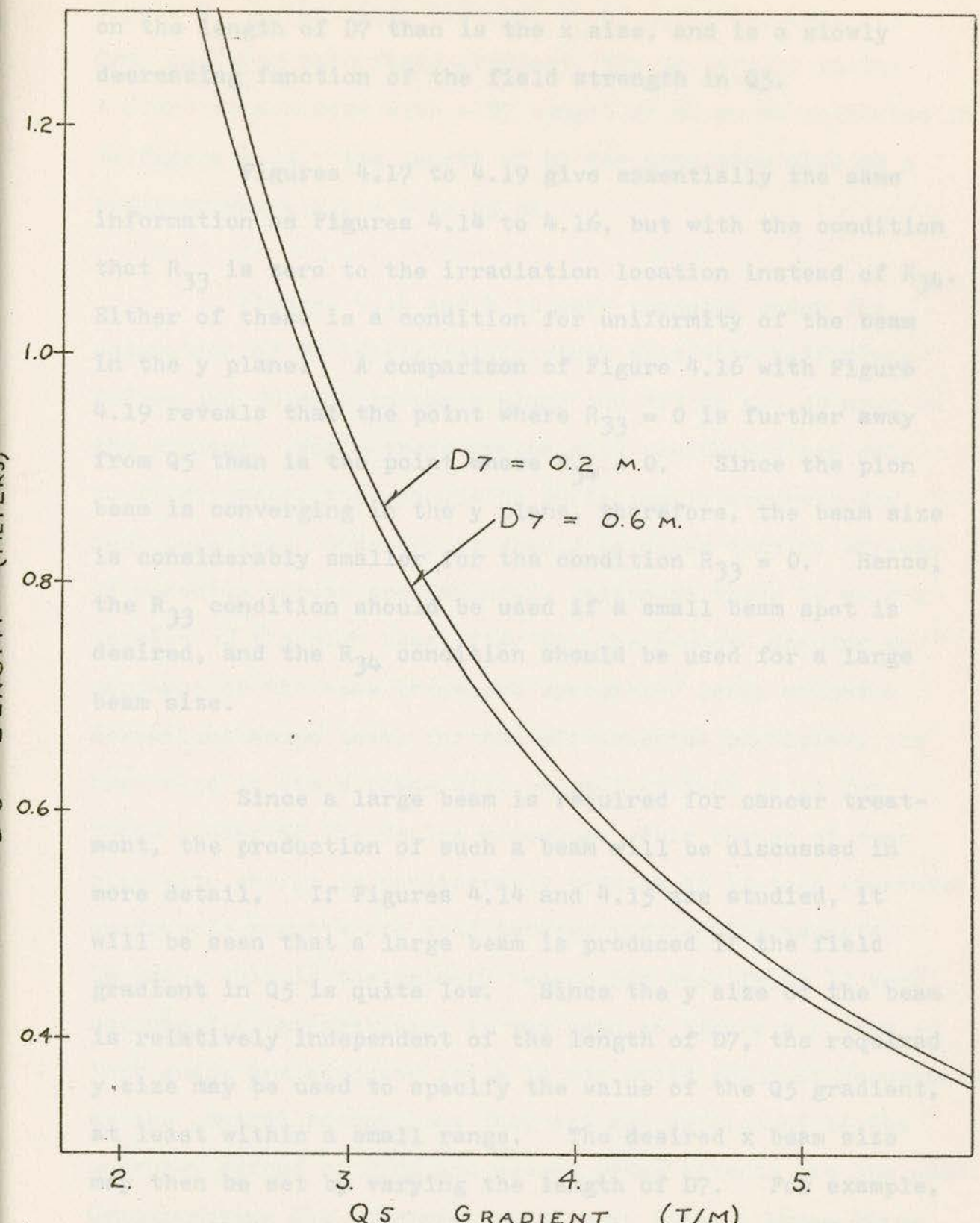

Fig. 4.19 Drift distance from Q5 to a position where $R_{33} = 0$ and the beam is uniform to first order in the y plane.

on the length of D7 than is the x size, and is a slowly decreasing function of the field strength in Q5.

Figures 4.17 to 4.19 give essentially the same information as Figures 4.14 to 4.16, but with the condition that R_{33} is zero to the irradiation location instead of R_{34}. Either of these is a condition for uniformity of the beam in the y plane. A comparison of Figure 4.16 with Figure 4.19 reveals that the point where $R_{33} = 0$ is further away from Q5 than is the point where $R_{34} = 0$. Since the pion beam is converging in the y plane, therefore, the beam size is considerably smaller for the condition $R_{33} = 0$. Hence, the R_{33} condition should be used if a small beam spot is desired, and the R_{34} condition should be used for a large beam size.

Since a large beam is required for cancer treatment, the production of such a beam will be discussed in more detail. If Figures 4.14 and 4.15 are studied, it will be seen that a large beam is produced if the field gradient in Q5 is quite low. Since the y size of the beam is relatively independent of the length of D7, the required y size may be used to specify the value of the Q5 gradient, at least within a small range. The desired x beam size may then be set by varying the length of D7. For example, suppose that a pion beam 10 x 10 cm is required. From

Figure 4.15, the field gradient on Q5 should be near 1.5 T/m, and with this field gradient, the 10 cm size in the x plane is achieved with a D7 length of 44 cm as indicated in in Figure 4.14. The length of D8 for this beam size at a position where $R_{34} = 0$ is 65 cm.

Figures 4.14 and 4.19 were produced under the assumption of an initial ellipsoidal beam with half sizes 0.2 cm and 50 mrad in the x plane and 2.5 cm and 50 mrad in the y plane. While these graphs give the beam sizes only to first order, they should be sufficiently accurate for most purposes. However, it should be noted that no effects of momentum spread are included. Although there is no dispersion of the pion beam after B2, the reduced angular acceptance of the beam transport system for large momentum deviations means that, for the off-momentum particles, the beam size in the x plane will be smaller than it is for those closer to the design momentum. This change of beam size with energy is considerably reduced if 12 inch aperture quadrupole magnets are used between the bending magnets. In fact, this is the primary reason for specifying 12 inch magnets for the triplet. It was seen in Figure 4.2 that 10 inch quads are adequate for a 10 msr solid angle of acceptance at the central energy, but they are not sufficient if the momentum spread of ±10% and second order effects are included. Consequently, the aperture requirement for the three large quadrupoles must be increased to 12 inches.

4.1.4 Tolerance Calculations

One further topic should be discussed before second order effects are studied. Since the computer program TRANS has the facilities necessary for calculating the tolerances on the magnetic fields and the magnet rotations, these specifications will be given here. For further details on the methods of calculation, see Lobb (1972).

For the current tolerances on the quadrupole magnets, the change of beam spot size at the end of the system due to a unit fractional change in the quadrupole excitation current is calculated for each of the quadrupoles in the system. The most critical current supply tolerances are those of quadrupoles Q2, Q3, and Q4. A 1% change in the current results in a change in beam spot size of 6.9% in the x plane for Q2, 6.8% change in the y plane for Q3, and 4.1% change in the x plane for Q4. For the other two quadrupoles, the effect of a 1% current change is less than 2% change in the final beam spot size.

The results for the individual magnets are added in two ways: simple addition to simulate a current change if all of the magnets were run from a single control circuit, and in quadrature to simulate random changes in independent power supplies. In the first case, the result is a 9.5% change of beam spot size in the x plane and 2.8% change in the y plane; in the second, random 1% changes

result in an 8.1% change in the x size, and a 5.6% change in the y size. If all magnets are regulated by a single source, the current variation that would be allowed for a 10% change of beam spot size is ±1.05%; if the magnets have independently regulated power supplies, the RMS current variation allowed is 1.23%.

The effect of varying the current in the bending magnets is not to change the first order beam spot size or the waist positions, but rather to increase the time-average beam spot size due to shifting of the optic axis of the system. If a time-average increase of beam spot size of 10% is allowed, then the bending magnets must have their current regulated to ±0.32%. Current supplies are easily regulated to 0.1%; neither the tolerance on the bending magnet current nor that for the quadrupole current should cause any difficulty.

The quadrupole rotation tolerances are calculated in much the same manner as the current tolerances: each of the quadrupole magnets is separately given a rotation of 1 mrad about the optic axis. Then the change of beam size at the end of the system is calculated for each rotation. The magnets that are most sensitive to rotations are Q2 and Q4. The fractional changes of beam spot size due to 1 mrad rotations are 8.6×10^{-5} and 6.9×10^{-5} respectively, both in the y plane. The RMS total fractional

change in beam spot size due to independent rotations of the quadrupoles is 2.0×10^{-5} in the x plane and 1.1×10^{-4} in the y plane. From these two numbers, the allowed RMS value for the quadrupole for an allowed 10% change in beam spot size is calculated to be 30 mrad (1.7 degrees). This angular alignment tolerance should be very easy to achieve.

In order to calculate the bending magnet rotation tolerances, the bending magnets are given 10 mrad rotations about the optic axis at the entrance of the magnet. The effect of this rotation of B1 is to change the x spot size by only .003% and the y size by .13%; for B2, the rotation causes an increase in the beam size of .02% in both the x and y planes. These changes are completely negligible.

Because of unavoidable asymmetries in the construction of the magnets, all beam transport magnets have a certain amount of higher harmonic magnetic fields such as sextupole, octupole, and higher multipole fields. The method of calculation of the tolerances on the higher harmonics is to trace a number of representative rays through the beam transport system with and without the presence of these higher harmonic fields and to measure the effects of these fields by the changes in the final co-ordinates of these trajectories. The calculations are performed so that the tolerances are upper limits on the sensitivity of the design to the presence of higher harmonic fields.

Because the beam is so large in the x plane inside quadrupole Q2, the final trajectories are most sensitive to higher harmonic error fields in this magnet. A 1% component of a sextupole or higher order multipole field in this magnet as measured at a radius of 4 inches may cause an increase of beam spot size of as much as 7%. For the other magnets, 1% sextupole field in quadrupoles Q3 and Q4 can cause less than 4% change in the final beam size, and in magnets Q1 and Q5, 1% multipole fields increase the beam spot size by less than 1%. Since magnets are commonly designed and built to have their multipole field components less than 1% of the quadrupole field as measured near the full aperture, there should be no problem with the harmonics tolerances on these magnets.

In short, none of the tolerances on the magnet rotations, power supply stability, or higher harmonic field components in the quadrupoles should be at all difficult to meet.

4.2 Second Order Effects.

4.2.1 Rotation of the Momentum Focal Plane

Three important effects in the beam transport system that are attributable to second order aberrations will be discussed in this section. They are: rotation of the momentum focal plane, beam non-uniformity, and variation of the beam size with energy at the irradiation location. The first problem is relatively easy to eliminate, the second is a little more difficult, and the third is one that may not be completely solved. The tilt of the focal plane in the middle of Q2 arises because a magnetic field has less effect on particles with high momentum than it does on those with lower momentum. Because of this effect, a chromatic aberration arises in the quadrupoles and bending magnets that results in an increase of focal length of a magnetic lens with the energy of the particles that are transmitted. The beam is dispersed between the two bending magnets with a focus at the center of Q3, but because the high-momentum particles come to a focus further downstream in the transport system than the low-momentum particles do, the focal plane is no longer perpendicular to the optic axis, but appears rotated as shown in Figure 4.20. Brown (1967) has shown that the angle of rotation of a focal plane can be calculated at a position where $R_{12} = 0$ (as it is in the middle of Q3) from the formula

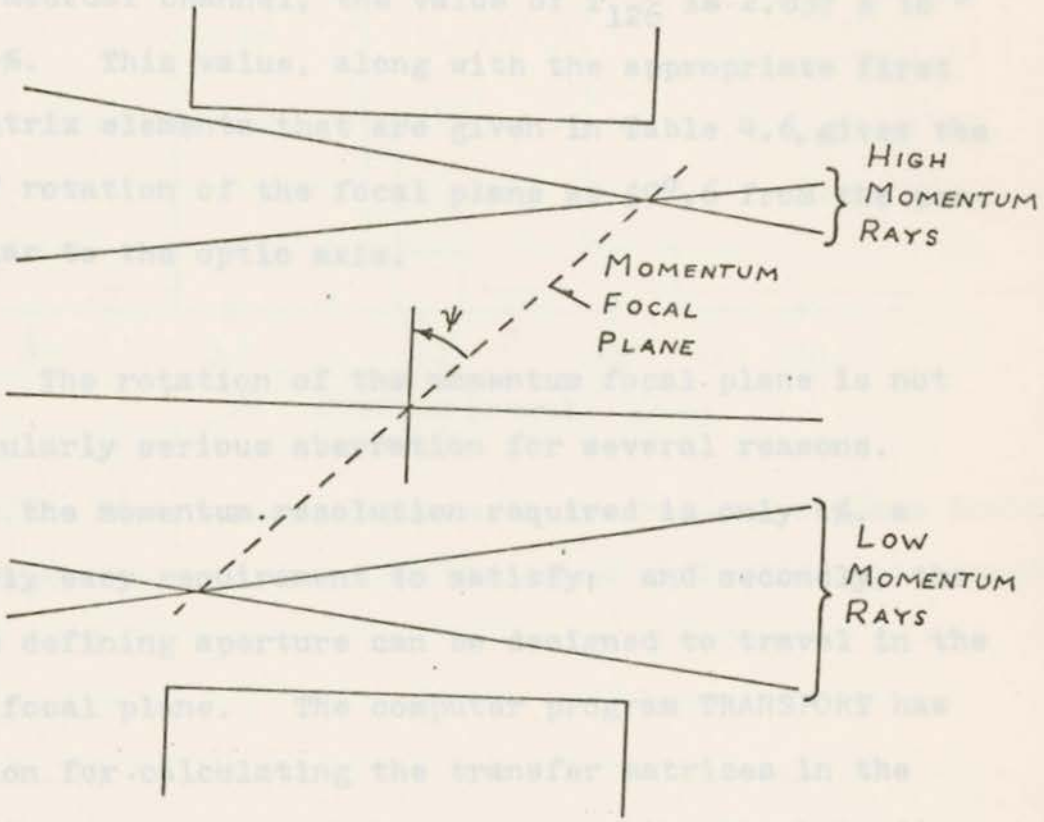

Fig. 4.20 The rotation of the momentum focal plane in Q3.

$$\tan \psi = \frac{T_{126}}{R_{22} R_{16}} \qquad 4.1$$

Recall from Chapter 2 that T_{126} is the Taylor series coefficient giving the change in x due to the product $x'_o \delta_o$. For the medical channel, the value of T_{126} is 2.837×10^{-3} cm/mrad-%. This value, along with the appropriate first order matrix elements that are given in Table 4.6, gives the angle of rotation of the focal plane as $59^{o}.6$ from the perpendicular to the optic axis.

The rotation of the momentum focal plane is not a particularly serious aberration for several reasons. Firstly, the momentum resolution required is only 1%, a relatively easy requirement to satisfy; and secondly, the momentum defining aperture can be designed to travel in the rotated focal plane. The computer program TRANSPORT has the option for calculating the transfer matrices in the rotated focal plane, so that one may examine the beam distribution in this plane with the program NPFLUX. Using this procedure, the x plane histograms of beams with different momenta were calculated to second order with the results shown in Figure 4.21. The two beams are seen to be well separated in space. The resolution due to a momentum defining aperture that travels in the rotated focal plane would be approximately 0.7% of the design momentum.

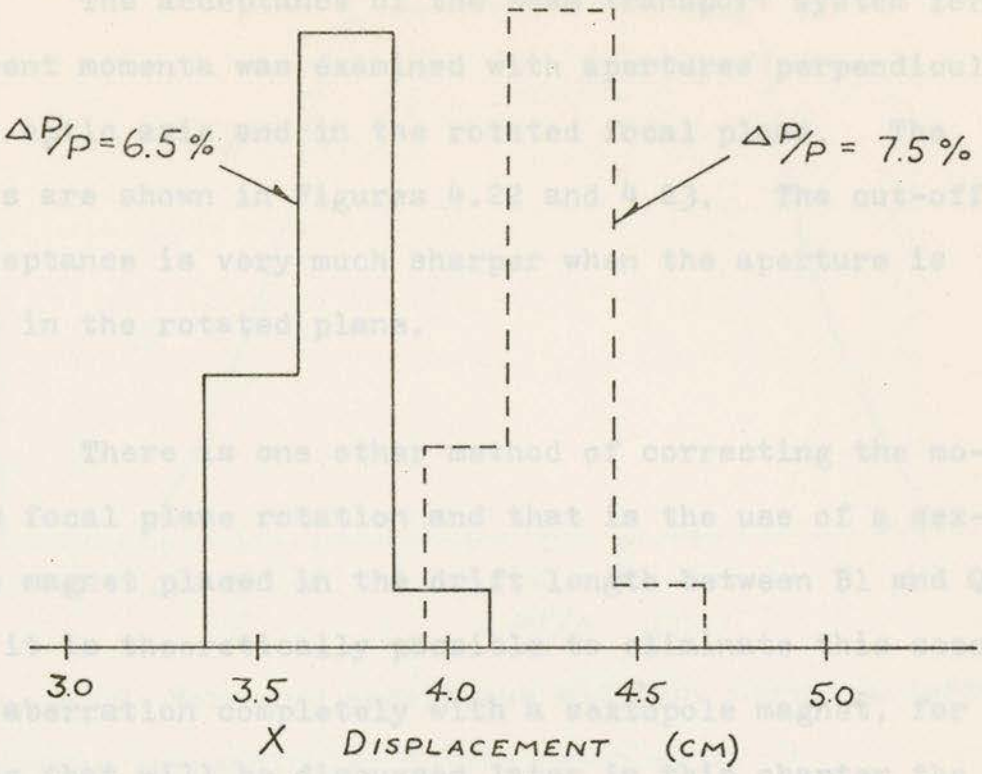

Fig. 4.21 Pion beam histograms in the rotated x plane inside Q3 showing the separation of the beams with different momenta.

The acceptance of the beam transport system for different momenta was examined with apertures perpendicular to the optic axis and in the rotated focal plane. The results are shown in Figures 4.22 and 4.23. The cut-off of acceptance is very much sharper when the aperture is placed in the rotated plane.

There is one other method of correcting the momentum focal plane rotation and that is the use of a sextupole magnet placed in the drift length between B1 and Q2. While it is theoretically possible to eliminate this second order aberration completely with a sextupole magnet, for reasons that will be discussed later in this chapter the recommended design will have a focal plane rotation of approximately 8 degrees. Whether or not sextupole magnets are used in the final design, it has been shown that the required momentum resolution can be achieved with a proper design of the momentum-defining aperture.

4.2.2 Beam Non-uniformity and Its Correction With Curvatures of the Bending Magnet Pole Edges

The second problem mentioned above is that of beam non-uniformity at the irradiation location due to second order aberrations. Whereas the first order histograms of Figures 4.11 and 4.13 show that the beam is uniform to first order, those given in Figures 4.24 and 4.25 show the results of including all second order effects in the beam transport calculations. Compared to the first order results, the

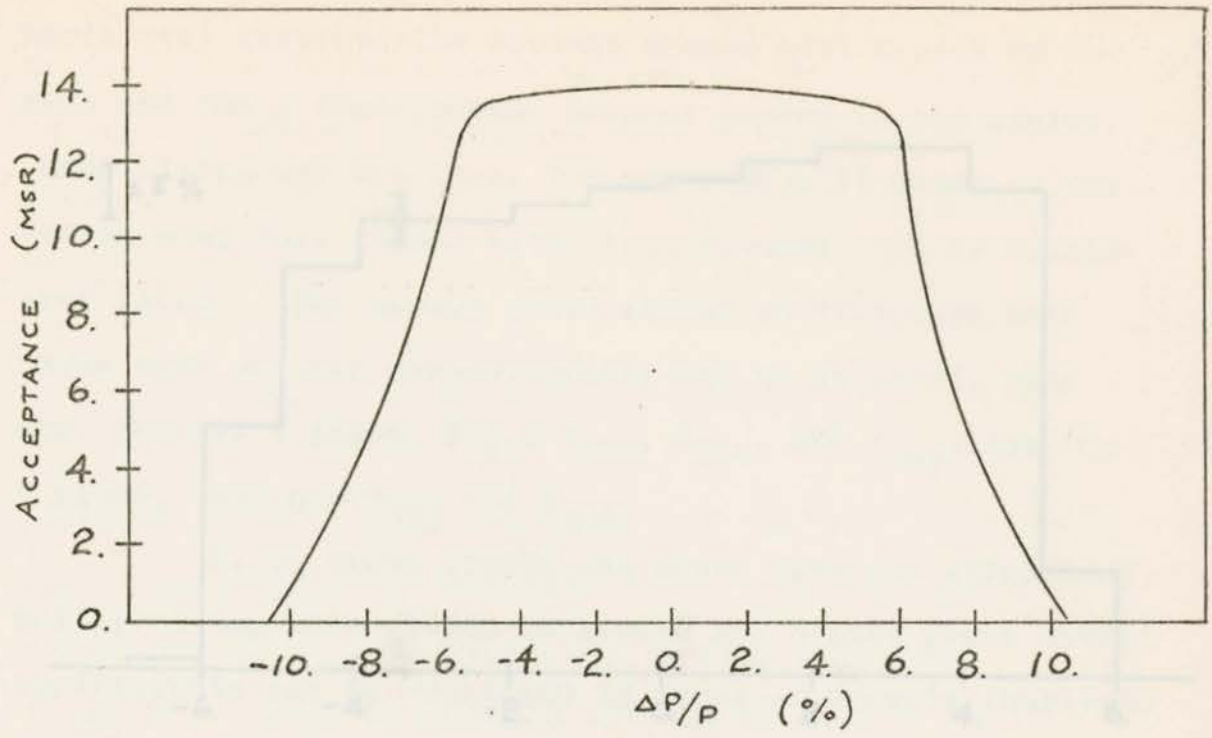

Fig. 4.22 Momentum acceptance with the momentum-defining aperture perpendicular to the optic axis.

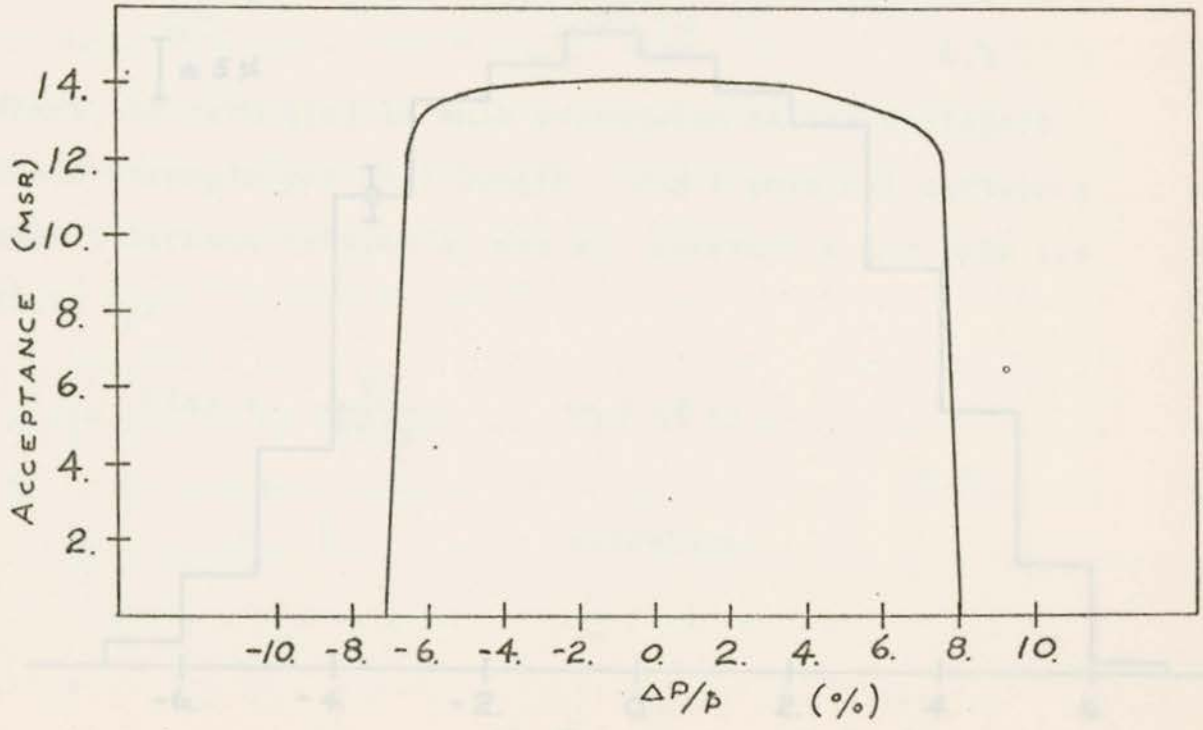

Fig. 4.23 Momentum acceptance with the momentum-defining aperture in the rotated focal plane.

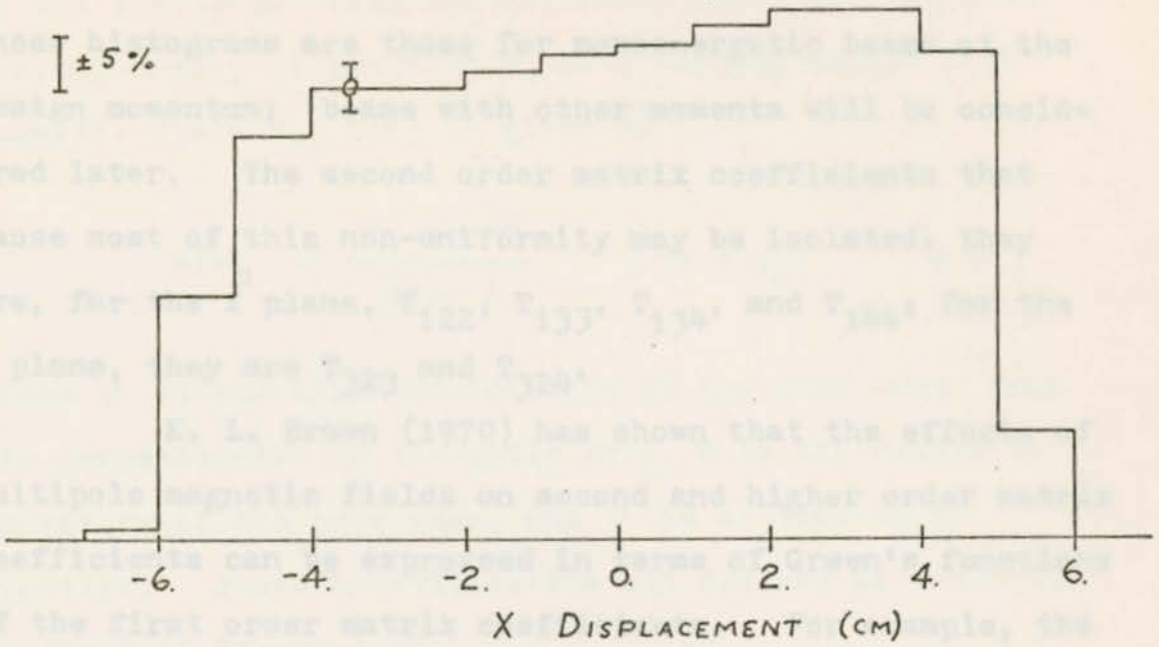

Fig. 4.24 Pion beam distribution at the irradiation location in the x plane (second order).

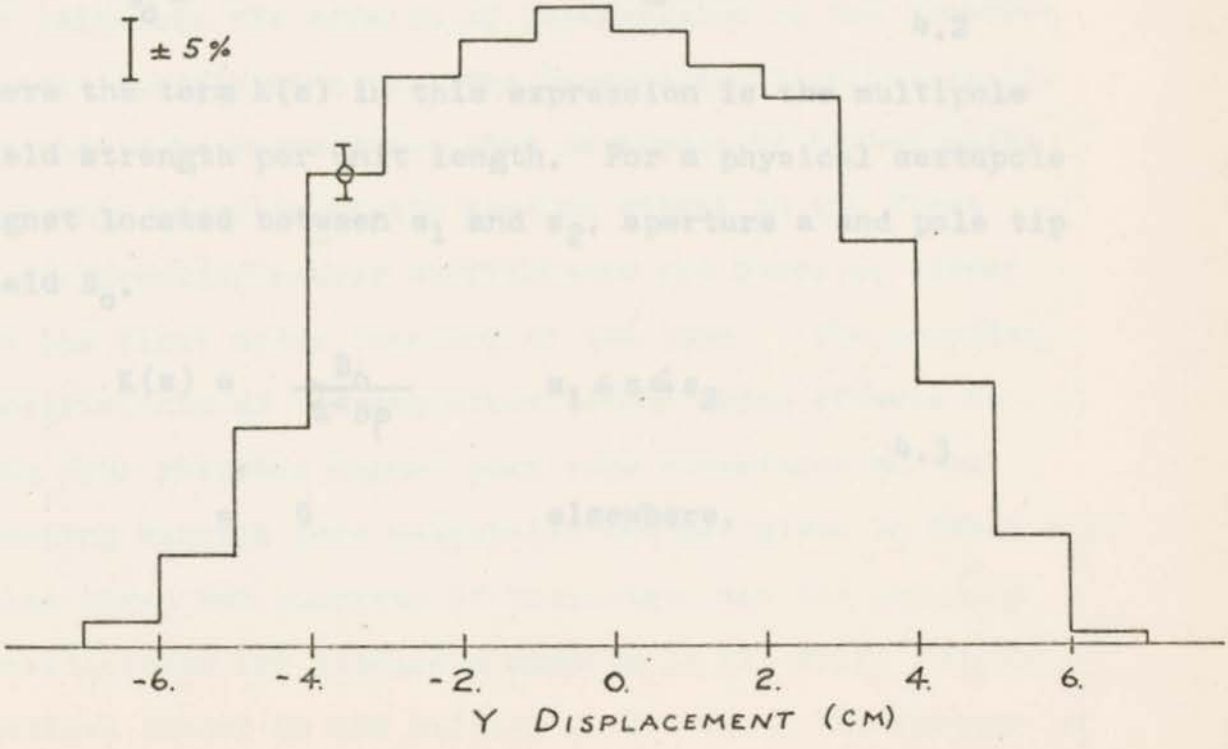

Fig. 4.25 Pion beam distribution in the y plane at the irradiation location (second order).

horizontal distribution becomes skewed with a peak on one side and the y distribution becomes peaked in the center. These histograms are those for monoenergetic beams at the design momentum; beams with other momenta will be considered later. The second order matrix coefficients that cause most of this non-uniformity may be isolated: they are, for the x plane, T_{122}, T_{133}, T_{134}, and T_{144}; for the y plane, they are T_{323} and T_{324}.

K. L. Brown (1970) has shown that the effects of multipole magnetic fields on second and higher order matrix coefficients can be expressed in terms of Green's functions of the first order matrix coefficients. For example, the effect of a sextupole field on the coefficient T_{126} at position t in the system is given by

$$\Delta T_{126} = -\int_0^t \left[R_{12}(t)R_{11}(s) - R_{12}(s)R_{11}(t)\right] R_{12}(s)R_{16}(s)K(s)ds \qquad 4.2$$

where the term K(s) in this expression is the multipole field strength per unit length. For a physical sextupole magnet located between s_1 and s_2, aperture a and pole tip field B_o,

$$K(s) = \frac{B_o}{a^2 B\rho} \qquad s_1 \leq s \leq s_2 \qquad 4.3$$

$$= 0 \qquad \text{elsewhere.}$$

where $B\rho$ is the magnetic rigidity of the particles. If the sextupole field arises from a contoured magnetic field boundary at position S_o on a bending magnet with magnetic field B_o, K(s) is given by

$$K(s) = \frac{B_o \sec^3\beta}{2B\rho\ R} \cdot \delta(s - s_o) \qquad 4.4$$

where β is the angle of rotation of the pole edge from the perpendicular to the optic axis, R is the radius of curvature of the pole edge, and δ is a Dirac delta function. These quantities are all defined as positive as drawn in Figure 4.26.

If it is desired to modify the second order aberrations with sextupole fields, then it is necessary to calculate the effects of these fields on the transfer matrix coefficients from the Green's function integrals. It should be pointed out that sextupole or higher multipolarity magnetic fields have no effect on the first order transfer matrix coefficients and hence no effect on the first order behavior of the beam. The coupling coefficients of the important second order effects to the four possible magnet pole edge curvatures on the bending magnets were calculated and are given in Table 4.7. Also given for purposes of comparison are the coupling coefficients for sextupole magnets in the drift lengths between B1 and Q2 and between Q4 and B2. The changes in

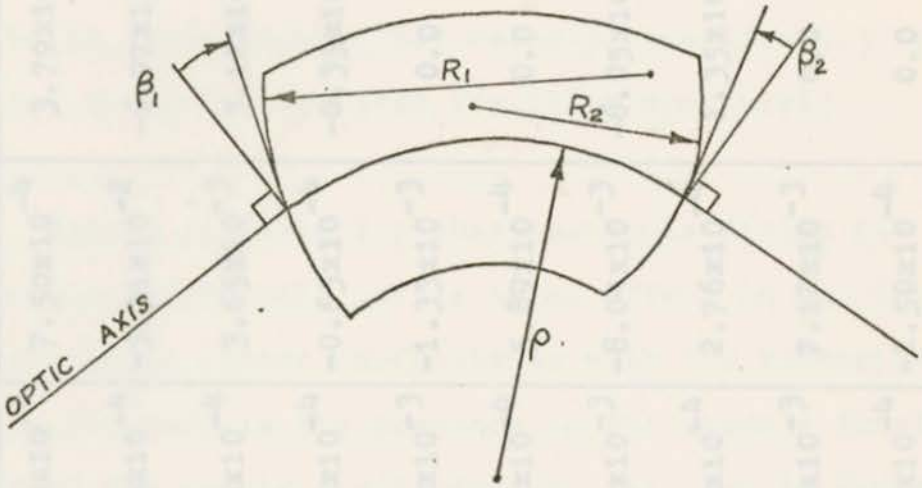

Fig. 4.26 A bending magnet with rotated, curved pole edges. All quantities are defined as positive in the directions shown above.

Matrix coefficient	Uncorrected value	f_1 (C_{11})	f_2 (C_{12})	f_3 (C_{21})	f_4 (C_{22})	f_5 (S_1)	f_6 (S_2)
T_{122}	1.30×10^{-4}	-3.27×10^{-4}	-8.40×10^{-4}	7.50×10^{-4}	3.79×10^{-4}	5.47×10^{-3}	-4.12×10^{-3}
T_{133}	-7.02×10^{-2}	5.35×10^{-3}	4.50×10^{-4}	-5.31×10^{-2}	-6.97×10^{-2}	-5.85×10^{-2}	2.22×10^{-1}
T_{134}	6.47×10^{-3}	1.64×10^{-3}	5.83×10^{-4}	3.65×10^{-3}	3.12×10^{-3}	5.02×10^{-3}	-2.10×10^{-2}
T_{144}	1.32×10^{-4}	1.25×10^{-4}	1.72×10^{-4}	-0.63×10^{-4}	-0.35×10^{-4}	-1.16×10^{-3}	4.96×10^{-4}
T_{126}	-1.73×10^{-2}	0.0	-1.49×10^{-3}	-1.33×10^{-3}	0.0	2.43×10^{-2}	1.82×10^{-2}
T_{166}	-7.27×10^{-3}	0.0	-6.59×10^{-4}	5.89×10^{-4}	0.0	2.72×10^{-2}	-2.04×10^{-2}
T_{323}	-1.27×10^{-2}	-3.68×10^{-3}	-1.14×10^{-3}	-8.04×10^{-3}	-6.05×10^{-3}	-9.13×10^{-3}	5.07×10^{-2}
T_{324}	-5.58×10^{-4}	-5.63×10^{-4}	-6.79×10^{-4}	2.76×10^{-4}	1.35×10^{-4}	4.23×10^{-3}	-2.40×10^{-3}
T_{336}	-7.46×10^{-2}	0.0	-1.01×10^{-3}	7.12×10^{-3}	0.0	-2.08×10^{-2}	-1.13×10^{-1}
T_{346}	1.09×10^{-2}	0.0	-6.00×10^{-4}	-2.50×10^{-4}	0.0	9.38×10^{-3}	5.35×10^{-3}

Table 4.7 The coupling coefficients of the second order matrix elements to the sextupole fields.

the second order aberrations can be calculated from the coefficients in this table with the formula

$$T_{1mn} = f_1 c_{11} + f_2 c_{12} + f_3 c_{21} + f_4 c_{22} + f_5 s_1 + f_6 s_2 \qquad 4.5$$

where f_i are the coupling coefficients of T_{1mn} to the sextupole fields, c_{ij} is the curvature (1/radius in meters) of the j'th edge of the i'th bending magnet, and s_i is the pole tip field of the i'th sextupole magnet (aperture assumed to be 10 cm radius, but refer to Equation 4.3 for calculating the pole-tip field for other apertures).

Notice in Table 4.7 that sextupole fields due to pole edge curvatures have little or no effect on the chromatic aberrations (those coefficients with the subscript 6). The reason for this is the presence in the Green's function integrals of the matrix coefficient R_{16} as seen in Equation 4.2. Since this first order coefficient is zero everywhere except between B1 and B2, a sextupole magnetic field must be placed between the two bends to have any effect on chromatic aberrations. At the entrance of B1 and the exit of B2, $R_{16} = 0$, and at the exit of B1 and the entrance of B2, R_{16} is very small. For this reason, the effects of pole edge curvatures on the chromatic aberrations are negligible. Sextupole magnets must be used if these aberrations are to be modified.

Neglecting the possible use of sextupole magnets for the moment, let us examine the possibilities of correcting some of the second order abberations with the use of pole edge curvatures alone. With just four variables available, it is obviously impossible to eliminate all of the second order coefficients, so we must try to eliminate the worst effects and hope that the others do not get out of hand.

There are many ways of attacking the problem of minimizing six functions of four variables. The most successful method seems to be to choose the three most sensitive functions (second order matrix coefficients) and set them equal to zero with the added constraint that the maximum curvature is a minimum. This last condition assures that the solution will be physically possible. Another reason for formulating the problem this way is that it allows a straightforward graphical solution. For example, setting T_{122}, T_{323} and T_{324} equal to zero at the position of a 10 x 10 cm beam spot requires $C_{11} = -1.063$, $C_{12} = -.366$, $C_{21} = -1.063$, and $C_{22} = .030$. The minimum radius of curvature for this solution is approximately 95 cm, a mild curvature for a bending magnet with bending radius 69 cm.

The results of a second order calculation using these curvatures are much better than expected: in addition

to the three coefficients mentioned, several others (including T_{144}, T_{244} and T_{424}) are much smaller than before, while none of the other coefficients are significantly worse than with no pole edge curvatures at all. The beam histograms shown in Figures 4.27 and 4.28 demonstrate that the beam is almost completely uniform in both planes. In fact, the distributions are every bit as good as the first order histograms in Figures 4.11 and 4.13.

This is not to suggest, however, that pole edge curvatures on the bending magnets are the solution to all of our problems. For one thing, the second order effects have been minimized for one particular beam size and position. If the field gradient of Q5 is changed, or if Q5 is moved farther from B2 to change the beam size at the irradiation location, the aberrations may be as large as or larger than those with no pole edge curvatures. Since the curvatures result from metal shims placed on the bending magnets, which themselves will be buried in concrete shielding, there will be no way of changing the curvatures once they are installed.

This situation is not completely unacceptable because there are other ways of varying the beam size. Moveable apertures may be placed at several places in the beam transport system similar to the aperture that limits the beam divergence in the y plane that was placed between B1

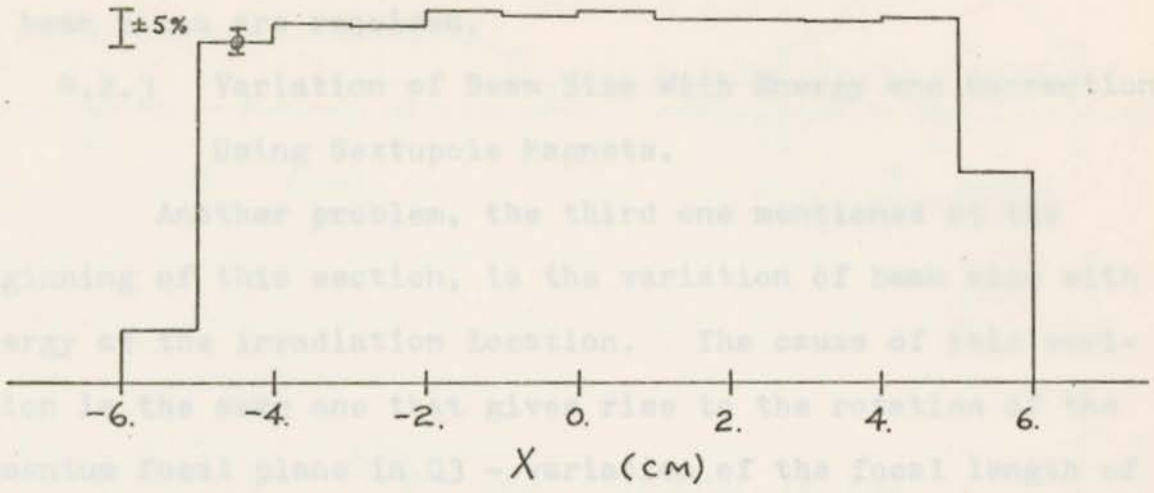

Fig. 4.27 Pion distribution in the x plane with second order correction using curved pole edges on the bending magnets.

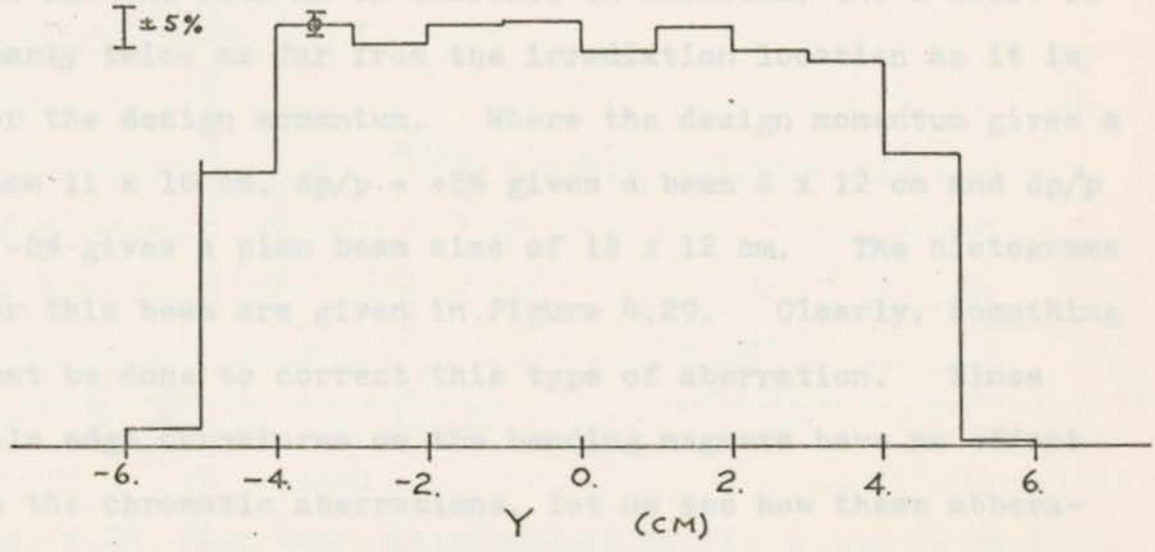

Fig. 4.28 Pion distribution in the y plane at the irradiation location after correction with curved pole edges.

and Q2. Such slits to limit the beam size would mean some loss of intensity, especially for smaller beam sizes, because they would intercept much of the pion beam when smaller beam sizes are required.

4.2.3 Variation of Beam Size With Energy and Correction Using Sextupole Magnets.

Another problem, the third one mentioned at the beginning of this section, is the variation of beam size with energy at the irradiation location. The cause of this variation is the same one that gives rise to the rotation of the momentum focal plane in Q3 - variation of the focal length of a focussing magnet with the momentum of the beam that is being transmitted. For the design momentum, the pion beam is roughly parallel in the y plane but is diverging quite strongly from the narrow waist in the x plane some distance before the irradiation location. For a beam with an 8% increase in momentum, the x waist occurs almost at the irradiation location, and for one with an 8% decrease in momentum, the x waist is nearly twice as far from the irradiation location as it is for the design momentum. Where the design momentum gives a beam 11 x 10 cm, $dp/p = +8\%$ gives a beam 2 x 12 cm and $dp/p = -8\%$ gives a pion beam size of 18 x 12 cm. The histograms for this beam are given in Figure 4.29. Clearly, something must be done to correct this type of aberration. Since pole edge curvatures on the bending magnets have no effect on the chromatic aberrations, let us see how these abberations can be corrected with sextupole magnets.

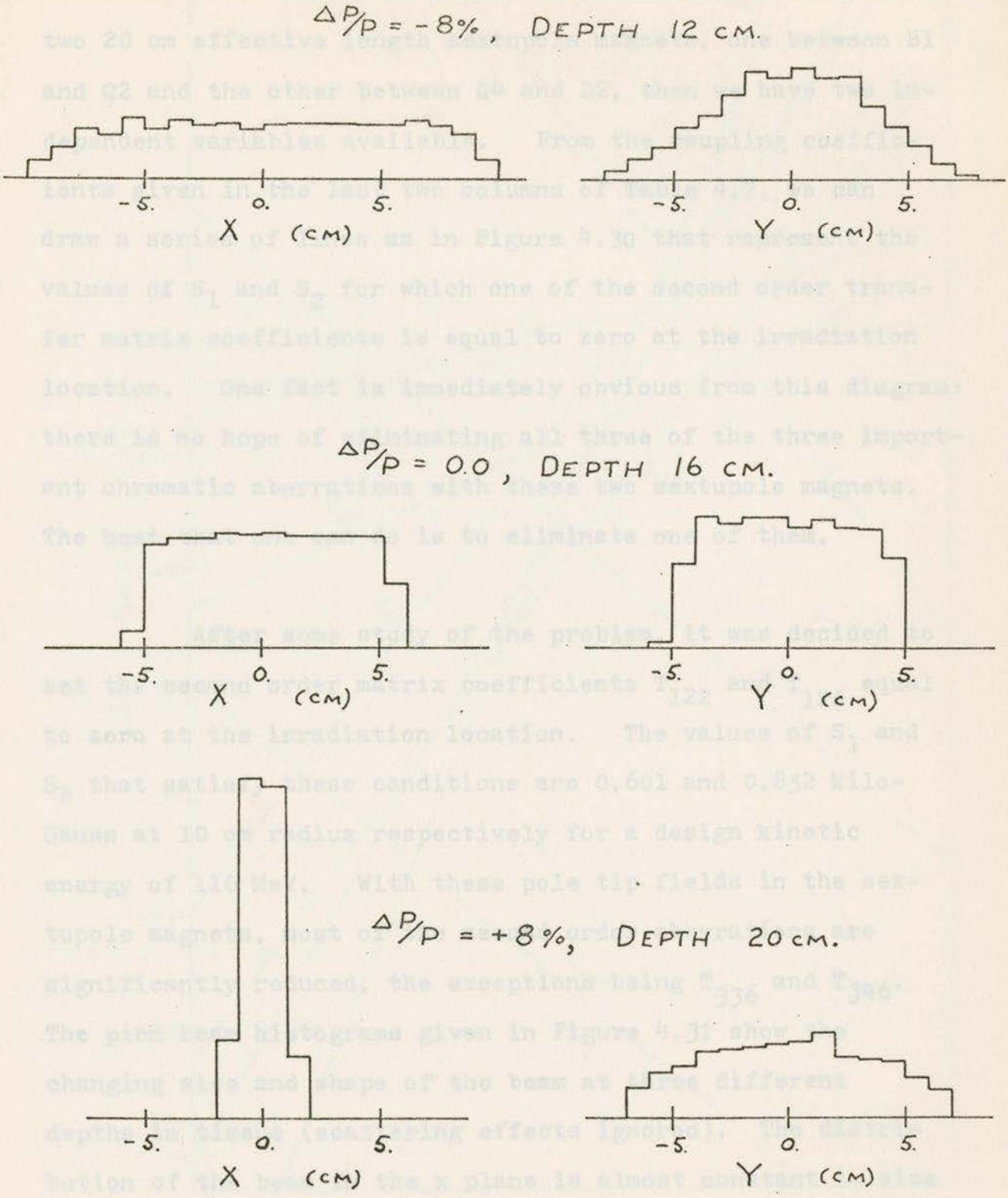

Fig. 4.29 Pion beam distributions at 12, 16 and 20 cm depth with correction of some second order aberrations with pole-edge curvatures.

If we assume no second order correction other than two 20 cm effective length sextupole magnets, one between B1 and Q2 and the other between Q4 and B2, then we have two independent variables available. From the coupling coefficients given in the last two columns of Table 4.7, we can draw a series of lines as in Figure 4.30 that represent the values of S_1 and S_2 for which one of the second order transfer matrix coefficients is equal to zero at the irradiation location. One fact is immediately obvious from this diagram: there is no hope of eliminating all three of the three important chromatic aberrations with these two sextupole magnets. The best that one can do is to eliminate one of them.

After some study of the problem, it was decided to set the second order matrix coefficients T_{122} and T_{126} equal to zero at the irradiation location. The values of S_1 and S_2 that satisfy these conditions are 0.601 and 0.852 kilo-Gauss at 10 cm radius respectively for a design kinetic energy of 110 MeV. With these pole tip fields in the sextupole magnets, most of the second order aberrations are significantly reduced, the exceptions being T_{336} and T_{346}. The pion beam histograms given in Figure 4.31 show the changing size and shape of the beam at three different depths in tissue (scattering effects ignored). The distribution of the beam in the x plane is almost constant in size and nearly uniform at all depths, while the beam spreads

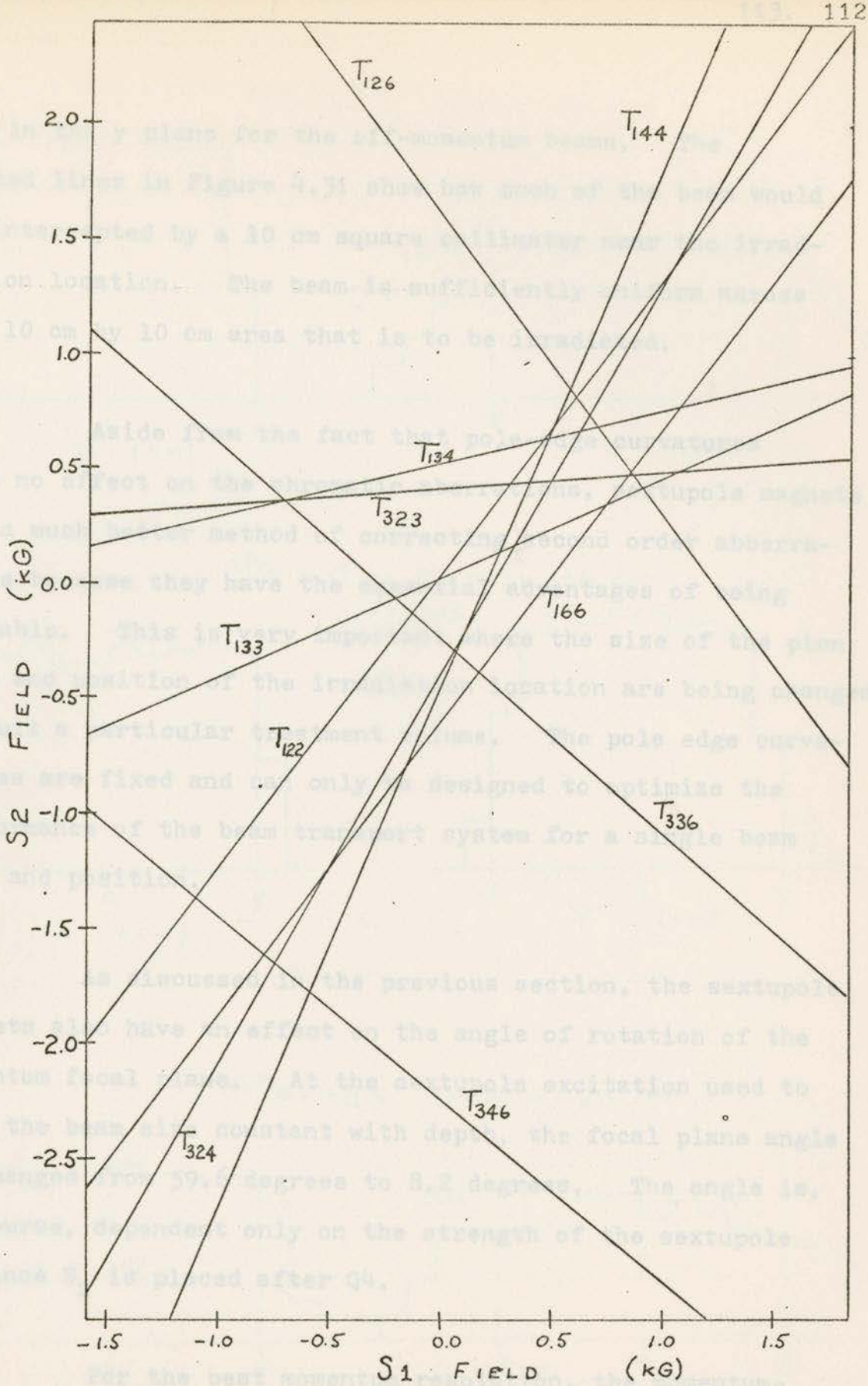

Fig. 4.30 The elimination of second order aberrations using sextupole magnets. Along each of the lines, one of the second order matrix coefficients is equal to zero.

out in the y plane for the off-momentum beams. The dotted lines in Figure 4.31 show how much of the beam would be intercepted by a 10 cm square collimator near the irradiation location. The beam is sufficiently uniform across the 10 cm by 10 cm area that is to be irradiated.

Aside from the fact that pole-edge curvatures have no effect on the chromatic aberrations, sextupole magnets are a much better method of correcting second order abberrations because they have the essential advantages of being variable. This is very important where the size of the pion beam and position of the irradiation location are being changed to suit a particular treatment volume. The pole edge curveatures are fixed and can only be designed to optimize the performance of the beam transport system for a single beam size and position.

As discussed in the previous section, the sextupole magnets also have an effect on the angle of rotation of the momentum focal plane. At the sextupole excitation used to make the beam size constant with depth, the focal plane angle is changed from 59.6 degrees to 8.2 degrees. The angle is, of course, dependent only on the strength of the sextupole S_1 since S_2 is placed after Q4.

For the best momentum resolution, the momentum-defining aperture should be placed exactly in the focal plane,

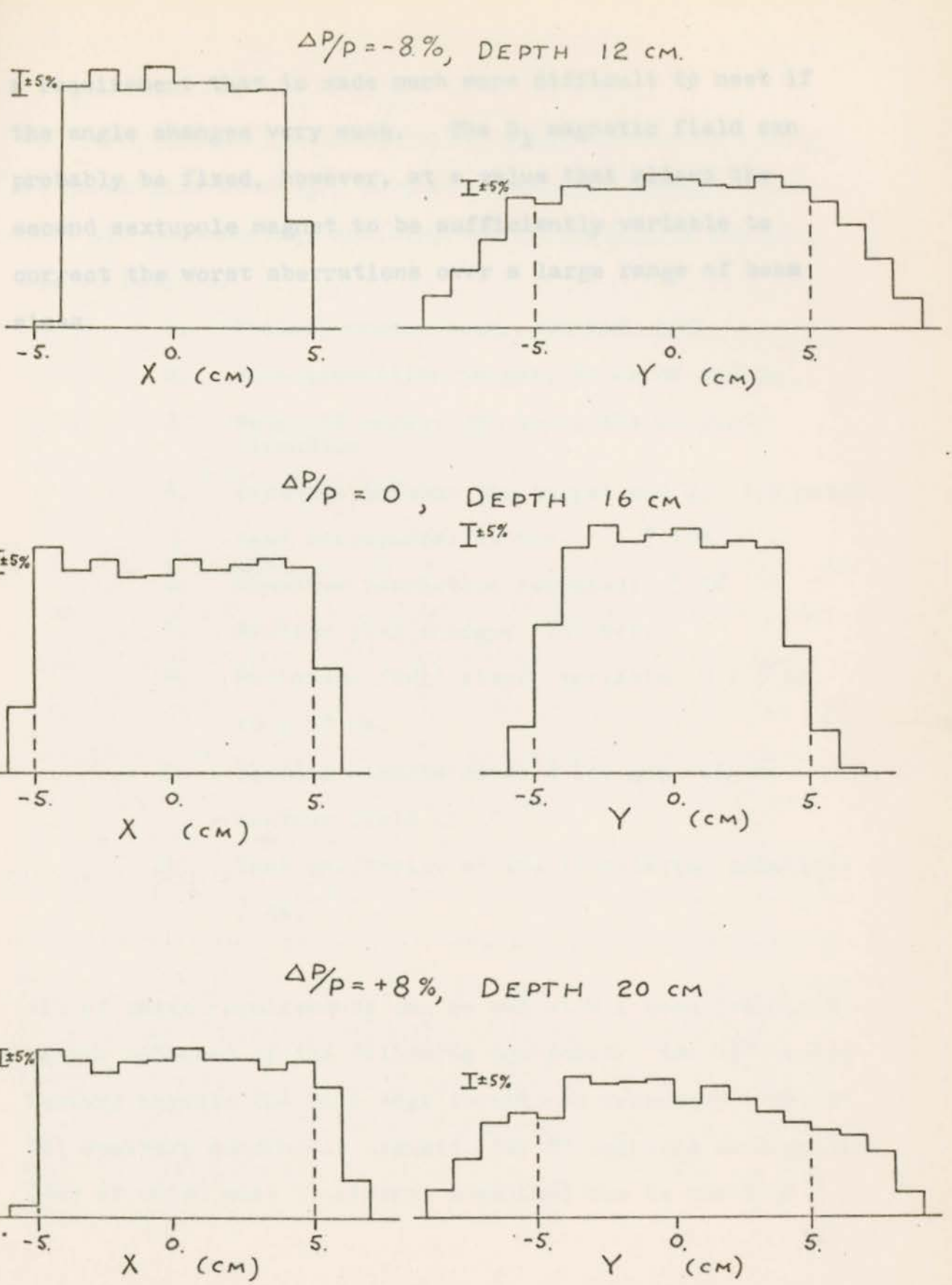

Fig. 4.31 Pion beam distributions at depths of 12, 16 and 20 cm after correction with two sextupole magnets. No pole edge curvatures are used.

a requirement that is made much more difficult to meet if the angle changes very much. The S_1 magnetic field can probably be fixed, however, at a value that allows the second sextupole magnet to be sufficiently variable to correct the worst aberrations over a large range of beam sizes.

5. SUMMARY AND CONCLUSIONS

The design criteria for a beam transport system to transmit a secondary beam of negatively charged pions into the Radiobiology-Radiotherapy Laboratory at TRIUMF are as follows:

1. Primary proton beam: 500 MeV, 100 A.
2. Pion production target: 10 cm of carbon
3. Take-off angle: 30° above the forward direction
4. Distance between the target and Q1: 1.0 meter
5. Beam acceptance: 10 msr, $= \pm 10\%$
6. Momentum resolution required: $\pm 1\%$
7. Maximum pion energy: 110 MeV.
8. Radiation field size: variable, 3 x 3 to 10 x 10 cm.
9. Bending magnets used: 6 in. gap height, maximum field 10 kG.
10. Beam uniformity at the irradiation location: $\pm 5\%$.

All of these requirements can be met with a beam transport system composed of the following equipment; two 45° sector bending magnets (no pole edge curvatures necessary), three 12" aperture quadrupole magnets, two 8" aperture quadrupoles (one of which must be mineral insulated due to the high

radiation field near the production target), two sextupole magnets with effective length 20 cm, and three adjustable beam limiting apertures. One of these apertures is to be in the x plane in the momentum focal plane inside quadrupole Q3 to define the pion momentum range transmitted, one is to be placed in the y plane between B1 and Q2 (possibly inside sextupole S1) to improve the uniformity of the beam and to regulate intensity, and the third will be located near the irradiation location to define the final pion beam size in both the x and y planes.

The length of the beam transport system is approximately 7.0 meters, which implies a 50% loss of beam intensity at 80 MeV due to in-flight decay of the pions before they reach the irradiation location. This position is 6.9 feet above the proton beam at a perpendicular distance of 13.7 feet, 12.0 feet downstreat of target T3. According to Batho(1970), the floor level of the Radiation Laboratory is at an elevation of 270.75 feet and the elevation of the proton beam is 268.5 feet, so that the irradiation location is 4.6 feet above the floor of the laboratory. This height is equal to the maximum allowable height if a 12" false floor is installed; if for any reason the beam transport system before B2 must be lengthened, a smaller take-off angle may be necessary to reduce the height of the irradiation location.

The last quadrupole magnet before the end of the transport system, Q5, should have a range of movement of 40 cm to provide a continuous range of beam sizes. Since the shielding around the target T3 extends to 12 feet from the proton line, Q5 will be entirely embedded inside the shielding, as shown in Figure 5.1. The irradiation location will vary from 1.3 to 3.6 feet from the wall, depending on the beam size required.

Much work remains to be done on the design. Some changes will be necessary as designs are chosen for the beam transport magnets. One of the most critical areas of the design in this respect is the first two magnets, Q1 and B1. The effective length of Q1 should be increased somewhat so that the magnetic field can be made more uniform. In all of the beam transport calculations performed so far, "hard-edge" fields have been assumed. A hard-edge field is one that assumes some constant value over a specified interval, and is equal to zero outside this region. Since a magnetic field always takes some distance for the transition from maximum field to zero, the hard-edge model is necessarily an approximation to physical reality. It has been suggested (Alexander and Reeve (1971)) that this assumption should be carefully checked with computer programs capable of simulating "soft-edge" magnetic fields, possibly using field data measured from existing magnets.

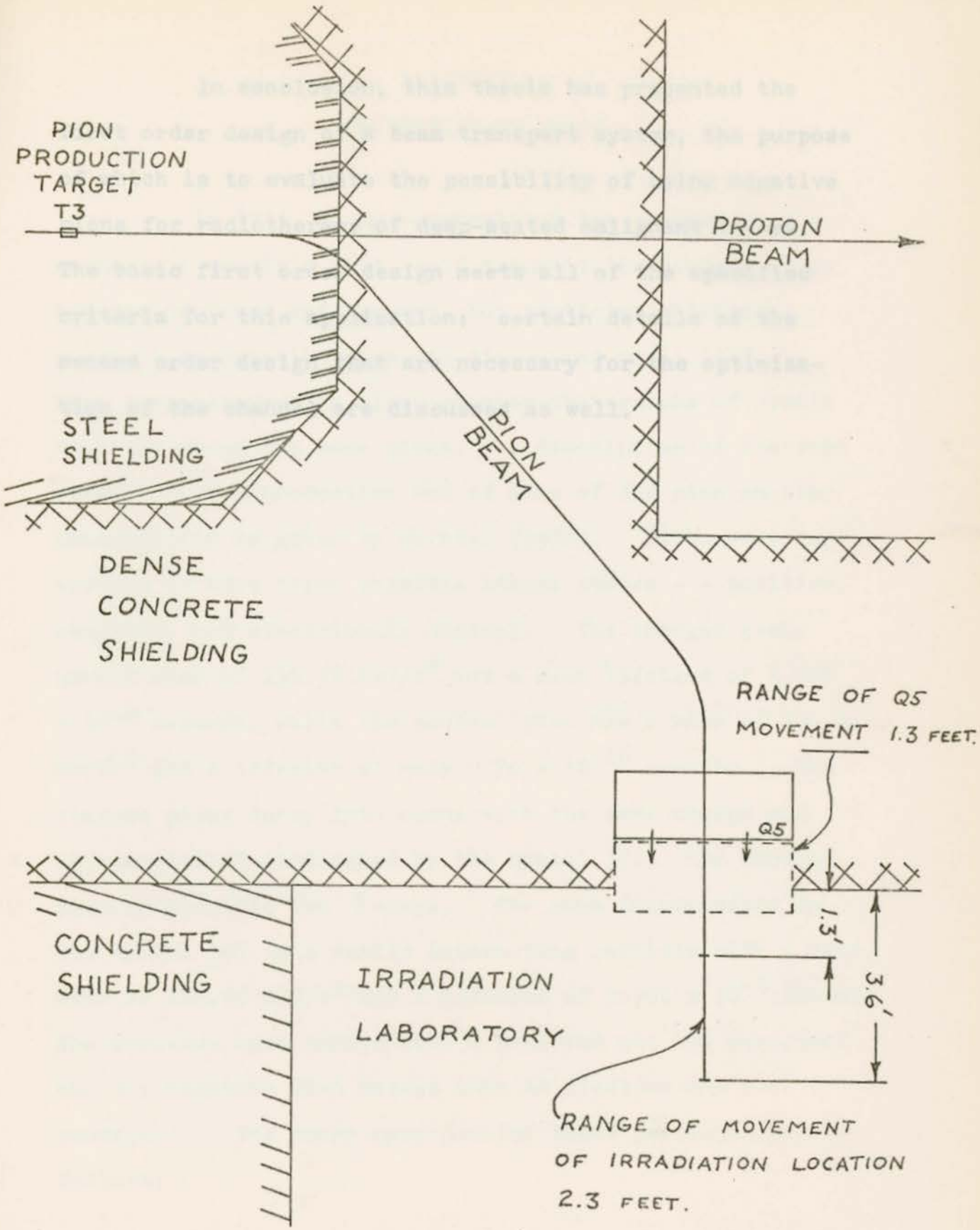

Figure 5.1 The position and range of movement of Q5 and the irradiation location relative to the shielding around target T3.

In conclusion, this thesis has presented the first order design of a beam transport system, the purpose of which is to evaluate the possibility of using negative pions for radiotherapy of deep-seated malignant tumors. The basic first order design meets all of the specified criteria for this application; certain details of the second order design that are necessary for the optimization of the channel are discussed as well.

APPENDIX I

PROPERTIES OF PIONS

In 1935, H. Yukawa predicted the existence of a subnuclear particle that could transmit the nuclear force between neutrons and protons, but particles matching Yukawa's description were not discovered until 1947. They were observed in cloud chamber photographs of cosmic rays and given the name pions. A description of the processes of pion production and of some of the pion nuclear interactions is given by Marshak (1952). Pions were discovered to have three possible charge states - - positive, negative, and electrically neutral. The charged pions have a mass of 139.58 MeV/c^2 and a mean lifetime of 2.604 x 10^{-8} seconds, while the neutral pion has a mass of 134.97 MeV/c^2 and a lifetime of only 0.76 x 10^{-16} seconds. The charged pions decay into muons with the same charge and into neutrinos (indicated by the symbol ν); the neutral pion decays into two γ-rays. The muon (represented by the symbol μ) is a weakly interacting particle with a rest mass of 105.66 MeV/c^2 and a lifetime of 2.198 x 10^{-6} seconds. The positive muon decays into a positron and two neutrinos and the negative muon decays into an electron and two neutrinos. The decay equations for these particles are as follows:

$$\pi^+ \longrightarrow \mu^+ + \nu \qquad \text{I.1a}$$

$$\pi^- \longrightarrow \mu^- + \nu \qquad \text{I.1b}$$

$$\pi^\circ \longrightarrow \gamma + \gamma \qquad \text{I.1c}$$

$$\mu^+ \longrightarrow e^+ + \nu + \bar{\nu} \qquad \text{I.1d}$$

$$\mu^- \longrightarrow e^- + \nu + \bar{\nu} \qquad \text{I.1e}$$

The symbol $\bar{\nu}$ represents an antineutrino. The most recent measurements of the properties of these particles may be found in the Review of Particle Properties (1970).

In spite of the very short lifetime that pions have, they may be created with velocities large enough that a sufficient fraction of them arrives at the end of a beam transport system before they decay. The number of pions that survive a given flight distance can be calculated using the formulae of relativistic kinematics. The symbols that will be used are;

e = 2.7183, the base of natural logarithms

c = the velocity of light in vacuum (meters per second)

β = the ratio of the velocity of the particle to the velocity of light in vacuum.

m = the rest mass of the particle (MeV/c^2)

t = the mean particle lifetime (sec.)

T = particle kinetic energy (MeV)

P = Particle momentum (MeV/c)

F = fraction of particles that does not decay.

L = length of the flight path (meters)

D = decay length (meters)

$B\rho$ = magnetic rigidity (Tesla-meters)

The relativistic time dilation factor γ is found from

$$\gamma = \frac{T}{mc^2} + 1 \qquad \text{I.2}$$

and from this factor, the velocity of the particle can be found from

$$\beta = \frac{\sqrt{\gamma^2-1}}{\gamma} \qquad \text{I.3}$$

That mean lifetime, which is the time taken to reduce the particle number by a factor of 1/e, is lengthened due to the relativistic velocities at which the pions travel, so the relativistic decay length, which is the distance travelled in one mean lifetime, is found from Equation I-4.

$$D = \beta c \gamma t \qquad \text{I.4}$$

To calculate the fraction of pions that survives for a given

distance, L, one must use the equation

$$F = e^{-\frac{L}{D}} \qquad \text{I.5}$$

These relations have been used to calculate values of γ, D and F for a 7.0 meter flight path for pion energies between 10 and 150 MeV for Table I.1. The mean decay length and the fraction of pions that survives to the end of a seven meter beam transport system are plotted as functions of pion kinetic energy in Figures I.1 and I.2. The distance seven meters was chosen because the pion channel for the TRIUMF Medical Facility is approximately seven meters in length.

Also useful for some purposes are values for the momentum (P), the magnetic rigidity ($B\rho$), and the ratio of the particle's velocity to that of light in vacuum (β). These quantities are calculated from the formulas

$$P = c\beta m\gamma \qquad \text{I.6}$$

and

$$B = \frac{P \times 10^6}{c} \qquad \text{I.7}$$

and are given for a range of values of pion kinetic energy in Table I.2. The magnetic rigidity of a particle is equal to the product of the radius of curvature of a particle's trajectory in a magnetic field and the magnitude of the

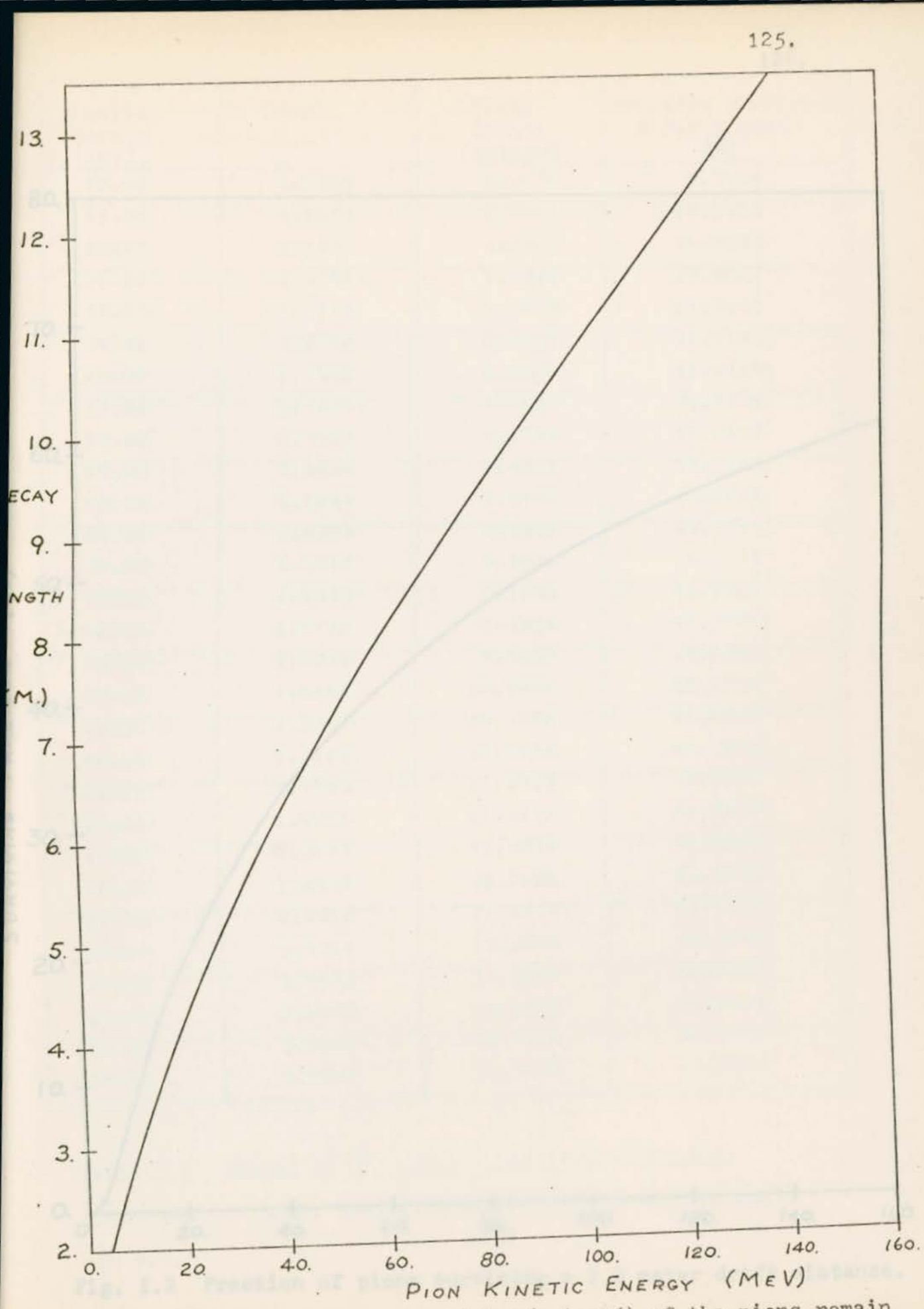

Fig. I.1 Mean distance at which 1/e (=37%) of the pions remain

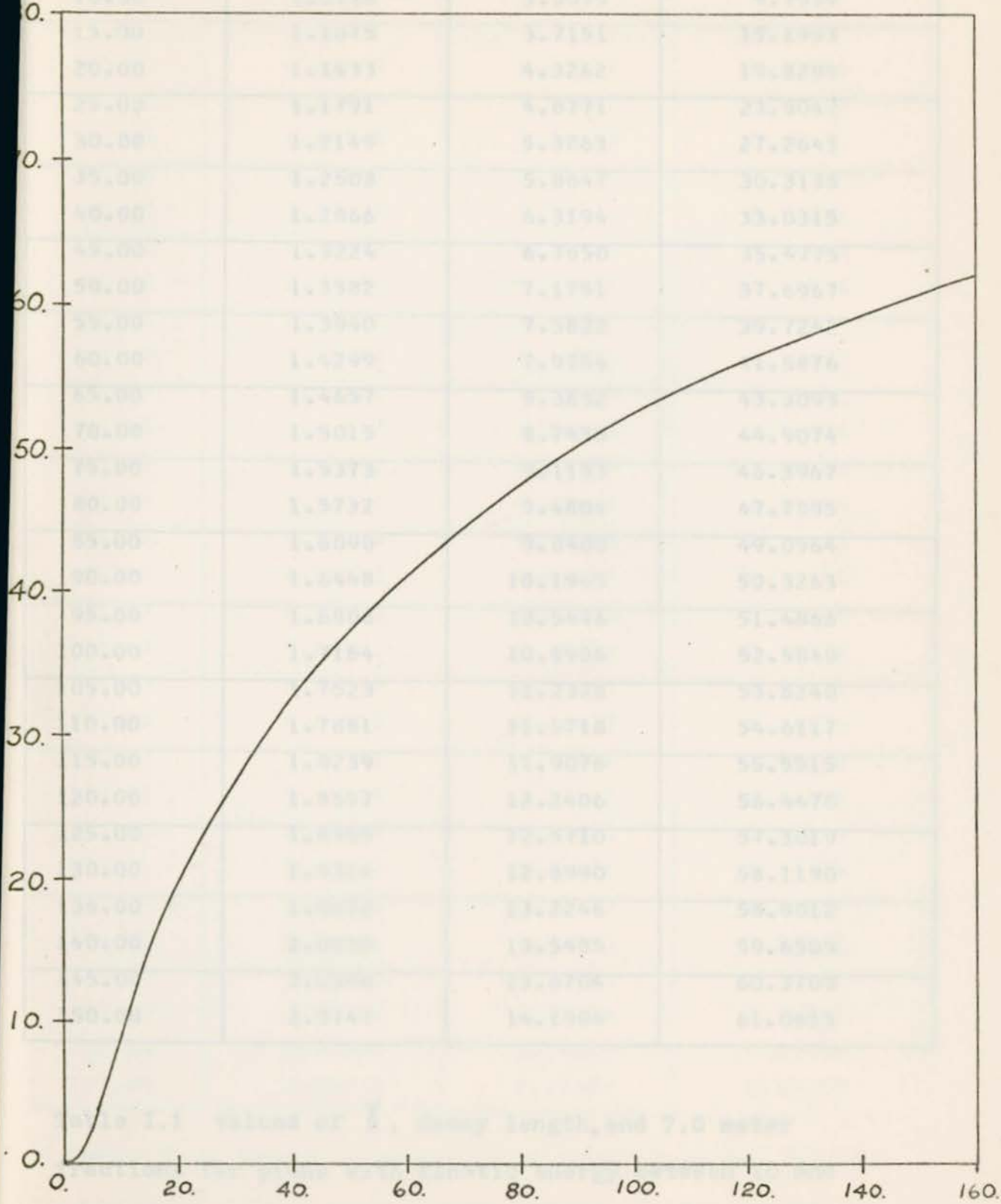

Fig. I.2 Fraction of pions surviving a 7.0 meter drift distance.

Kinetic Energy (MeV)	Gamma	Decay Length (meters)	Fraction Surviving a 7.0 m drift (%)
10.00	1.0716	3.0075	9.7539
15.00	1.1075	3.7151	15.1953
20.00	1.1433	4.3262	19.8284
25.00	1.1791	4.8771	23.8047
30.00	1.2149	5.3863	27.2643
35.00	1.2508	5.8647	30.3135
40.00	1.2866	6.3194	33.0315
45.00	1.3224	6.7550	35.4775
50.00	1.3582	7.1751	37.6967
55.00	1.3940	7.5822	39.7242
60.00	1.4299	7.9784	41.5876
65.00	1.4657	8.3652	43.3093
70.00	1.5015	8.7438	44.9074
75.00	1.5373	9.1153	46.3967
80.00	1.5732	9.4804	47.7895
85.00	1.6090	9.8400	49.0964
90.00	1.6448	10.1945	50.3263
95.00	1.6806	10.5446	51.4866
100.00	1.7164	10.8906	52.5840
105.00	1.7523	11.2328	53.6240
110.00	1.7881	11.5718	54.6117
115.00	1.8239	11.9076	55.5515
120.00	1.8597	12.2406	56.4470
125.00	1.8955	12.5710	57.3019
130.00	1.9314	12.8990	58.1190
135.00	1.9672	13.2248	58.9012
140.00	2.0030	13.5485	59.6509
145.00	2.0388	13.8704	60.3703
150.00	2.0747	14.1904	61.0613

Table I.1 Values of γ, decay length, and 7.0 meter fractions for pions with kinetic energy between 10 and 150 MeV.

Kinetic Energy (MeV)	Magnetic Rigidity (T/m)	Momentum (GeV/c)	Beta
10.00	0.17937	0.05377	0.35950
15.00	0.22157	0.06643	0.42972
20.00	0.25802	0.07735	0.48472
25.00	0.29087	0.08720	0.52984
30.00	0.32124	0.09631	0.56791
35.00	0.34977	0.10486	0.60064
40.00	0.37689	0.11299	0.62918
45.00	0.40287	0.12078	0.65434
50.00	0.42792	0.12829	0.67670
55.00	0.45221	0.13557	0.69672
60.00	0.47584	0.14265	0.71476
65.00	0.49890	0.14957	0.73110
70.00	0.52148	0.15634	0.74595
75.00	0.54364	0.16298	0.75952
80.00	0.56542	0.16951	0.77196
85.00	0.58686	0.17594	0.78340
90.00	0.60801	0.18228	0.79395
95.00	0.62888	0.18853	0.80371
100.00	0.64952	0.19472	0.81276
105.00	0.66993	0.20084	0.82116
110.00	0.69014	0.20690	0.82899
115.00	0.71017	0.21290	0.83630
120.00	0.73003	0.21886	0.84313
125.00	0.74974	0.22477	0.84952
130.00	0.76930	0.23063	0.85552
135.00	0.78873	0.23646	0.86116
140.00	0.80804	0.24224	0.86646
145.00	0.82723	0.24800	0.87145
150.00	0.84632	0.25372	0.87617

Table I.2 Values of magnetic rigidity, momentum and β for pions with kinetic energy between 10 and 150 MeV.

magnetic field. For example, a 110 MeV pion with a magnetic rigidity of 0.69 Tesla-meters will bend with a radius of curvature 0.69 meters in a magnetic field of 1 Tesla (10 kilogauss).

The range of pions in an absorber has not been measured very well to date, but the range as a function of energy can be calculated if the range-energy relation is known for some other charged particle. For the same kinetic energy, the ratio of the range of a proton to the range of a pion is equal to the ratio of the proton mass to the pion mass. This simple relation is discussed further by Weinstein (1964). Since the range of protons is well-known (see, for example, Attix and Roesch (1968)), the range of pions can easily be approximated. A plot of the range in water as a function of kinetic energy is given by Figure I.3.

Another useful graph that may be derived from the range-energy curve is Figure I.4 which gives the momentum range that is required to irradiate a given thickness of absorber as a function of the design energy of the transport system. For example, assume that the beam transport system transmits a momentum range of $\pm$ 8% of the design momentum, and a tumor thickness of 8 cm is to be irradiated. Figure I.4 shows that the design energy of the

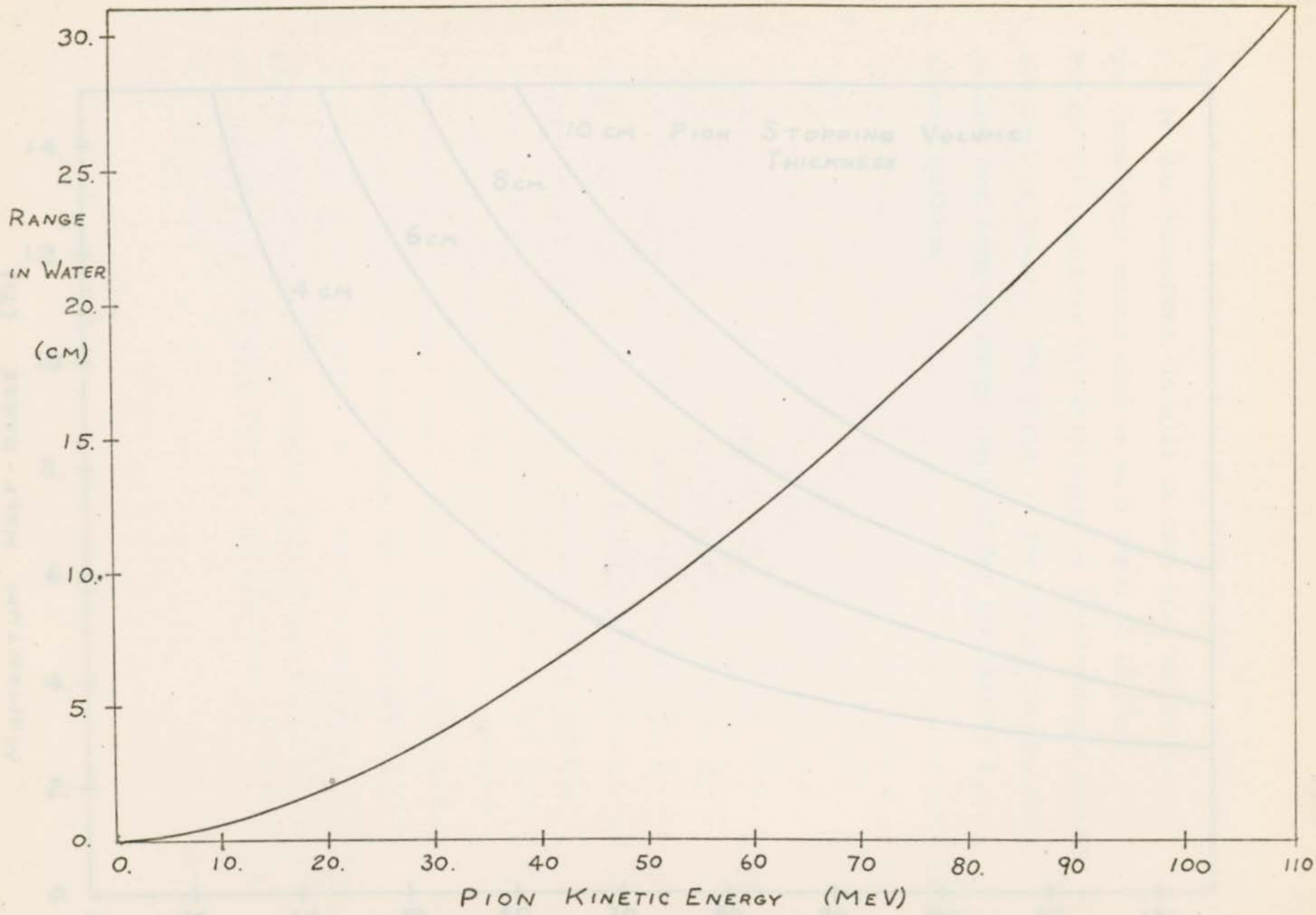

Fig. I.3 Range of pions in water.

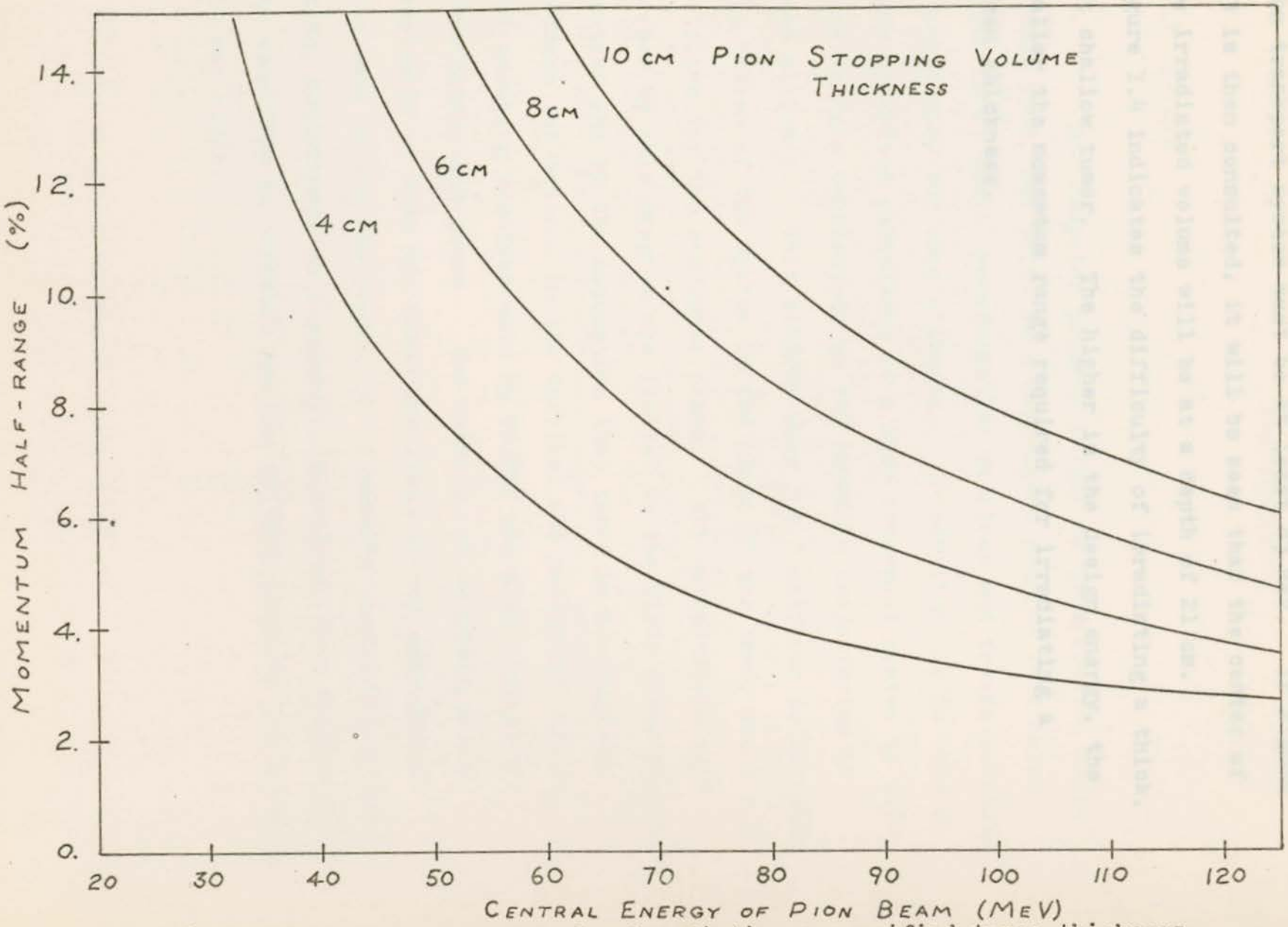

Fig I.4 Required momentum range for irradiating a specified tumor thickness.

beam transport system must be at least 83 MeV. If Figure I.3 is then consulted, it will be seen that the center of the irradiated volume will be at a depth of 21 cm. Figure I.4 indicates the difficulty of irradiating a thick, but shallow tumor. The higher is the design energy, the smaller the momentum range required for irradiating a given thickness.

APPENDIX II COMPUTER PROGRAMS FOR BEAM TRANSPORT CALCULATIONS.

II.1 TRIUMF

The computer program TRIUMF as described by Tautz (1968, 1969, and 1970) is a high-speed program that calculates first order transformation matrices and tracks particle trajectories and beam ellipses. In addition, it is able to vary specified parameters of a beam transport system to satisfy certain constraints on the particle trajectories or beam ellipses. This program uses 3 x 3 matrices to describe the action of the system in the plane of the bend, and 2 x 2 matrices for the conjugate plane. All calculations performed by this program are limited to the first order approximation and by the assumption that there is no coupling between the motions in the vertical and horizontal planes. The matching routines used by TRIUMF are also limited in flexibility and power. For example, no constraints are available to keep the field gradients of two quadrupoles the same during the design of a symmetric quadrupole triplet. Also, convergence to a solution is unlikely if a drift length is specified as variable and the initial guess at the solution is not close.

II.2 TRANS

The computer program TRANS (Chan and Lobb (1970)) is another tracking and matching program which, like TRIUMF, uses the first order approximation for all of its beam optics calculations. TRANS, however, uses the 6 x 6 matrix formalism of Brown (1967) so that the effects of coupling of the motions in the vertical and horizontal planes may be treated with this program. TRANS tracks beams represented by ellipsoids in a six dimensional phase space. More general matching facilities are offered with this program than with TRIUMF. TRANS is able to set any transfer matrix or beam ellipse matrix coefficients to a specified value by varying any of the parameters of the beam transport system. The program TRANS is intermediate in size between the relatively small, but fast TRIUMF and the large, slow TRANSPORT.

II.3 TRANSPORT

The computer program TRANSPORT (Brown and Howry (1970)) is the most general program available for use on problems in beam optics. TRANSPORT is able to include elements such as solenoids, sextupole magnets, and accelerator sections as well as all types of beam transport system elements mentioned previously. In addition to the tracking of six dimensional phase space ellipsoids and matching of first order matrix elements and beam parameters, TRANSPORT also can calculate the second order matrix coefficients. The list ov available constraints in the matching problems is essentially complete, but the arrival at correct solutions to some problems depends on the accuracy of the initial guess at the solution. If the initial conditions are sufficiently close to satisfying the constraints, then TRANSPORT can refine the solution to any specified accuracy.

II.4 NPFLUX

The program NPFLUX (R.Hutson, 1970) uses the first and second order transformation matrices calculated by TRANSPORT to do trajectory tracking. From a specified particle source size, NPFLUX chooses a large number of trajectories for which all initial positions and directions are equally probable. These trajectories are then tracked through the beam transport system to a rectangular grid at the end. The output of the program gives the solid angle of acceptance of the system, the places in the system where some of the trajectories have exceeded the beam tube size, and the vertical and horizontal distributions of the particles that would arrive at the end of the system.

II.5 ACCEPTANCE

This program written by Harrison and Lobb (1968) calculates the beam acceptance in initial phase space of a system of quadrupoles and uniform field bending magnets. Using the same matrix formalism as is used in the program TRIUMF, ACCEPTANCE can find the limiting apertures in the system, transform these limits back to the phase space at the origin of the system, and show exactly how each element limits the beam that will pass through the system. Since it is assumed that the motions in the vertical and horizontal planes are independent, rectangular apertures must be used for all elements. This program treats the quadrupole second-order chromatic aberrations directly by calculating the quadrupole strength parameters appropriate to the particle momentum.

BIBLIOGRAPHY

Alexander, J. H. and Reeve, P. A. 1971. TRIUMF Internal Report VPN-71-21.

Anderson, H. L. et al. 1964. Phys. Rev. 133, B392.

Bacon, G. E. 1969. Neutron Physics. (Wykeham Publications, London).

Banford, A. P. 1966. The Transport of Charged Particle Beams. (E. and F. N. Spon Ltd., London).

Batho, H. F. et al. 1968. Proposal for a Radiobiology and Radiotherapy Facility Using a Negative Pi-meson Beam from TRIUMF submitted to the Health Resources Fund.

Batho, H. F. 1970. Private communication.

Boone, M. L. M. and Wiley, A. L. 1971. IEEE Trans. Nucl. Sci. NS-18, #3, 36.

The British Columbia Cancer Treatment and Research Foundation, 1970. A Radiobiology-Radiotherapy Laboratory at TRIUMF and a Radiology Department at the British Columbia Cancer Institute. Vancouver, B. C.

Brown, K. L. 1967. Stanford Linear Accelerator Center Report SLAC-75.

Brown, K. L. and Howry, S. K. 1970. Stanford Linear Accelerator Center Report SLAC-91.

Casarett, A. P. 1968. Radiation Biology. (Prentice-Hall Inc., Englewood Cliffs, N. J.).

Chan, C. and Lobb, D. E. 1970. TRIUMF Internal Report VPN-70-4.

Curtis, S. B. and Raju, M. R. 1967. Lawrence Radiation Laboratory Report UCRL-17606.

Curtis, S. B. and Raju, M. R. 1968. Rad. Res. 34, 239

Curtis, S. B. 1971. Rad. Res. 46, 557.

Evans, R. D. 1955. The Atomic Nucleus. (McGraw-Hill Book Company, Inc., New York).

Fowler, P. H. and Perkins, D. H. 1961. Nature, 198, 524.

Fowler, P. H. 1965. Proc. Phys. Soc. 85, 1051.

Fowler, P. H. and Mayes, V. M. 1967. Proc. Phys Soc. 92, 377.

Goldstein, H. 1950. Classical Mechanics. (Addison-Wesley Publishing Company, Inc., Reading, Mass.).

Guthrie, M. P. et al. 1968. Nucl. Instrum. and Meth. 66, 29.

Harrison, R. W. and Lobb, D. E. 1968. TRIUMF Report TRI-68-7.

Hirt, W. et al. 1969. CERN Report CERN-69-24.

Hutson, R. 1970. Private communication.

Johns, H. E. and Cunningham, J. R. 1969. The Physics of Radiology, 3d edition. (Charles C. Thomas, Springfield, Illinois).

Kaplan, H. S. 1970. Proceedings of the Third LAMPF Users Meeting, LA-4397-MS.

Larson, J. D. 1971. IEEE Trans. Nucl. Sci. NS-18, #3, 1088.

Lawrence Radiation Laboratory, 1970. Review of Particle Properties. Lawrence Radiation Laboratory Report UCRL-8030.

Leighton, R. B. 1959. Principles of Modern Physics. (McGraw-Hill Book Company, Inc., New York).

Lobb, D. E. 1970. Nucl. Inst. and Meth. 82, 331.

Lobb, D. E. 1972. Methods for Calculating the Effects of Errors Which Increase the Beam Spot Size at the End of a Beam Transport System, submitted to Nucl. Inst. and Meth.

Lobb, D. E. 1972. TRIUMF Internal Report VPN-72-1.

Marshak, R. E. 1952. Meson Physics. (McGraw-Hill Book Company, Inc., New York).

Meredith, W. J. and Massey, J. B. 1968. Fundamental Physics of Radiology. (John Wright and Sons, Ltd., Bristol).

Meyerhof, W. 1967. Elements of Nuclear Physics. (McGraw-Hill Book Company, Inc., New York).

Penner, S. 1961. Rev. Sci. Instr. 32, 2.

Raju, M. R. and Richman, C. 1969. Lawrence Radiation Laboratory Report UCRL-18806.

Reeve, P. A. 1971. TRIUMF Internal Report VPN-71-11.

Richman, C. et al. 1964. Lawrence Radiation Laboratory Report UCRL-11387.

Richman, C. et al. 1966. Am. J. Roentgenol. 96, 177.

Rosen, L. 1968. Nucl. Applic. 5, 379.

Steffen, K. G. 1965. High Energy Beam Optics. (John Wiley and Sons Inc., London).

Sullivan, A. H and Baarli, J. 1968. Phys. Med. Biol. 13, 435.

Tautz, M. F. 1968. TRIUMF Report TRI-68-5. See also:
Tautz, M. F. 1969. TRIUMF Internal Report VPN-69-8, and
Tautz, M. F. 1970. TRIUMF Internal Report VPN-70-26.

Vogt, E. W. and Burgerjon, J. J. (editors) 1966. TRIUMF Proposal and Cost Estimate. University of British Columbia.

Weinstein, R. 1964. The Interaction of Radiation with Matter. (McGraw-Hill Book Company, Inc., New York).

Surname: HARRISON Given Names: ROBERT WILLIAM

Place of Birth: Comox, B. C. Date of Birth: July 18, 1946

Educational Institutions Attended, with Dates of Entering and Leaving:

UNIVERSITY OF VICTORIA 1964 to 1968

Degrees, Diplomas, Etc., Awarded, with Dates and Names of Institutions:

B.Sc. 1968 UNIVERSITY OF VICTORIA, VICTORIA

Honours and Awards:

Publications:

R. W. Harrison and D. E. Lobb, A Program to Calculate the Phase Space Acceptance of a Beam Transport System, TRIUMF Report TRI-68-7, October, 1968.

THE UNIVERSITY OF VICTORIA LIBRARY

MANUSCRIPT DISSERTATION (or THESIS)

AUTHORITY TO DISTRIBUTE

AUTHOR: This dissertation may be lent or microfilm copies made available:

(a) Without restriction [redacted]

(b) With the restriction that, for a period of five years (until)the written approval of the following is required:

(1) The Chairman, School of Graduate Studies .....

(2) The Author .....

(3) both the Chairman, School of Graduate Studies, and the Author .....

BORROWERS: The borrower undertakes, by signing below, to give proper credit for any use made of the dissertation, and to obtain the consent of the author if it is proposed to make extensive quotations, or to reproduce the dissertation in whole or in part.

Signature of Borrower	Address	Date